FINAL REPORT

Shoreline Evolution and Coastal Resiliency at Two Military Installations: Investigating the Potential for the Loss of Protecting Barriers

SERDP Project RC-1702

MAY 2014

Rob. L. Evans
Jeffrey Donnelly
Andrew Ashton
Woods Hole Oceanographic Institute

Kwok Fai Cheung
Volker Roeber
University of Hawaii

SERDP
DOD ▪ EPA ▪ DOE

REPORT DOCUMENTATION PAGE

Form Approved
OMB No. 0704-0188

1. REPORT DATE *(DD-MM-YYYY)*	**2. REPORT TYPE**	**3. DATES COVERED** *(From - To)*
	Final	08/24/2009-05/01/2014

4. TITLE AND SUBTITLE
Shoreline Evolution and Coastal Resiliency at Two Military Installations: Investigating the Potential for and Impacts of Loss of Protecting Barriers

5a. CONTRACT NUMBER
W912HQ-09-C0043

5b. GRANT NUMBER
W912HQ-09-C0043

5c. PROGRAM ELEMENT NUMBER

6. AUTHOR(S)
Rob. L. Evans, Jeffrey Donelly, Andrew Ashton, Kwok Fai Cheung, Volker Roeber

5d. PROJECT NUMBER
RC-1702

5e. TASK NUMBER

5f. WORK UNIT NUMBER

7. PERFORMING ORGANIZATION NAME(S) AND ADDRESS(ES)

Woods Hole Oceanographic Institution, 266 Woods Hole Rd, Woods Hole, MA 02543

8. PERFORMING ORGANIZATION REPORT NUMBER

9. SPONSORING / MONITORING AGENCY NAME(S) AND ADDRESS(ES)
SERDP

10. SPONSOR/MONITOR'S ACRONYM(S)

11. SPONSOR/MONITOR'S REPORT NUMBER(S)

12. DISTRIBUTION / AVAILABILITY STATEMENT
Approved for public release; distribution is unlimited

13. SUPPLEMENTARY NOTES

TABLE OF CONTENTS

List of Figures

List of Tables

List of Acronyms

ACE	Accumulated Cyclone Energy
ADCIRC	A system of computer programs for solving time dependent, free surface circulation and transport problems in two and three dimensions
AIWW	Atlantic Intracoastal Waterway
AMM	Atlantic Meridional Mode
AMO	Atlantic Multidecadal Oscillation
AMS	Accelerating Mass Spectrometer –a technique for dating carbon bearing samples
BOSZ	Boussinesq Ocean and Surf Zone model
Ca	Calcium
CFAMS	Continuous Flow Accelerating Mass Spectrometer
CFSR	Climate Forecast System Reanalysis
CHIPS	Coupled Hurricane Intensity Prediction System
CL	Marine Corps Base Camp Lejeune
CMIP	Coupled Model Intercomparison Project
ENSO	El Nino Southern Oscillation
EAFB	Eglin Air Force Base
GCM	Global scale numerical Climate Model
dGPS	Differential Global Positioning System
GPR	Ground Penetrating Radar -a geophysical technique which uses high frequency radar signals to map subsurface structure
UH-ORE	The University of Hawaii high resolution inundation and wave modeling package
IPCC	Intergovernmental Panel on Climate Change
ITCZ	Inter-Tropical Convergence Zone
LIDAR	LIght Detection And Ranging - an optical remote sensing technology used to determine information (such as distance to) of a remote target
MJO	Madden-Julian Oscillation
MDR	Main Development Region (of tropical cyclones)
MSL	Mean Sea Level
NAO	North Atlantic Oscillation
NCAR	National Center for Atmospheric Research
NCEP	National Centers for Environmental Prediction –A division of the National Weather Service
NEOSURGE	A long-wave model describing water levels forced by tides and wind and wave setup
NOAA	National Oceanic and Atmospheric Administration
NOSAMS	National Ocean Sciences Accelerating Mass Spectrometer
OSL	Optically Stimulated Luminescence
PDF	Probability Density Function
PHM	Parametric Hurricane Model
QBO	Quasi-Biennial Oscillation
RMW	Radius of Maximum Wind
SLR	Sea-Level Rise
SLOSH	Sea, Lake, and Overland Surges from Hurricanes

Sr	Strontium
SST	Sea Surface Temperature
SWAN	Simulation of WAves Nearshore
Ti	Titanium
WHOI	Woods Hole Oceanographic Institution
WIS	Wave Information Study
WW3	WaveWatch 3
XRF	X-Ray Fluoresence

Keywords

Coastal Barrier; Sea-Level Rise; Tropical Cyclones; Storm Surge

Acknowledgements

We would like to thank those who assisted us in the field and in the laboratory, especially Stephanie Madsen, Emily Carruthers, Buzz Friend, Trevor Harrison, Skye Moret, Michael Toomey, Pete Van Hengstrum and students from the Northeastern University Co-op program. Cape Abilities work crews are thanked for constructing sediment traps.

We gratefully thank staff at Eglin Air Force Base and the Jackson Guard, especially Brett Williams for assistance with research permits and access to the installation grounds. Glen Barndollar is thanked for making it easy for us to work on Santa Rosa Island. Bob Miller is thanked for co-ordinating our efforts with respect to protected habitats.

We would like to than Susan Cohen for facilitating access to Camp Lejeune. We also acknowledge scientific advice, input and data provided by the DCERP funded team working at Lejeune, especially from Tony Rodriguez and Jesse McNinch.

The project was funded by the Strategic Environmental Research and Development Program (SERDP).

1. Abstract

Objectives

This project evaluates the impacts of sea-level rise (SLR), in conjunction with storms, on the barrier islands fronting Eglin Air Force Base (EAFB), Florida and at Marine Corps Base Camp Lejeune (CL), North Carolina, using prescribed SLR scenarios. Both installations face open oceans and include coastal barriers that dynamically respond to rising seas and currently protect significant backbarrier infrastructure. However, the geologic history, geometry and environmental setting of each system are different; in particular, the extent of back-barrier lagoon as well as the wave and storm exposure varies between the two sites.

Coastal barriers (barrier islands and spits) act as a buffer, protecting estuarine ecosystems and the upland from direct assault by the ocean, particularly during large storms. Under the conditions of moderate SLR experienced over the last several millennia, barriers formed and migrated landward through overwash processes, allowing barriers to maintain themselves. However, the dramatically increased rates of projected SLR significantly exceed those seen in the last 6,000 years, raising a concern that barriers may be unable to survive intact. The loss of the protective barrier beach would leave backbarrier areas exposed to the open ocean and to more frequent and severe storm-induced flooding. Barriers provide protection to a number of U.S. military installations, including the two we focus on in this study.

Key questions addressed in our study are:

1) How will protective barriers respond to 0.5, 1.0, 1.5, and 2.0 m of SLR over the coming century? For these SLR scenarios, what is the potential that barriers will no longer be able to keep up with sea level and will drown completely? How do the constraints of local geographic and geologic settings affect the potential for drowning?
2) How do storms, and variability in storm activity, work in concert with SLR to exacerbate barrier loss or impact barrier morphology?

Technical Approach

The project features an integrated field and modeling approach to understand the impacts of SLR on the barriers fronting EAFB and CL. This includes using sedimentary approaches to evaluate the long-term storm history of each region. The two sites were selected as they are both subject to relatively frequent impacts from tropical cyclones, yet have different tidal ranges and wave climates. CL has the added exposure to longer duration, but less intense nor'easter storm events.

In order to address the questions outlined above, we have worked to determine the natural oceanographic and sediment transport processes that control barrier morphology and migration (and potentially drowning). We have developed a numerical model of barrier evolution over the centennial timescale appropriate for the SLR scenarios considered. Numerical modeling

approaches were also used to generate a synthetic suite of 10,000 storms for each site. These storm parameters were fed into the National Oceanic and Atmospheric Administration (NOAA) Sea, Lake and Overland Surge from Hurricanes (SLOSH) model to generate storm and storm-surge return intervals for both locations. High-resolution inundation modeling was run for select storms at both sites and includes consideration of a nor'easter event at CL.

Results

Under modern climate conditions, the 1/100 year event at EAFB corresponds to a ~3m surge event. In contrast, the return interval for a 2m surge event at CL is 240 years. In both cases, barrier drowning has a profound impact on back-barrier surge levels, even for relatively modest increases in sea level. This is also true for Nor'easter events at CL. Under modern conditions nor'easter events seem unlikely to overtop the barrier but instead remove sediment from the beachface and transport it offshore, most of which is available for transport onshore during calmer conditions.

The geomorphic model demonstrates the importance of overwash in maintaining intact barriers as sea level rises. Given the uncertainty in quantifying future overwash rates, the model is able to provide envelopes of different shoreline change behaviors for different potential overwash fluxes. Estimates of modern overwash flux rates at both sites are below the quantity required to maintain barrier geometries over centennial timescales.

Long-term storm histories for each region show a consistent picture of Holocene storm history for the Gulf of Mexico and for the US Atlantic coast when integrated with other regional studies. Our data show that storminess across both basins has been highly non-stationary over the past thousands of years, revealing a geologic precedent for significant changes in storm climate. Periods of enhanced storm activity in the past have had significant impacts on barrier morphology.

Benefits

Our program highlights several critical issues that should be specifically evaluated or taken into consideration as part of any vulnerability assessment for installations fronted by or which rely on barrier beach systems. These include:

- Determining the geometry and geology of the entire system with a reasonably high level of precision and detail.
- Analysing storm recurrence intervals for a given region.
- Understanding of across-barrier sediment transport.
- Running a detailed suite of inundation models with a large ensemble of storm events that are plausible for a specific location or installation.
- Evaluating the historical record in a given area to understand the long-term risk of storm impacts.

2. Objective

This project evaluates the impacts of SLR, in conjunction with storms, on the barrier islands fronting EAFB, Florida and at CL, North Carolina, using prescribed sea-level scenarios. Both installations face open oceans and include coastal barriers that will dynamically respond to rising seas (as opposed to fully engineered or protected harbors, which will mostly be passively affected by higher sea levels).

SLR has the potential to affect existing coastal infrastructure through both passive and dynamic mechanisms. Higher sea levels inundate coastal regions, leaving them more susceptible to flooding and damage from storms. The hazards associated with this passive inundation can be reasonably estimated using current tools. However, the coast is not a bathtub—increased sea levels enhance the ability for waves to reorganize the coast, typically resulting in increased shoreline retreat by moving sediment either offshore into deeper waters or onshore by overwashing the existing coast.

Coastal barriers (barrier islands and spits) act as a buffer, protecting estuarine ecosystems and the upland from direct assault by the ocean, particularly during large storms. Under the conditions of moderate SLR experienced over the last several millennia, barriers formed and migrated landward through overwash processes, allowing barriers to maintain themselves. However, the dramatically increased rates of projected SLR significantly exceed those seen in the last 6,000 years, raising a concern that barriers may be unable to survive intact. The loss of the protective barrier beach would leave backbarrier areas exposed to the open ocean and to more frequent and severe storm-induced flooding. Barriers provide protection to a number of U.S. military installations, including EAFB and CL. This project has combined field and modeling approaches to better understand the dynamic responses of barriers to accelerated SLR and the impacts of subsequent inundation by severe storms.

Key questions addressed in our study are:

1) How will protective barriers respond to 0.5, 1.0, 1.5, and 2.0 m of SLR over the coming century? For these SLR rates, what is the potential that barriers will no longer be able to keep up with sea level and will drown completely? How do the constraints of local geographic and geologic settings affect the potential for drowning?

2) How do storms, and variability in storm activity, work in concert with SLR to exacerbate barrier loss or impact barrier morphology?

In order to address these questions, we need to determine the natural oceanographic and sediment transport processes that control barrier morphology and migration (and potentially drowning). Although many models of coastal change have been developed, most of these models are highly

calibrated and are intended to operate at the temporal scales of engineering projects, offering little possibility of forecasting never-seen behaviors. Other models that focus on long-term geologic timescales envision slow, steady changes, assuming that the coast maintains an 'equilibrium' configuration. We have developed a model that examines key decadal sedimentary and oceanographic parameters to project barrier behavior through the coming century.

For each site, we have estimated the vulnerabilities from major storms based upon current climatology, as changing storm patterns could play as large a role as SLR alone in determining the future morphology of the protecting barriers. We have also evaluated the long-term storm history for each region and use these to examine natural variability in storminess and the impact this non-stationarity has on barrier behavior.

3. Background

3.1 Eglin Air Force Base Site: The Santa Rosa/Destin Barrier System

EAFB, FL, located on Choctawhatchee Bay and Santa Rosa Sound, is protected by the Santa Rosa/Destin Barrier system (Fig. 1). Mean tidal range is about 40cm (Stone, 1991). Ocean waves dominantly approach from the south-southeast, with average heights of 0.8m that rarely exceed 2m in height. Santa Rosa Island extends nearly 100km west of Destin to Pensacola Pass and is separated from the mainland by Santa Rosa Sound.

The island has been characterized as a composite barrier (a modern barrier combined with a stranded Pleistocene barrier) by Otvos (1982) and is thought to have formed in the late Holocene (also see Stone, 1991; Stone et al., 2004). The barrier primarily consists of quartz sand that is sourced from eroding Pleistocene deposits at Grayton Beach to the east (Stone, 1991; Stone et al., 1992; Stone and Stapor, 1996). Choctawhatchee Bay is a large back-barrier estuary occupying over 300km^2. East Pass is the principal inlet to the estuary and has a well-developed flood tidal delta (Morang, 1992). This inlet is maintained and is substantially larger than it was ~100 years ago. Immediately landward of the flood tidal delta is an area of over 40km^2 that is over 9m deep, with some depressions as deep as 12m. During periods of rising sea-level, this deep back-barrier could contribute to barrier drowning, serving as a sediment sink.

The Eglin region has been significantly impacted by at least 9 tropical cyclones since 1851 (Landsea et al., 2004). Most recently, three category 3 storms have hit the area in 1995 (Opal), 2004 (Ivan), and 2005 (Dennis). In addition, Hurricane Georges (a category 2 storm) hit the region in 1998. Barrier surveys at Santa Rosa Island before and after Georges reveal the landward transport of sand during the event (Stone et al., 1999). Hurricanes Ivan and Dennis also resulted in landward transport of sand into the back-barrier environment associated with hurricane-induced overwash (Houser, 2008; 2009).

Much of the EAFB infrastructure is protected by the Santa Rosa/Destin barrier system and modifications to, or loss of the barrier could have profound impacts on the vulnerability of the base to future storms. However, portions of the barrier itself are Air Force property and house military infrastructure. These sections of barrier are also used for training exercises. The Air Force recently completed reconstruction of the access road through this section of barrier at a cost of around $50 million. Similar investments have been made to preserve base-associated buildings and infrastructure along this otherwise undeveloped stretch of coast.

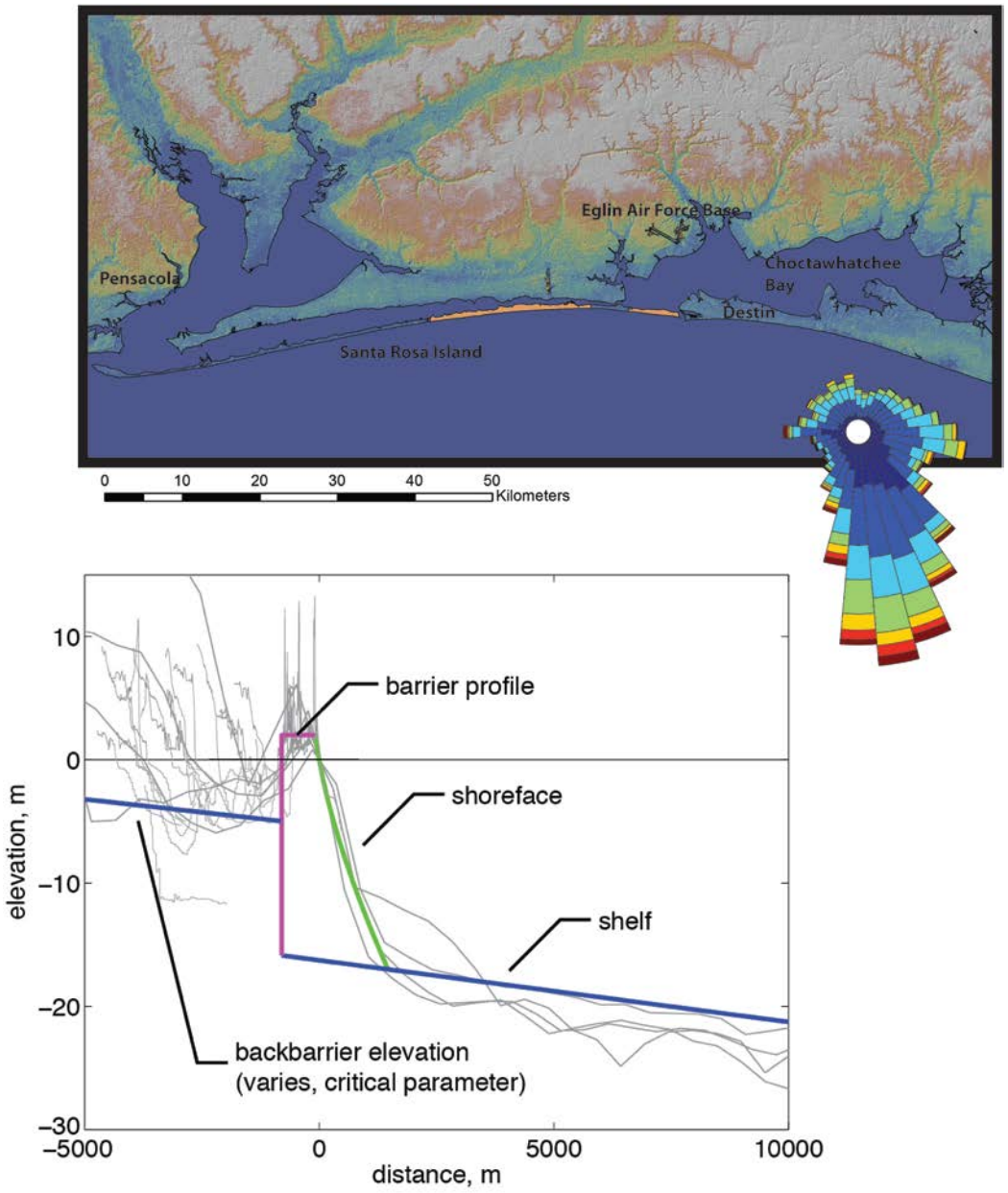

Figure 1. A map of the EAFB region showing the extent of Santa Rosa Island. Areas on the barrier shaded orange are military property. Also shown is the windrose diagram for the region showing the prevailing wind direction. Waves dominantly approach from the south-southeast, driving westward alongshore sediment transport. The lower panel shows a series of combined bathymetric and topographic profiles along Santa Rosa Island overlain with simple representative shelf, shoreface, and barrier width geometries used in numerical model simulations.

Given the funnel shape of Choctawhatchee Bay, it may be subjected to significant focusing of surge during some tropical cyclone scenarios, particularly if the protecting barrier is lost to increasing SLR rates. Increases in wave energy in the bay could also result in erosion of uplands that could potentially threaten existing infrastructure. Changes in barrier configuration associated with future SLR could result in increased susceptibility of bay-bottom sediments to erosion during hurricane landfalls that could mobilize contaminated sediments (Hemming et al., 2005) and pose significant water quality issues. Further, Santa Rosa Island provides important habitat for several threatened and endangered species including Santa Rosa Beach Mouse, Green Sea Turtle, Loggerhead Sea Turtle, Snowy Plover, Least Tern and also fauna such as Reindeer lichen. Understanding future changes in barrier morphology constitutes a critical first step for developing appropriate wildlife management strategies.

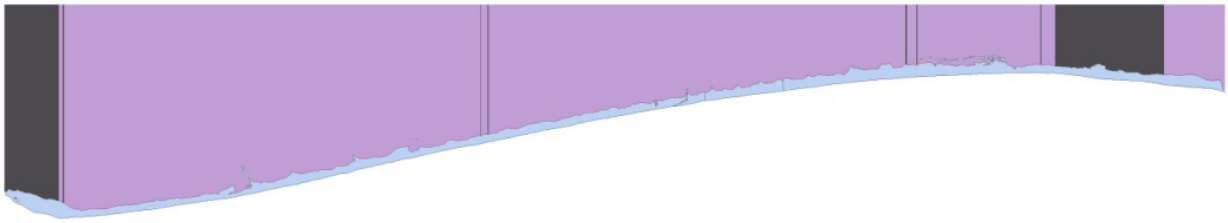

Figure 2. The motion of the shoreline along Santa Rosa Barrier between 1855 and 2001. Most of the barrier has been retreating (pink regions), but sections of the westernmost and eastern barrier have seen accretion (grey regions).

Historic shorelines along Santa Rosa Island show relatively modest changes in position, with the exception of the western end of the island where it has extended westwards of Fort Pickens due to westward alongshore sediment transport. Most of the barrier shoreline has been migrating landward since records began in 1855 (Fig. 2), with the exception of regions around Fort Pickens and the eastern section of the barrier fronting Choctawhatchee Bay which have accreted (Fig. 3). There has been significant migration of the barrier immediately to the east of Fort Pickens, a low lying section of barrier that is often seen to be the most vulnerable section to storms. The change in the East Pass Inlet morphology can be seen in Figure 3. The modern-day inlet cuts through what was, in the mid-late 1800's, a continuation of the Holocene barrier that connected up with what is now the southwestern part of Destin. At that time, the inlet flowed to the east between the Pleistocene and Holocene barriers.

Figure 3. Historic shorelines on portions of Santa Rosa Island. (Top) changes in the westernmost portion of the barrier around Fort Pickens (Lower) changes in the east inlet location around Destin (Shoreline data from the USGS).

3.2 Marine Corps Base Camp Lejeune, North Carolina

The Onslow Bay Barrier system is a transgressive barrier that fronts portions of CL and the New River Estuary (Fig. 4). The New River Inlet, with a well-developed flood tidal delta, occupies the mouth of the estuary. This region has been described as a submarine headland, produced by the Oligocene Silverdale Formation, a limestone and sandstone unit that outcrops at the mouth of the New River estuary (Riggs et al., 1995). The north portion of Onslow barrier is a cuspate shoreline with a virtually continuous and high dune ridge, relatively wide beaches, well-developed back-barrier marshes, and a recurved accretionary beach ridge. This stretch of shoreline has historically

been accreting at rates of about 2m/yr (Cleary and Hosier, 1987). The southern portion of the barrier has a narrow shoreface, a discontinuous scarped foredune ridge, is overwashed frequently during storms, and experiences erosion rates as large as 6m/yr. Significant portions of this barrier complex are underlain by estuarine sediments (Riggs et al., 1995) that often outcrop in the surf zone during storms. Mean tidal range in the area is approximately 1.2m (NOAA, 2008). The sea-level history for the North Carolina region has been reported by Kemp et al., (2009), with a measured rate of relative SLR during the twentieth century of 3.0–3.3 mm/yr.

The return period for historic hurricanes (sustained winds in access of 33m/s) impacting this region is about 10 years (Elsner and Kara, 1999). This region of North Carolina has experienced several landfalling hurricanes during the most recent active period. Hurricanes Bertha and Fran made landfall in 1996 at category 2 and category 3 intensity respectively (Pasch and Avilla, 1999). In 1998 Hurricane Bonnie made landfall as a category 3 storm (Pasch et al., 2001). Hurricane Floyd made landfall in 1999 at category 2 intensity (Lawrence et al., 2001). Earlier in the 20th century Hurricane Hazel made landfall in 1954 as a strong category 3 storm (Davis, 1954). Most of these storms caused significant storm surge and modifications to coastal barriers in the region.

In addition to the previous geological investigations (see Riggs et al., 1995 for review), the geological evolution of this site has recently been the focus of a large DCERP program (http://www.serdp.org/Program-Areas/Resource-Conservation-and-Climate-Change/Natural-Resources/Coastal-and-Estuarine-Ecology-and-Management/RC-1413). Data from the DCERP program have been used in our analysis.

Much of the CL infrastructure is located up the New River estuary on relatively high bluffs. However, some infrastructure and training grounds are located in more vulnerable low-lying areas near the estuary or on the barrier or back-barrier. In addition, the New River estuary may be subjected to significant focusing of surge during some tropical cyclone scenarios, particularly if the inlet is widened or the protecting barrier is lost to increasing SLR. Increased surge in wave energy in the estuary could also result in erosion of bluffs that could potentially threaten existing infrastructure.

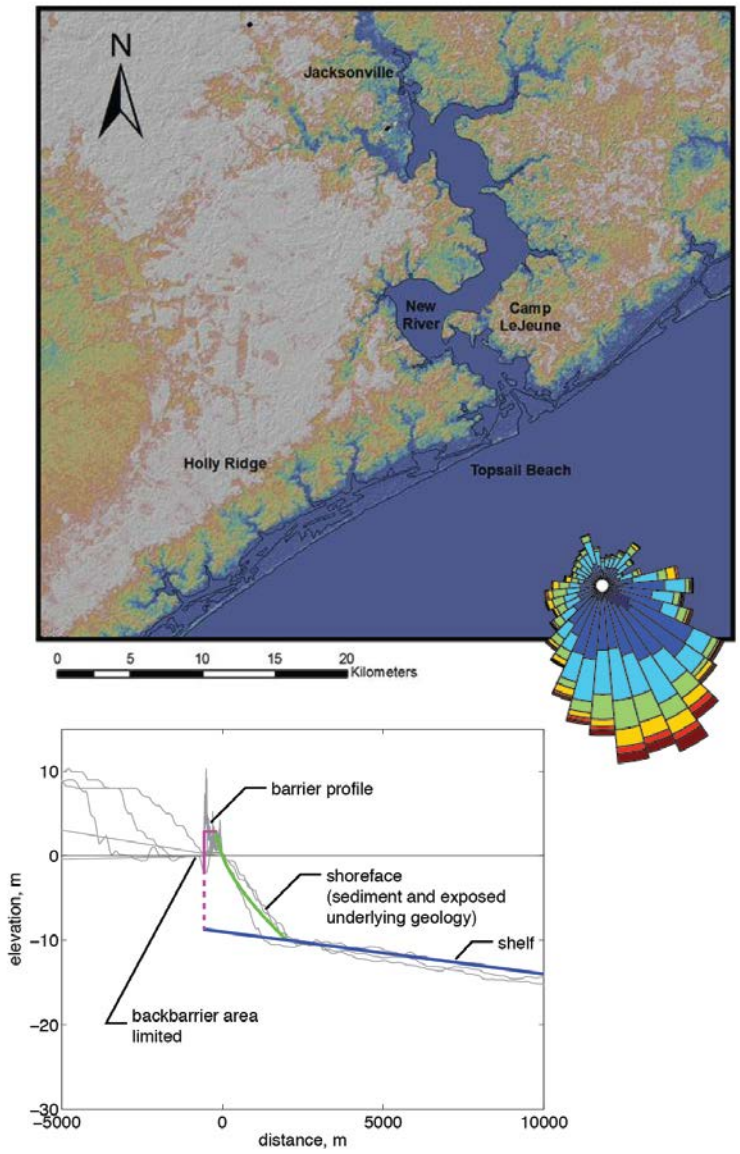

Figure 4. A map of the region surrounding CL, North Carolina. Also shown is the windrose diagram for the region showing a prevailing wind from the south-southeast. The lower panel shows the representative cross section through the barrier system used in modeling. In contrast to EAFB, the barrier at CL is quite narrow, has a smaller vertical extent of the active shoreface and has a much more limited backbarrier region.

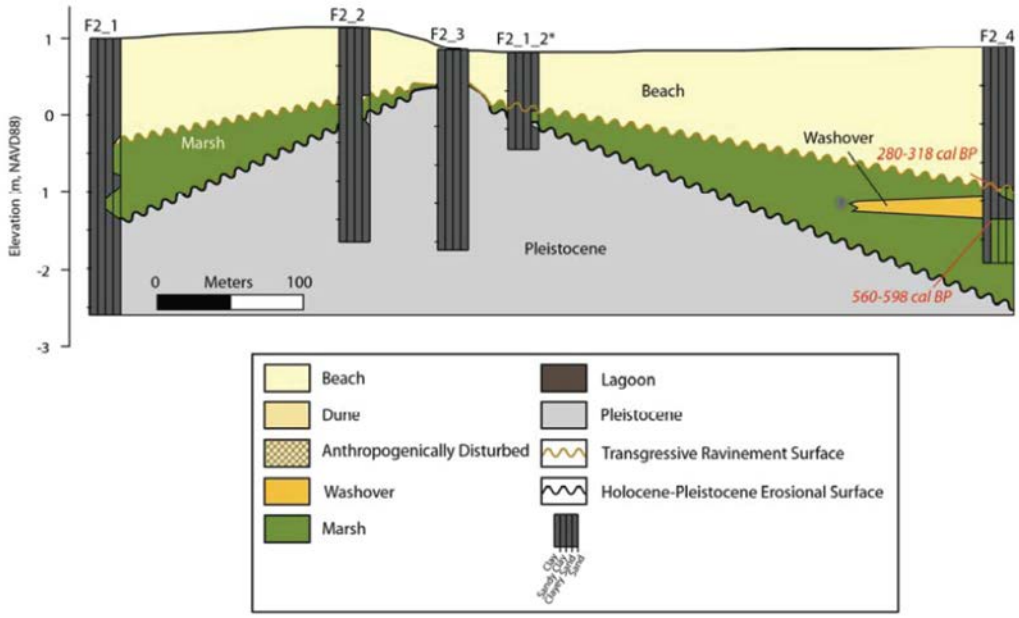

Figure 5. A geologic cross section through the barrier system fronting CL. The figure is a product of the DCERP program and is provided courtesy of A. Rodriguez. The DCERP team have identified and quantified a number of overwash deposits in the barrier (Foxgrover, 2009).

The Onslow Beach barrier system fronting CL is thinner in vertical extent (~several meters) than Santa Rosa Island. Another significant difference between the two settings is the near absence of a backbarrier lagoonal system at CL, although the Atlantic Intracoastal Waterway (AIWW) was excavated immediately behind the barrier. In the study area, the barrier lies between the New River Inlet at the southern end, and Brown's Inlet to the north. Offshore, sediment supply is limited with extensive hardbottom conditions and outcropping limestone (Riggs et al., 1996) and recent sidescan and sub-bottom imaging carried out as part of the DCERP project show thin sediment cover (Foxgrover, 2009).

4. Materials and Methods

4.1 Seismic Methods

Chirp seismic data were used to map subbottom sediments and to identify locations for coring. Data were collected with an Edgetech 512i chirp-seismic unit navigated with a Trimble ProXRT differential Global Positioning System (dGPS) unit. Data were imported into Kingdom Suite software for processing and visualization.

4.2 Ground Penetrating Radar Coverage

Extensive ground penetrating radar (GPR) data was collected on Santa Rosa Island. GPR data were collected with a Mala Geoscience system with a 250MHz antenna. For land profiles, the radar unit was pulled behind a vehicle and was in contact with the road surface. Data were generally spatially referenced through use of a Trimble ProXRT dGPS unit, with real-time Omnistar differential correction, mounted on the antenna.

The GPR profiles collected consist of continuous profiles along the length of the barrier, collected to identify the locations of past inlets and breaches in the barrier, a series of across barrier profiles which have the potential to identify erosional and constructional strata in the barrier, and more targeted studies on overwash fans identified through aerial photographs.

4.3 Sedimentary Analyses for Storm History

Cores were collected in a variety of locations to provide a storm history of the study areas over the late Holocene. For the Eglin region, work was combined with other studies by our group to produce a storm history for the Northern Gulf of Mexico extending back 5000-6000 years. At CL, a series of cores provide a history over the last 8000 years.

Cores were collected using a vibracoring rig. In most cases, the vibracore has a companion overlapping surface drive collected with a piston corer, to better preserve the less consolidated upper meter of sediments. The surface drive and vibracore from each location are typically combined into a composite core by matching visually distinctive bedding and trends in geochemical data. The cores are then split and described using the classification method from Schnurrenberger et al. (2003).

Cores of interest were scanned on an ITRAX Corescanner, typically at 200 micron increments with a 0.4s dwell time, to obtain radiographic images and at 1 mm increments with a 10s dwell time to obtain elemental abundance data. Surface samples were analyzed for elemental abundances using

an INNOV-X systems Alpha 4000 handheld X-ray fluorescence (XRF) analyzer with a 90s dwell time.

We obtain grain size data by sampling the core at continuous (typically 1cm) increments and separating the samples into two parts; one part is weighed and then dried overnight in a convection oven at 100˚C to determine the water content, and the other part is weighed and wet-sieved at 32 microns to remove the clay particles that solidify when the samples are dried. The fraction of water determined on the subset of samples that were dried in the oven is used to approximate the bulk dry mass of the samples that were sieved. The sieved samples are combusted in a muffle furnace at 550˚C for four hours to remove all organic material and wet-sieved again at 32 microns post-combustion, dried, and weighed (Dean, 1974). The mass of dried sediment remaining after the sieving and combustion processes is divided by the bulk dry mass of that sample, approximated using the water fraction from the subset of samples that were dried in the oven immediately after sampling, to determine the percent of sediments that is greater than 32 microns in diameter relative to the bulk dry mass. These samples are then wet-sieved at 63 microns to determine the percent of the dry bulk sediments that is sand sized and greater, which we refer to as "%sand".

Age models come from a combination of ^{14}C ages on intact bivalve halves obtained using the Continuous-Flow Accelerated Mass Spectrometer (CFAMS) method at the National Ocean Sciences Accelerating Mass Spectrometer (NOSAMS) facility (Roberts et al., 2011) and organic ^{14}C ages on plant macrofossils that were strategically sampled near major density transitions detected in the radiographic images obtained from the cores to maximize age control at major sedimentological transitions. Recent age markers are obtained using push-cores which are typically sampled at five-centimeter increments and these samples are analyzed using Gamma ray spectrometry analysis to determine levels of ^{137}Cs and ^{210}Pb down core.

4.4 Sediment Transport

The transport of sediment across the barrier system is a critical parameter for understanding long-term barrier behavior. We used several methods to estimate the onshore sediment fluxes on Santa Rosa Island. Determining overwash volumes at CL was part of the independent DCERP project (Foxgrover, 2009).

LIght Detection And Ranging (LIDAR) data collected before and after hurricane events can be differenced and used to assess changes in morphology of the beach related to storm erosion and sediment transport. The changes in morphology can be compared to flow velocities calculated by high-resolution wave models as part of our modeling exercise.

Aerial photographs were used to identify overwash fans, sediment deposited on the back portion of the barrier beach by identifiable events. In the field, these fans were sampled by push-coring to estimate their thickness. Return intervals of storm surge, estimated from our synthetic storm analysis (sections 4.6-4.9), provide a time frame from which a crude flux estimate can be calculated.

While in the field, it was apparent that potentially significant volumes of the very fine sediment that makes up the Santa Rosa barrier can easily be transported by aeolian processes (wind blown). In an attempt to estimate this flux of sediment, we deployed a series of sediment traps within the military facility on Santa Rosa Island (Fig. 6.). The sediment traps were based on a design used by the DCERP team at CL (Ridge et al., 2011). The traps use pressure sensor data-loggers installed in buried fluid filled tubes, with the increase in pressure as sediment accumulates. Traps were deployed for roughly 1 year and were visited at roughly 4 month intervals. Four transects were set up with groups of traps placed across the barrier. In some cases, traps had filled, in which case the numbers available represent a lower bound on the flux of sediment over that time period. Traps were manufactured through a partnership with Cape Abilities, a local non-profit that finds work for people with disabilities.

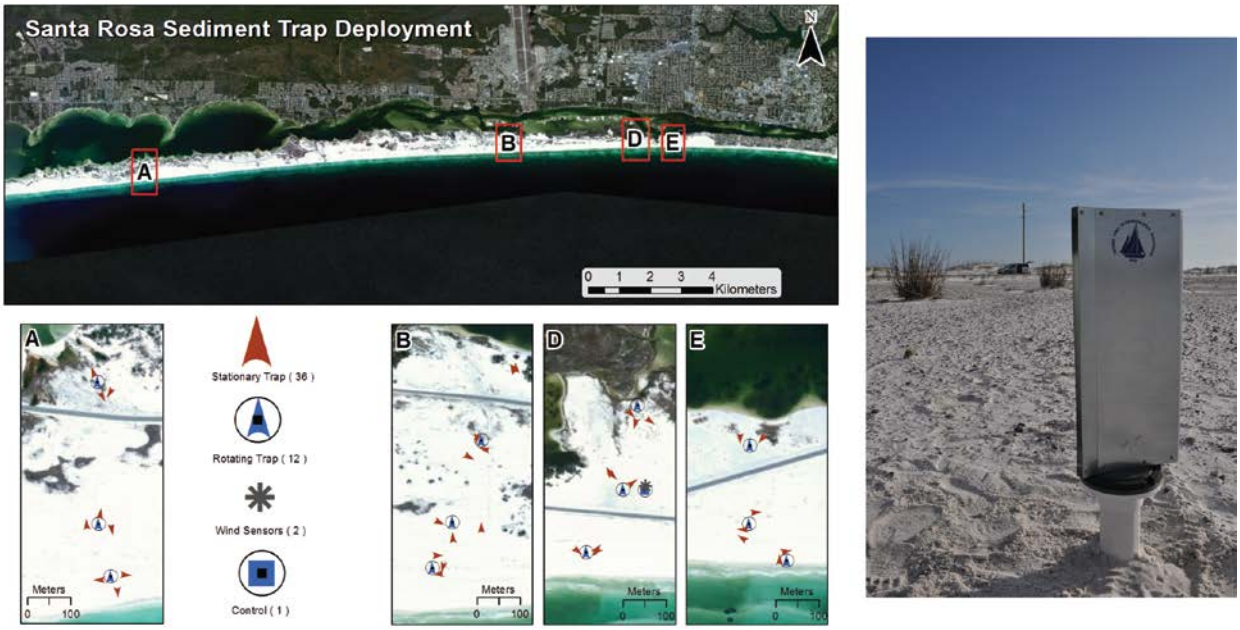

Figure 6. The locations of sediment traps deployed across Santa Rosa Island. An example of one of the traps is shown at right. The rotating traps were experimental and generally ceased to spin due to sand interfering with the rotation mechanism.

4.5 OSL Dating of Dunes

We have used Optically Stimulated Luminescence (OSL) methods to provide age estimates of dunes on Santa Rosa Island. OSL is a technique used to provide an estimate of the time since a sample was exposed to direct sunlight (e.g., Madsen and Murray, 2009). Many crystalline materials are able to store charge for long periods, but direct exposure (or stimulation) from sunlight can release this charge. Once sediments are buried, beyond the reach of sunlight, a charge can accumulate through interaction with cosmic rays and natural radiation. If samples are taken without exposing the sediment to sunlight, then this charge can be released and measured in the laboratory, giving an estimate of the time since burial. OSL is typically able to provide dating for recent burial events (years to several thousand years) and, because the material dated is crystalline, it does not rely on the presence of organic material to provide an age estimate. Dating of the samples was done at the University of Illinois, Chicago, in the Luminescence Dating Research Laboratory.

4.6 Storm Data Generation and Storm Impact Assessment

We have used a synthetic climatology approach to estimating the population of storm surge expected at both EAFB and CL. In this approach, storms are generated in a hurricane model using a random draw of observed genesis locations based on the space-time probability distribution for documented events (Emanuel et al., 2006). These disturbances are then propagated through randomly generated wind fields whose statistics conform to those obtained from atmospheric observations over the last 40 years (i.e. National Center of Environmental Prediction (NCEP) and National Center for Atmospheric Research (NCAR) reanalysis data, Kalnay et al., 1996). The time-varying intensity for each synthetic storm is calculated deterministically based on the monthly means for the thermodynamic state of the ocean and atmosphere, as well as wind shear data obtained from simulated wind field data. Since the size of a storm has a strong effect on the character of storm surge, we randomize the radius of maximum wind by taking a random draw from the climatological distribution of sizes. These steps of initiation, propagation, intensity evolution are repeated many times to produce a large sample (typically 10^5) of synthetic storms throughout the Atlantic Basin. A filter is then applied to select for storms that come within a specified radius of a site of interest. The result is a large (10^4), regional synthetic archive of storms that span the range of modern climatology. A full discussion of the method, including a comparison of the statistics with observed tropical cyclones from 1980 and 2005 (from NOAA Best Track data set; Landsea et al., 2004) is given by Emanuel et al. (2008).

Once a large sample of hurricane scenarios are produced for a given climate scenario, the storm surge generated by each event is simulated using the NOAA SLOSH model (Jelesnianski et al., 1992). The SLOSH model is an operational, numerical model used by the National Hurricane Center to simulate hurricane storm surges in a time-sensitive, forecast capacity.

SLOSH applies internal wind and pressure models to generate the wind and pressure fields to drive the surge simulation (Jelesnianski et al., 1992). Also, it takes the storm pressure deficit, ΔP, as input (in addition to storm position and size information) and uses an empirical relationship to estimate $V_{max,}$ the maximum vortex-relative wind speed (m/s), from the values of ΔP and R_{max}, the radius of maximum wind (RMW). The empirical relationship may not be valid, especially for large storms (Jelesnianski et al., 1992), and the information of V_{max}, even when it is available, is not used.

Although the topography embedded within SLOSH is low resolution, the model runs quickly allowing a large number of storms to be analyzed for surge levels. SLOSH does not compute wave-runup. We have compared estimated surge levels from SLOSH and the University of Hawaii high resolution modeling package for a small set of storms and are comfortable that surge levels from SLOSH are reasonable (see Section 4.12).

Inputs for the SLOSH model are storm position, speed and direction of motion, central pressure, and radius of maximum wind—all outputs from the simulated hurricane climatology model. SLOSH uses a system of polar, hyperbolic, and elliptical grids, called basins. The spacing between the model grid points ranges from 0.5km near the coast to about 7km in the domain farthest away from the shore. SLOSH also includes parameterizations for some sub-grid features, including barriers to flow, breaks in barriers, channel flow, variable friction due to vegetation and one-dimensional flow in rivers. The topographic and bathymetric data used by the model come from the U.S. Geological Survey and NOAA's National Geophysical Data Center. Landscape elevations for each SLOSH grid cell are determined by averaging these higher-resolution geographic data. The model uses storm central surface pressure to generate a parameterized wind field and calculates surface stresses based on storm winds and motion. These stresses are integrated forward in time with the storm track in order to calculate the water levels generated in each grid cell during the event. The result of this approach is an ensemble of storms and surge levels specific to the study site. This ensemble allows us to quantify statistics of surge levels and return intervals of major events.

4.7 Radius of Maximum Wind Model

The RMW critically affects both the magnitude and distribution of surge associated with a storm. This can be the most challenging aspect of forecasting a storm surge as the extent of coastal flooding can be very sensitive to the structure of the wind field, which is difficult to measure and even more difficult to forecast. In lieu of observed RMW values for most events, we modeled the evolution of this variable by assuming partial angular momentum conservation of inflowing air as it travels from a storm's outer radius (R_o) to the RMW. Again, the R_o is defined here as the radius

at which the wind field becomes indistinguishable from the ambient flow. Based on an analysis of North Atlantic storm size statistics (Demuth et al., 2006, Kossin et al., 2007), Dean et al. (2009) found R_o has a mean value of 392km, and this was used as a constant for the historic surge simulations in this paper. The RMW evolution was then modeled according to:

$$(V_{\max} \times R_{\max}) + \frac{f \times R_{\max}}{2} = \frac{\alpha \times f \times R_o^{\,2}}{2},$$

where V_{max} is the maximum vortex-relative wind speed (m/s), R_{max} is the radius of maximum wind(m), f is the latitude-dependent Coriolis parameter (s^{-1}) and α is the dimensionless fraction of angular momentum that is conserved. V_{max} and f are either provided by the statistical-deterministic model or can be determined from its output. The fraction of angular momentum conservation, $\alpha \approx 0.43$, was treated as a constant and estimated empirically by finding the mean value of the solution to the above equation for R_{max} using observations from Dean et al. (2009) and comparing the predicted R_{max} to the observed RMW values. The evolution of RMW for each historic storm was calculated at each time step.

4.8 RMW Model for Synthetic Storms

In the same way that a good estimate of RMW is critically important to forecasting storm surge during a particular event, a realistic distribution of RMW is likewise required when attempting to simulate the full range of events likely to affect a location over a long period of time. Indeed, it may be simpler to model surge distributions, based on reasonable RMW distributions, than it is to model the surge of a particular event where a very good estimate of the RMW is required. Dean et al. (2009) found R_o follows a lognormal distribution around its geometric mean value of 392km. Since R_o is known to vary the least of all hurricane size metrics throughout a storm's lifetime (Frank, 1977), R_o was treated as a random variable with each draw from the lognormal distribution kept as a constant for each storm. As before, partial angular momentum conservation was used to model the RMW evolution for each storm, but in this case RMW is a random draw from the climatological lognormal distribution.

4.9 Synthetic Storm Dataset Generation

A large number of synthetic storms are generated (N = 10,000) having maximum wind speeds of at least 40 knots while within 500km of a desired location. For each storm, a genesis point is randomly selected from a distribution constructed from historical track data going back to 1970 (NOAA 2007). This genesis distribution is a function of location and time of year in the model. Once initiated, 2-hr storm displacements were calculated using the beta and advection model (Marks, 1992) where 850 and 250mb environmental steering flows vary randomly but in accordance with the mean, variance and co-variances of the NCAR/NCEP reanalysis data for the North Atlantic. The steering flows at these pressure levels were also made to have kinetic energies

that obey the ω^{-3} power law of geostrophic turbulence. Vertical wind shear, an important factor in the development and intensification of hurricanes, was calculated directly from the modeled steering flows at the two pressure levels. Thus, the dependence of vertical shear on storm track was incorporated into the model.

The Coupled Hurricane Intensity Prediction System (CHIPS), a deterministic numerical model, was used to simulate the maximum, vortex-relative wind speed of each storm along its simulated track (Emanuel et al., 2004). The model, which assumes axisymmetric storm structure and includes a one-dimensional ocean, employs climatological values of potential intensity and upper ocean thermal structure to model the intensity evolution of each synthetic storm. CHIPS calculates the maximum wind speed using an angular momentum coordinate scheme that maximizes model resolution where it is most crucial – in the storm eyewall. The impact of wind shear on storm intensity is dealt with parametrically in CHIPS.

Storm positions are modeled directly by the statistical-deterministic storm model; however, variables other than latitude and longitude had to be determined through other means. Storm forward speed was found first by using consecutive storm positions to solve the Haversine formula for the distance traveled along a spherical earth. This distance was then divided by the time increment ($\Delta t = 2$ hours) to solve for storm translation speed. The bearing, or compass direction in degrees, of storm motion was similarly calculated from successive latitude and longitude observations.

The entire suite of storm tracks are run through NOAA's SLOSH model giving a low-resolution estimate of storm surge for the region of interest. These results can be analysed statistically to give distributions of storm surge as a function of storm parameters, yielding return intervals for specific surge events for the range of sea-level rise scenarios. This approach was not suitable for modeling nor'easter events at CL. The high resolution modeling package described in the next section was used to estimate the surge generated by a nor'easter (see section 4.10.2 which also outlines some of the technical difficulties intrinsic to this effort).

4.10 High Resolution Surge/Wave Modeling

High resolution modeling of specific storm events was carried out using a nested modeling package, including a wave-modeling tool developed at the University of Hawaii. For a given storm event this allows us not only to estimate storm surge, but also to calculate flow velocities across a small subdomain of the model during the peak of the storm and to relate these velocities to sediment transport.

4.10.1 University of Hawaii Model Package

Cheung et al. (2003; 2008) described the development and implementation of a model package for assessment of coastal flood hazards associated with storm surge and waves. The package utilizes a series of physics-based models to capture both large scale phenomena in the open ocean and small scale processes in coastal areas. The package is referred to below as the UH-ORE model.

The UH-ORE model package (Fig. 7) consists of Parametric Hurricane Model (PHM) (Phadke et al., 2003), Wave Watch 3 (WW3) (Tolman et al., 2002), NEOSURGE (Yamazaki et al., 2009; 2011), Simulating WAves Nearshore (SWAN) (Booij et al., 1999, Ris et al., 1999), and Boussinesq Ocean and Surf Zone Model (BOSZ) (Roeber et al., 2010). PHM calculates surface wind and pressure fields based on a hurricanes track, maximum sustained wind speed, and size. WW3, a third generation spectral wave model, takes as input surface winds and determines how the energy spectrum of waves change throughout the domain over time. NEOSURGE is a long wave model recently developed at the University of Hawaii to describe water levels forced by tides, wave setup (through radiation stress when coupled with SWAN), and wind setup. SWAN is a third generation spectral wave model which takes as input wind, bathymetry, and current to describe wave transformation in coastal areas. Lastly, BOSZ models a time series of individual waves propagating in relatively shallow water and runup onto land. This last model is able to capture the impact of individual waves, not just the average water level expected during a storm surge.

The most significant aspect of the storm surge modeling package is the two-way coupling between SWAN and NEOSURGE and the addition of BOSZ, which can accurately model breaking waves and individual wave propagation onto dry land. LIDAR survey data are used to generate the topographic surface used in the model. This advancement in model integration greatly enhances the accuracy of the computed surge and inundation. The modeling of individual waves throughout the surf zone onto land, which is essential in the impact of the hurricane, has not been considered in most other accepted storm surge models.

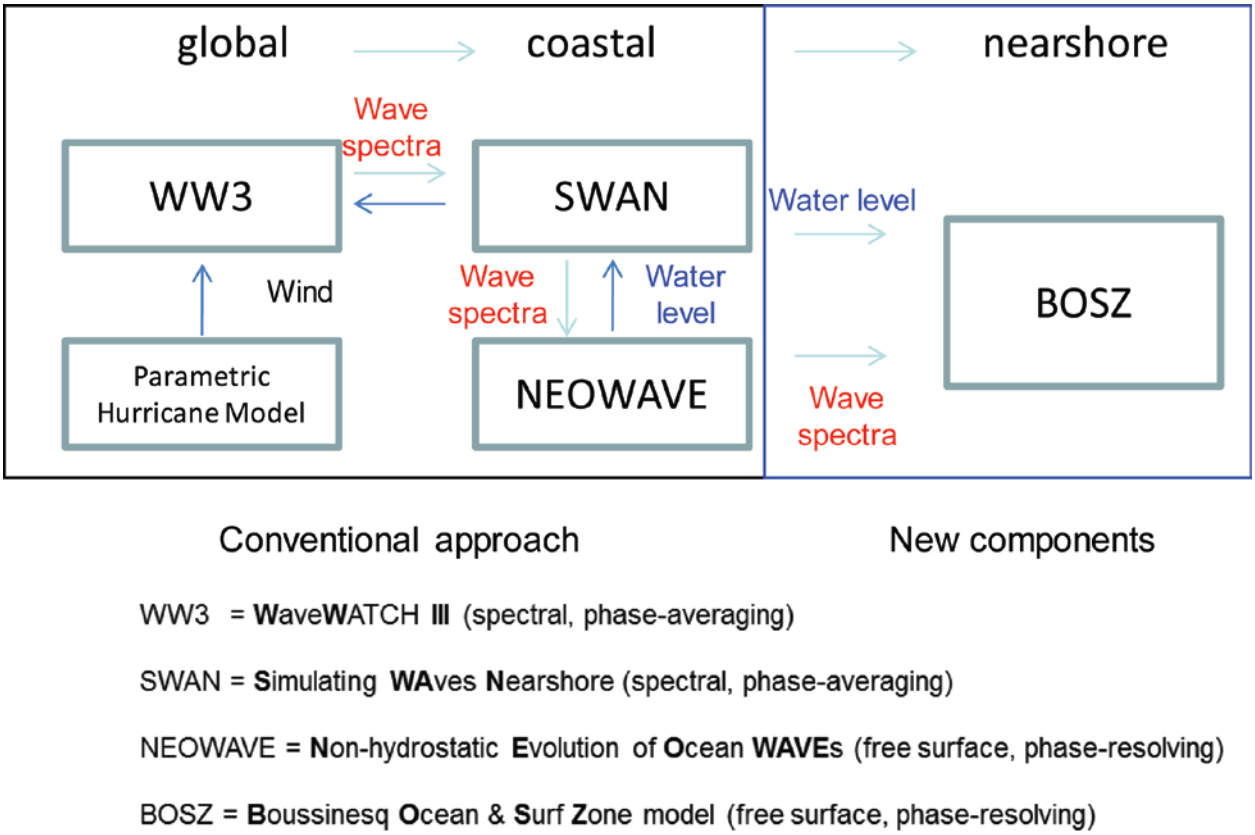

Figure 7. The University of Hawaii Storm Surge Model (UH-ORE) package flow chart.

4.10.2 Modeling Nor'easter Impacts

The UH-ORE model package used for the high resolution inundation modeling of hurricane events had to be slightly modified to account for the extra-tropical storm events near CL. The hurricane events for which the model is typically used are of relatively small scale and can be described by a cascade of model scenarios. Starting from the open ocean, the model package computes the wave and surge energy resulting from wind and barometric pressure forcings as a result of a parametric hurricane model. For extra-tropical storms with a much larger diameter, a parametric hurricane model cannot be used to properly account for the atmospheric conditions. Instead, we used a set of meteorological data from NOAA's Climate Forecast System Reanalysis (CFSR) data (http://cfs.ncep.noaa.gov/cfsr/). This dataset includes global atmospheric data and provides the input conditions for the storm surge model in the form of wind and pressure fields for a large portion of the North Atlantic and around the study site. However, the CFSR dataset provides data only every 6 hours and shorter increments are necessary to ensure a smooth propagation of the low-pressure system.

To overcome this low sampling rate of atmospheric data, we decided to take advantage of the fact that the extra-tropical low-pressure systems cover a much larger area and move more slowly than typical hurricane events. The resultant storm surge is consequently less dynamic. Since we are interested in a maximum inundation and flow velocity scenario, we compute the storm surge from the combined setups of tides, barometric pressure and wind. The wind wave evolution results from a WW3 computation over the entire North Atlantic at 900m grid resolution to provide spectral boundary conditions for the nearshore domain computation. We also tested a finer resolution of 600m grid spacing to see whether the wave spectra change significantly around the outer banks but found that 900m resolution is sufficient to capture the open ocean processes.

The final inundation and flow velocities result from the Boussinesq-type nearshore wave model BOSZ with input of the WW3 wave spectrum at the offshore boundary 7km from the shoreline at around 20m water depth. The previously computed storm surge envelope serves as an initial condition on top of which the individual swell waves propagate towards shore. The grid resolution is 6m in the cross-shore and 8m in the longshore direction. The grid has about 3 million cells covering an approximately 7km by 18km domain.

4.11 Barrier Beach Evolution

Understanding the potential future evolution of Santa Rosa Island and the barrier system fronting CL required the development of a numerical model of geologic and geomorphic barrier evolution in response to SLR. The model addresses long-term evolution of barrier profiles by focusing on mass balances and sediment fluxes driven by barrier overwash coupled by the marine response of the shoreface. This simplified model approach helps define the necessary conditions for a barrier to survive sea-level rise based upon local variables, and also examines the sensitivity of the evolution of a barrier such as Santa Rosa Island to different overwash rates. Exploring a wide range of overwash flux rates is important as these quantities are difficult to constrain, particularly as projected and project-defined SLR rates significantly exceed current, historical, and recent geologic rates.

4.11.1 Morphodynamic Model Approach

The model approach (Lorenzo-Trueba & Ashton, 2014) focuses on two primary barrier components, or behavioral elements: the marine domain, represented by the active shoreface, and the terrestrial system, where the infrequent process of overwash controls landward mass fluxes (Fig. 8). The movement of these locations is controlled by the fluxes between them, the shoreface flux, Q_{SF}, which could be directed either offshore or onshore, and the overwash flux, Q_{OW}, representing the landward sediment transport during extreme events (or aeolian processes), is directed landwards.

Similar to previous models for sedimentary basin evolution (Lorenzo-Trueba et al., 2009; 2012; 2013; Lorenzo-Trueba and Voller, 2010), a key feature of this model is that it considers a cross section through a simple idealized geometric configuration (Fig. 9). The model represents a significant simplification as it only involves a coupled system of four ordinary differential equations. This simplicity allows the model response to be explored for a wide range of parameter values. Moreover, the model demonstrates that internal barrier-system dynamics can lead to more complex behaviors than suggested by existing morphodynamic models. The model utilizes a time-integrated approach, averaging over short-term events to focus on the long-term interactions between sediment fluxes and the preexisting geometric template. The model is fully morphodynamic, in that it accounts for out-of-equilibrium behaviors and resolves morphology due to gradients in sediment fluxes, rather than geometric models such as those by Cowell et al. (1995) and Stolper et al. (2005).

4.11.2 Morphodynamic Model Description

The model is comprised of a linear shoreface profile with slope α(t) able to account for out-of-equilibrium behaviors, a subaerial portion of the barrier characterized solely by its width W and the elevation above mean sea-level (MSL), H, and a linear backbarrier lagoon with slope β (Fig. 9). The shoreface extends from the shoreline to an offshore depth D_T beyond which waves have a negligible effect and sediment transport becomes exceedingly low (Cowell et al., 1999). In this way, provided an initial geometric configuration and the required input parameters (Table 1), the evolution of the system can be fully determined with the rates of change of the shoreface toe dx_T/dt, shoreline dx_S/dt, backbarrier dx_B/dt, and height dH/dt. These rates can be expressed in terms of the SLR-rate ξ, the shoreface sediment flux Q_{SF}, and overwash flux Q_{OW} (these last two components are discussed below).

4.11.3 Overwash Fluxes

In order for the barrier system to persist and migrate landward during a period of significant SLR, the process of overwash must remove sediment from the seaward portion of the barrier and deposit it landward (Donnelly et al., 2006). Thinning of barriers below a threshold width tends to drive this overwash (Leatherman, 1979; 1983). In general, although SLR is considered to "drown" barriers, more horizontal accommodation volume than vertical accommodation volume is created by SLR due to the low slopes of the shoreface and continental slope (Fig. 9; note that figures 8-10 have substantial vertical exaggeration).

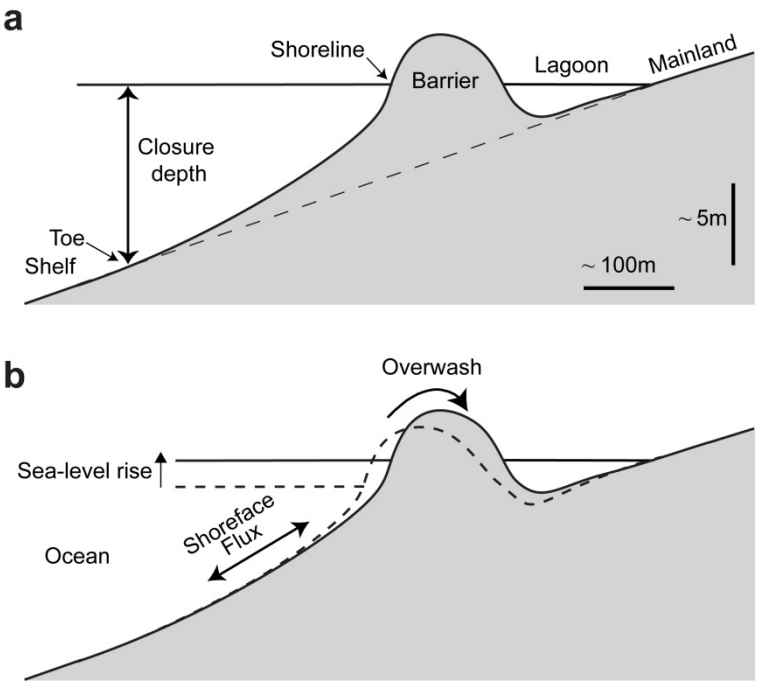

Figure 8. Schematic of a barrier profile showing the important geometrical interfaces, representing an overwashing barrier (with overwash flux Q_{ow}) coupled with a shoreface with fluxes that could be directed either onshore or offshore (Q_{sf}).

As an extension of the general concept of a critical, or 'equilibrium' barrier width (Leatherman, 1979; 1983) (w_e, m) and commensurate equilibrium barrier height (h_e, m), we define a 'barrier deficit volume' (V_d, m^3/m), which represents the difference, from a given shoreline location, between a current barrier configuration and one that is both high and wide enough such that overwash is presumed not to occur. This volume, akin to an 'accommodation space', can have both vertical and horizontal components (Fig. 10). The vertical component ($V_{d,v}$) grows with the passive drowning of the barrier itself, whereas the horizontal component ($V_{d,h}$) arises from the reduction in barrier width, and is dynamically affected by changes in the shoreline location itself. The growth of the horizontal deficit volume is also directly affected by the backbarrier geometry.

Overwash is handled simply— if the barrier width is below a threshold value, W_e, overwash onto the backbarrier occurs at a rate propotional to the width deficit ($W_e - W$). This description is expanded to incorporate the influence of barrier height on the overwash process as well; we define a critical height H_e beyond which overwash onto the top of the barrier occurs at a rate propotional to the heigth deficit ($H_e - H$). Additionally, we assume that there exists a maximum rate of potential barrier overwash $Q_{OW,max}$. Although this formulation vastly oversimplifies the complex process of barrier overwash (Donnelly et al., 2006; Roelvink, 2006; Roelvink et al., 2009; McCall et al., 2010), it bears resemblance to approaches used in other models (Jiménez & Sánchez-Arcilla 2004; Masetti et al., 2008; McNamara and Werner, 2008). Moreover, it encapsulates a general concept widely observed in natural systems: thinner and lower barriers overwash more frequently.

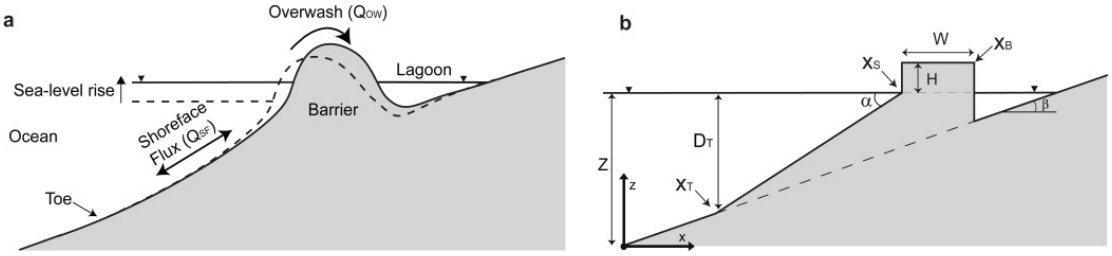

Figure 9. Cross-shore barrier model set-up and components.

The concept of a critical barrier width suggests that this deficit drives rollover barrier behavior. For long-term barrier stability, however, overwash must occur, but the rate of growth of this barrier deficit must eventually go to zero for a barrier to survive SLR. While this concept is obviously a simplification, it encapsulates the concept that low and thin barriers are more prone to overwash, and allows a focus on the primary flux balances. The deficit volume approach encapsulates two general concepts: 1) smaller barriers should overwash more frequently and 2) there exists a maximum rate of barrier overwash. This second assumption is reasonable insofar as there must exist some limit on overwash fluxes, We explore this second concept in the modeling simulations by varying the maximum flux in different model experiments.

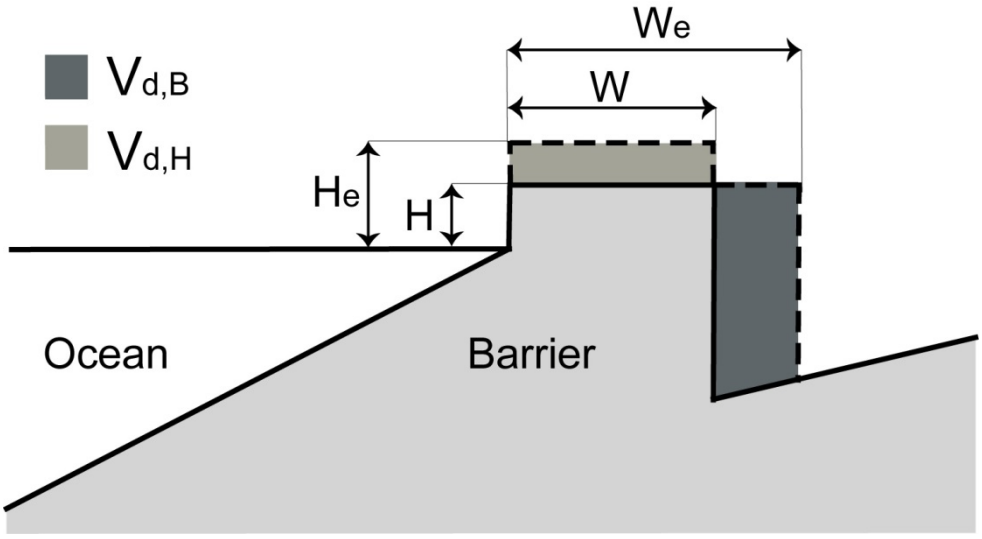

Figure 10. Schematic of the critical barrier island width concept and the top-barrier $V_{d,H}$, and back-barrier $V_{d,B}$ deficit volumes.

4.11.4 Shoreface Sediment Transport

We have found it necessary to revisit relationships for cross shore sediment transport on the shoreface using both shallow water and linear theory assumptions (Ortiz and Ashton, in prep).

Using energetics-based formulations for wave-driven sediment transport, we have developed a robust methodology for estimating the morphodynamic evolution of a cross-shore beach profile. The derived cross-shore sediment flux formula enables the calculation of a steady state (or dynamic equilibrium) profile based on three components of wave influence on sediment transport: two onshore-directed terms (wave asymmetry and wave drift) and an offshore-directed slope term.

Derived from Bagnold's energetics model (1963), Bowen (1980) presents a theoretical model for wave-driven cross-shore sediment transport. This approach, also adopted by Stive and de Vriend (1995) and similar to that of Bailard (1981), balances onshore-directed sediment transport by wave asymmetry and drift with offshore-directed slope terms. Although previous approaches have used shallow-water wave assumptions (Stive and de Vriend, 1995), as we are interested in transport on the lower shoreface where waves are typically not fully shoaled, we use linear Airy wave theory. For linear wave theory, we derive the following equation for cross-shore wave-driven sediment transport, or time-averaged suspended sediment transport flux, q_{sx}, (m^2/s):

$$q_{sx} = -K\frac{\pi^3 H^3}{T^3 w_s \sinh^3(kz)}\left[\frac{15\pi^2 H^2}{4TL\sinh^2(kz)} + \frac{9\pi^2 H^2}{4TL\sinh^4(kz)} + \frac{\pi^2 H^2 \beta}{w_s T^2 \sinh^2(kz)}\right]$$

where K, with units of s^2/m, is a coefficient based on sediment and fluid density, a friction factor, and suspended sediment transport efficiency factor. H, T, L, and k are wave characteristics: wave height (m), wave period (s), wave length (m), and wave number (m^{-1}). The water depth is defined by z (m) and the slope of the shoreface is β (m/m). For a long-term zero-flux condition, it is possible to solve for an equilibrium slope and equilibrium profile. This formulation yields an equilibrium profile with no dependence on wave height; instead, profile shape depends only on wavelength, wave period, and sediment fall velocity.

A shoreface bed evolution formulation can then be derived by combing the cross-shore sediment flux (q_{sx}) equation with the conservation of sediment mass. Similar to Swenson et al. (2005), we apply the Exner equation to find the change in depth over time by relating the negative divergence of sediment flux simplifying to an advection-diffusion equation, describing the bed evolution over time. Adapting approaches defining morphodynamic Péclet numbers from terrestrial geomorphology (Pelletier and Perron, 2012; Perron et al., 2009; Pritchard et al., 2009), from this advection diffusion equation, we calculate a morphodynamic, depth-dependent Péclet number for an equilibrium shoreface and find that diffusive terms are dominant throughout the shoreface.

From this formulation for shoreface bed evolution, we calculate a depth-dependent characteristic diffusional timescale of shoreface evolution (T_{diff}):

$$T_{diff} = \frac{x_{eq}^2 w_s^2 T^5 \sinh^5(kz)}{K\pi^5 H^5}$$

where w_s is the settling velocity of the sediment (m/s) and x_{eq} is the equilibrium cross-shore distance (m) calculated from an equilibrium shoreface geometry. The shoreface diffusivity is used to describe a depth-dependent characteristic response time. For typical values of deep-water wave height and wave period, shoreface response timescales get significantly large (over a 1,000 years) at depths between 10 and 30 meters, suggesting a type of morphodynamic "depth of closure." In other words, profile evolution and, in particular, sediment transport may continue beyond this depth but evolution of the shoreface shape becomes geologically slow and response to environmental changes driven by coastline change is virtually non-existent. On the other hand, using shallow-water wave assumptions instead of linear theory predicts greater sediment transport at depth and therefore a much deeper morphodynamic closure.

Following the concept of the dynamic equilibrium shoreface, within the numerical model, we simplify the shoreface slope into a linear average and calculate the shoreface sediment flux Q_{SF} based upon deviations from deviations from an equilibrium shoreface angle, α_e. The sediment flux can be directed either offshore or onshore, and aims to restore the shoreface equilibrium configuration α_e with a characteristic response rate K. Estimates for α_e and K can be calculated analytically in terms of the wave period T, the deep-water wave height during fair weather $H_{w,0}$, and the settling velocity w_s (Lorenzo-Trueba & Ashton, 2014).

Table 1: Parameters used in the morphodynamic model.

Symbol	Units (L: length; T: time)	Meaning	Proposed Methods (details given in Sect. 3.4)
$\dot{z}$	L/T	SLR rate	Literature review & radiocarbon / OSL dating to improve / extend SLR curves
β	-	backbarrier lagoon slope	Sediment core transects to determine antecedent topography (Pleistocene surface)
W_e	L	critical barrier width	Modern observation / stratigraphic models
H_e	L	critical barrier height	Modern observation / stratigraphic models
$Q_{OW,\max}$	L^3/L/T	maximum overwash sediment flux	Modern observation / stratigraphic data (after Carruthers *et al.* 2013)
$H_{w,0}$	L	deep-water wave height during fair weather	Hindcast wave-data analysis
T	T	wave period	
D_T	L	depth of the shoreface toe	
w_s	L/T	settling velocity	Grain-size analysis

4.12 Modeling Comparisons and Comments on Inundation Modeling

This section presents some benchmark comparisons between the SLOSH model and two other packages we have used: the UH-ORE model and ADCIRC, another commonly used inundation tool. We also share some thoughts and concerns on inundation modeling and discuss some of the pitfalls and approaches that should be best practice.

Storm surge and wave modeling involves many assumptions and approximations. Generally, a person working with numerical models might look at model results with more critical eyes than a person who is mostly working with lab and field data. From our experience, when we show results to planners, emergency managers, or politicians, the work is believed to be of good quality as long as it is somehow conclusive and good looking. For example, the designers of commercial model packages often put a lot of effort into the plotting style and visual appearance of the numerical model output, and less effort into the critical steps of model validation for each specific region modeled. If we cannot reproduce a known event, how can we have confidence in the results of an unseen event? That is why model validation is important. This process takes time, especially if the modeling work involves several models, as is the case for the UH-ORE model suite. We have validated our models extensively with a variety of laboratory and field data. For EAFB, we have used Hurricane Ivan as a benchmark, making sure that our results match, to within error, observed tide gauge data. An example of what is acceptable is shown in Figure 45, which shows the modeled and observed tides during the Nor'Ida nor'easter event at CL. The model does an excellent job reproducing the observations at the start of the event, but even here there is a ~0.5m systematic difference towards the end of the storm that is hard to explain. One possibility is that the local wind field has not been adequately captured in the data set used to parameterize the storm.

For the large suite of synthetic storms we have used NOAA's SLOSH model to calculate inundation levels. SLOSH does not incorporate high resolution digital elevation models, so that resolution of the inundation over a specific region is somewhat coarse, suggesting that estimates of inundation levels might be inaccurate. SLOSH adopts a highly parametric approach with the result that although SLOSH, ADCIRC, UH-ORE compare well offshore, they can often show differences nearshore where nonlinear processes are important that can only be accounted for by solving a set of nonlinear equations. The advantage of SLOSH is that it runs relatively quickly on a modest workstation, allowing all 10,000 storm tracks to be treated. We have carried out comparisons of inundation levels between SLOSH and the UH-ORE package for 4 specific storm tracks (Table 2). We have also compared SLOSH with ADCIRC for a larger number of storms impacting the eastern Gulf of Mexico (Figure 11).

When comparing SLOSH to the UH-ORE models we have used two domain sizes in SLOSH. The first of these, EGLL, is a larger domain with 8.7km resolution. The four corners of the domain are at (28.9N 97.6W), (30.5N 82.9W), (23.4N 98.7W), (25.1N 80.4W). The second domain, PN3 is

smaller but with a higher 0.68km resolution and is centered around Pensacola. The four corners of the PN3 domain are at (30.43N 87.22W), (30.27N 84.83W), (29.93N 87.87W), (28.56N 85.03W).

Track	EGLL	PN3	UH-ORE	R_o(km)
1	2.04	3.51	2.83	383
2	1.98	1.83	0.76	505
3	3.35	4.02	3.46	551
4	2.85	2.74	2.72	514

Table 2. Results of surge levels in m calculated for two domains in SLOSH (PN3, EGLL) and the UH-ORE model. The tracks are shown in Fig. 36. The last column shows the outer radius of each storm considered.

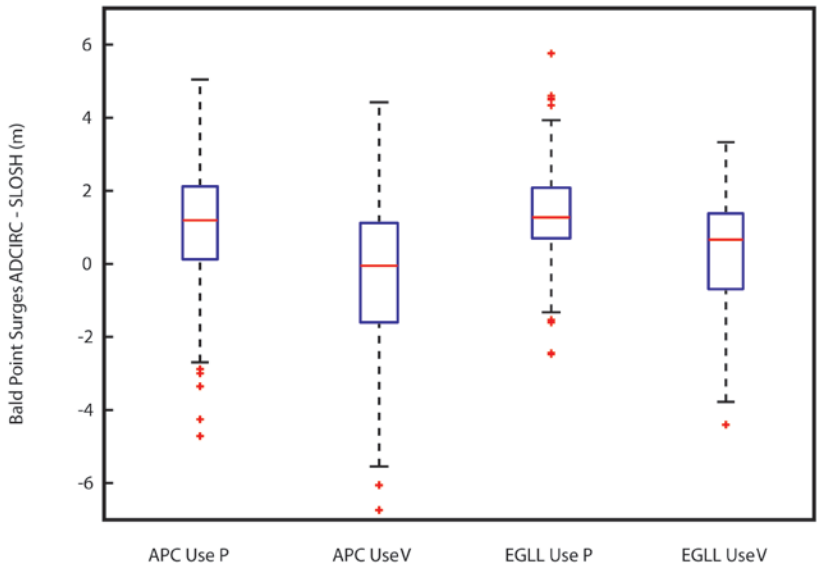

Figure 11. A comparison of surge values (shown as a differential) calculated by ADCIRC and SLOSH for a subset of 491 synthetic storms. Two modeling domains are considered: APC is a domain for the northeastern Gulf of Mexico and EGLL is a Gulf wide domain used for our analyses. Two cases are considered in each case, one using the pressure conditions of the storm and the other the storm velocity.

We have also run comparisons between SLOSH and ADCIRC (Fig. 11). To fully select the extreme events from historical tracks and from our large synthetic database, we applied two techniques: one is to use the (observed or simulated) ΔP as the input (denoted as useP) and the other is to use a calculated ΔP (denoted as useV) from the inverse of the SLOSH empirical relationship and the (observed or simulated) values of V_{max} and R_{max}, so that the intensity characteristic actually used is V_{max} (rather than ΔP). For this test, we have used two SLOSH simulation domains: the Apalachicola (APC) basin and the same EGLL basin as discussed above. The APC basin has relatively high resolution (~2 km around Apalachee Bay, Fl, to the east of EAFB), but it is small and neglects the effects of remotely-produced, coastally-trapped Kelvin waves, which are sometimes generated beyond the model domain and can travel into the area of interest. Using these two very different numerical grids further ensures the selection of all extreme events. Thus, we apply the SLOSH simulation to each of the 297 historical and 10,000 synthetic Apalachee Bay storms four times: using both basins each with useP or useV techniques. We select all storms that generate surges greater than 1.5 m near Bald Point, FL, in any of the four cases, resulting in a set of 40 historical and 451 synthetic extreme storm events. The selected synthetic set encompasses events with return periods of about 11 years and longer (in terms of the surge potential at Bald Point), based on the estimated storm frequency. All these selected extreme events are further analyzed with the ADICRC model. In most cases, a useP (useV) SLOSH-simulated surge is lower (higher) than the ADCIRC estimation, as the SLOSH empirical relationship between the maximum wind and pressure deficit underestimates the maximum wind when pressure data are used and overestimates the pressure deficit when the maximum wind data are used (compared to the estimations by the deterministic hurricane model). This bias becomes larger as the storm size increases. Therefore, the SLOSH wind-pressure relationship may fail to generate a realistic wind field, especially for large storms (Jelesnianski et al., 1992).

As is clear from Figure 11 there is considerable scatter for the surge estimates between storms of a given size (radius). This scatter represents the combined effects of many subtle and non-linear behaviors, most likely resulting from the limitations of the SLOSH model, but also related to how ADCIRC (which uses SWAN as a wave model) may not capture wave effects. For example, there is a clear difference in behavior between the SLOSH runs using velocity (useV) and pressure (useP). There are also differences between the two model domains, as discussed in the text. Thus, the discrepancies are not simply ascribable to systematic errors in SLOSH or to ADCIRC, but depend on the parameterisations of each model as well as whether the models are capturing specific basin wide phenomena as discussed above. To a large extent, the message of this section is do not simply run one model and take the results at face value, but understand the underlying physics contained in each model being used and know that it is adequate for the purpose. ADCIRC is certainly an appropriate model choice because the latest version includes a

spectral wave model to account for phase-averaged effects of storm waves (coupled with SWAN). This is commonly known as wave setup, which can increase the surge by up to 1 m. ADCIRC, however, is not as stable as the other models. We have worked with the developers of ADCIRC to model storm surges in Hawaii. It seemed that ADCIRC required excessive smoothing of the nearshore bathymetry (basically getting rid of the fringing reefs) and uses an unreasonably large friction coefficient near the coast - possibly to ensure stability of the model.

Somewhat counter-intuitively, the larger, coarser grid in SLOSH produces results that are more in agreement with both the UH-ORE and ADCIRC results. The primary reason for this is that there are specific surge behaviors in the eastern Gulf of Mexico, particularly relating to trapped Kelvin wave phenomena propagating northwestwards along the Florida coast, that are not captured by the smaller domain. This speaks to the need for a nested approach to modeling, similar to that included in the UH-ORE model, to capture the range of behaviors expected in a given region.

Our main criticism of the storm surge modeling community is that they typically don't consider inundation and impact of individual waves. The storm surge is mainly calculated from integrated phase-averaged quantities of the storm waves. Properly accounting for these individual storm waves has been an important part of the UH-ORE model development. As we discuss later, the individual waves are the primary driving force in sediment transport on the barrier island. Around smaller islands with steep bathymetry around, storm surge accounts for a small portion of the storm water level because of the steep slope. We often use Hurricane Iniki (1992) as an example. The tide gauge recorded a water level of around 1.5 m at the eye of Hurricane Iniki, but the debris line in the area reached the 9 m elevation contour. Observations of the damage and debris suggest high-energy storm waves propagate on an elevated water surface due to the storm surge, overtop the coastal dune system, and inundate large swaths of low-lying coastal land.

Another concern with the commonly used storm surge models such as ADCIRC, ECOM, FVCOM, and SLOSH is that they cannot describe supercritical or discontinuous flows. This is usually not a problem with inundation modeling as floodwater slows down on an upward slope. It becomes an issue when barrier or levee overtopping is involved. The water rushing down the back slope can transition into a supercritical flow and generate a hydraulic jump in the water behind the barrier. Existing models cannot describe these physical processes. The capabilities to calculate supercritical flow might receive more attention in the near future as researchers will try to understand the flow conditions that occurred during Typhoon Haiyan (2013). It seems that the storm surge travelled quickly, which would highlight the necessity of using advanced models, which can capture supercritical flow.

5. Results and Discussion

5.1 Generalized Barrier Beach Behavior Under Conditions of Accelerated Sea-Level Rise.

In general, the barrier model results demonstrate the importance of overwash in determining the morphodynamic behavior of a barrier system. Without overwash, SLR steepens the shoreface, sending sediment offshore as generally described by the Bruun rule (1962). For a barrier to maintain its shape as sea level rises, overwash must send sediment landwards. As a response, the shoreface is flattened, and sediment is sent onshore. This results in a different direction of shoreface flux if overwash is occurring than if there is no overwash. Although overwash drives considerable shoreline retreat, it also allows barriers to build additional subaerial land to compensate for SLR (Ashton and Ortiz, 2011).

When applied over centennial timescales, our model also demonstrates that the coupling of overwash with shoreface processes can lead to complex responses even with simple forcing conditions, including barrier drowning and discontinuous retreat. These are described below:

***Dynamic Equilibrium*:** At dynamic equilibrium, overwash and shoreface fluxes are sufficiently high and equivalent to maintain the geometric configuration of the barrier during landward migration. In this case, there is sufficient overwash to compensate for SLR, and the shoreface is capable of sending sediment onshore at a sufficient rate.

***Barrier drowning*:** When overwash fluxes are insufficient to maintain the landward migration rate required to keep pace with SLR, the barrier undergoes 'height drowning' (i.e., $H < 0$) (Fig. 12a). In this case the barrier fails even though it has maintained a sufficient width. Low overwash causes barrier height to undergo a continuous decay, with the barrier eventually drowning. Alternatively, large overwash fluxes can result in a different mode of barrier collapse. In 'width drowning', low onshore sediment transport from the shoreface is insufficient to maintain the barrier geometry during landward migration (i.e., $W < 0$) (Fig. 12b). In this case, the rate of shoreline migration significantly exceeds that of dynamic equilibrium, and consequently the width undergoes a rapid decay and eventually disintegrates.

***Discontinuous retreat*:** when the barrier system does not drown, it does not necessarily attain a constant landward migration rate. Model results (Fig. 13) demonstrate that, even with constant forcing (i.e., constant SLR rate and a linear backbarrier lagoon slope), the coupled overwash-shoreface system can undergo discontinuous retreat due to time lags in the shoreface response. These punctuated episodes of shoreline retreat are typically associated with sudden changes in

forcing conditions or complex geometries (Rodríguez et al., 2004; 2005; 2010; Storms & Hampson 2005; Masetti et al., 2008). However, these model results show that this complex behavior can also be caused by the intrinsic complexity of the system.

The simplicity of the model allows us to explore potential barrier behavior across a wide range of parameter values. In particular, barrier evolution can be very sensitive to changes in the backbarrier lagoon slope (Fig. 14). Barrier drowning is more likely to occur with flatter backbarrier slopes (small β) as the barrier must migrate landward faster to keep pace with SLR. Intuitively, faster rates of overwash should facilitate such rapid migration. However, this rapid overwash can outstrip the onshore flux from the shoreface, eventually leading to width drowning. As a result, as β decreases, the width-drowning region expands rapidly to take over most of the parameter space (Fig. 14). These results highlight the importance of the backbarrier environment on the barrier response to SLR. When the barrier system does not drown, it does not necessarily attain a constant landward migration rate. Note again that these behaviors tend to arise on centennial and longer scales when sea level rises to a greater height than the barrier itself. These results help guide an understanding of basic barrier evolution. Below, we present further model results applicable to the project-defined scenarios at the two project locations.

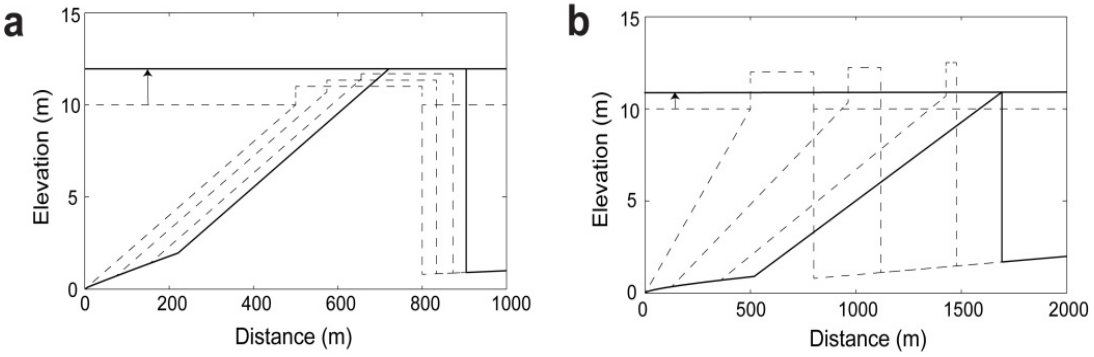

Figure 12. Profile evolution of modeled barrier-system response demonstrating (a) height and (b) width drowning.

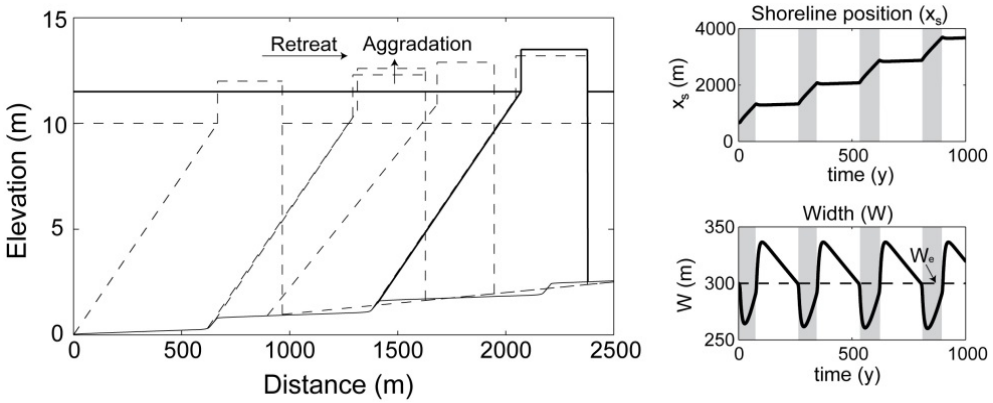

Figure 13. Profile evolution of modeled barrier systems response demonstrating discontinuous retreat. Figures on the right show the shoreline position and the barrier width over time. Note the alternation of rapid barrier migration, when the barrier width is below its critical value (i.e., $W<W_e$), and barrier aggradation, when the barrier is above its critical value (i.e., $W>W_e$).

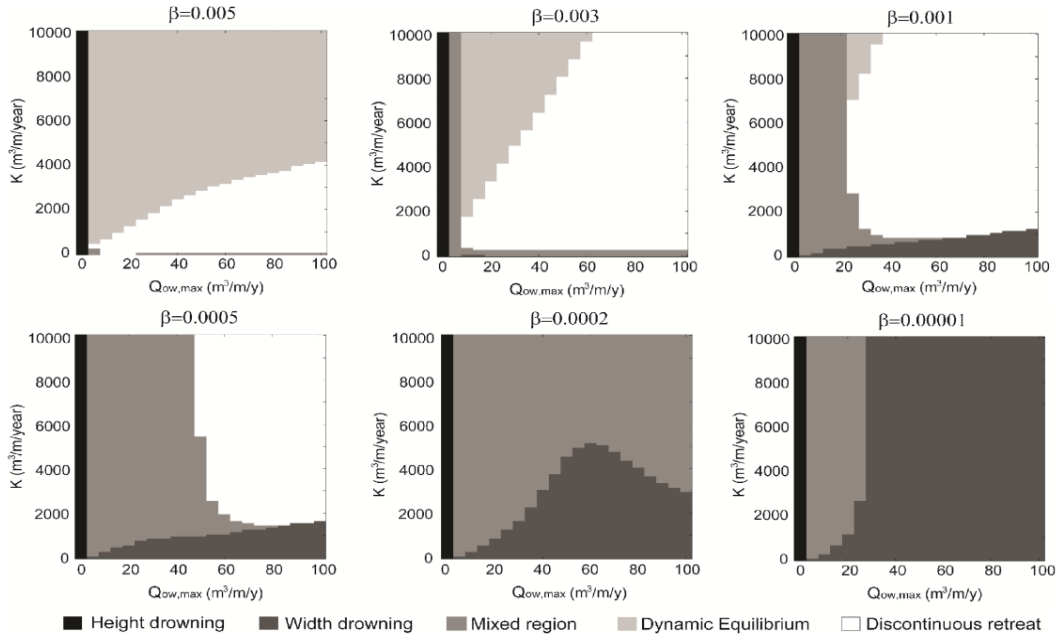

Figure 14. Regime diagrams as a function of the maximum overwash flux $Q_{OW,max}$ and the shoreface flux constant K for different values of the backbarrier lagoon slope β. SLR is a constant 2mm/yr in this simulation.

5.2 Eglin Air Force Base

5.2.1 Holocene History of Santa-Rosa Island

We have completed geological sampling and geophysical imaging at EAFB to determine a late Holocene Sea-level history for the region, to understand the structure and history of Santa Rosa Island, to establish a storm history for the region through the late Holocene, and to estimate volumes of overwash flux and aeolian sediment transport that feed into the barrier evolution model.

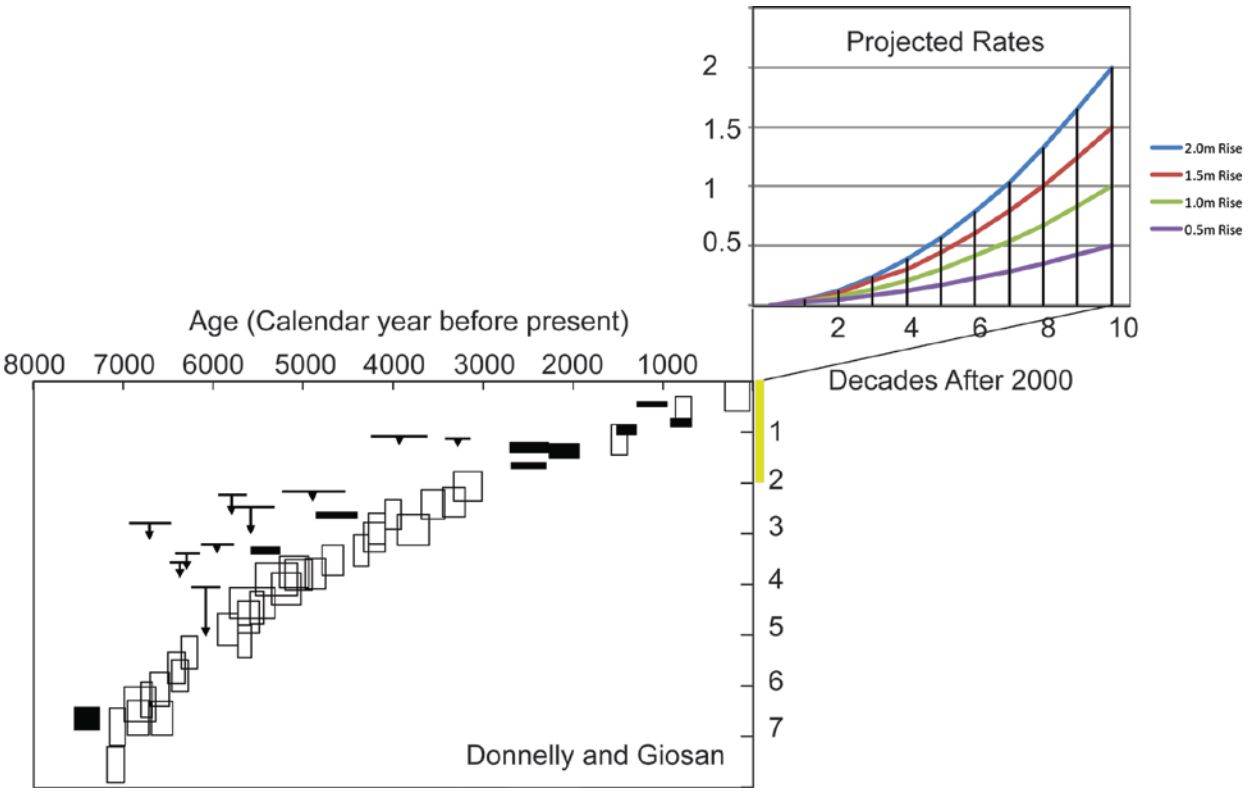

Figure 15. Regional sea-level in the southeastern US through the Holocene (Donnelly and Giosan, 2008) compared to those proscribed for this project. The proscribed rates encompass the range predicted for the coming century and represent a significant increase in the rate of SLR compared to the last few thousand years during which the Santa Rosa barrier has formed.

5.2.2 Sea Level History

A key part of understanding the late Holocene history of the region, particularly Santa Rosa Island, is to have good knowledge of the recent sea-level history. The sea level curves considered for this project represent a significant acceleration in rise rates over the coming century compared to the last few thousand years, although data over this period are patchy (Fig. 15). In particular, this region suffers from a paucity of valid sea-level index points, discrepancies between existing sea-level records, and temporal and spatial gaps in the existing records. Mid to late Holocene rates of relative SLR of 0.6 mm/yr accelerate in the later Holocene to over 2mm/yr. If we are to use our geomorphic data to understand recent barrier behaviors, then it should be done so with an understanding of the sea-level framework within which those changes occurred.

Recently, investigators have begun to extract high-resolution (cm- to m-scale vertical resolution and annual- to centennial-scale temporal resolution) records of relative sea-level changes from foraminifera and diatoms preserved in salt-marsh sediments using quantitative paleo-environmental reconstruction techniques (e.g., Kemp et al., 2009). Salt marsh sediments and, moreover, the foraminiferal assemblages therein are ideal for reconstructing past sea-level changes as they are intrinsically linked to the magnitude, frequency, and duration of tidal inundation (elevation) and can keep pace with moderate rates of SLR. The relationship between modern foraminifera and elevation is used to estimate past sea level from fossil foraminiferal assemblages in salt marsh sediment sequences dating back thousands of years. This, coupled with detailed composite chronologies of salt marsh sediments, can be developed using radiometric isotopes and independent stratigraphic age markers (e.g., Gehrels et al., 2008). Together, these techniques allow for the development of high precision estimates of former sea levels.

We have collected samples from marshes in the Eglin region which provide records of relative sea-level change from around ~5000 yrs before present. A sequence of cores was taken from a salt marsh in LaGrange Bayou off Choctawhatchee Bay, to identify the timing and magnitude of changes in the rates of relative SLR. We reconstruct past sea-level changes using 25-30 basal stratigraphic sections of peat cored (using a compaction-free Russian coring device) from marsh sediments overlying a gently-sloping basal sand deposit. Peat retrieved from such a basal contact is unlikely to have been significantly vertically displaced by auto-compaction (e.g., Bloom, 1964; Gehrels, 1999). Two modern transects were sampled from the upland to intertidal zone to determine the distribution of modern foraminifera relative to the duration and frequency of tidal exposure.

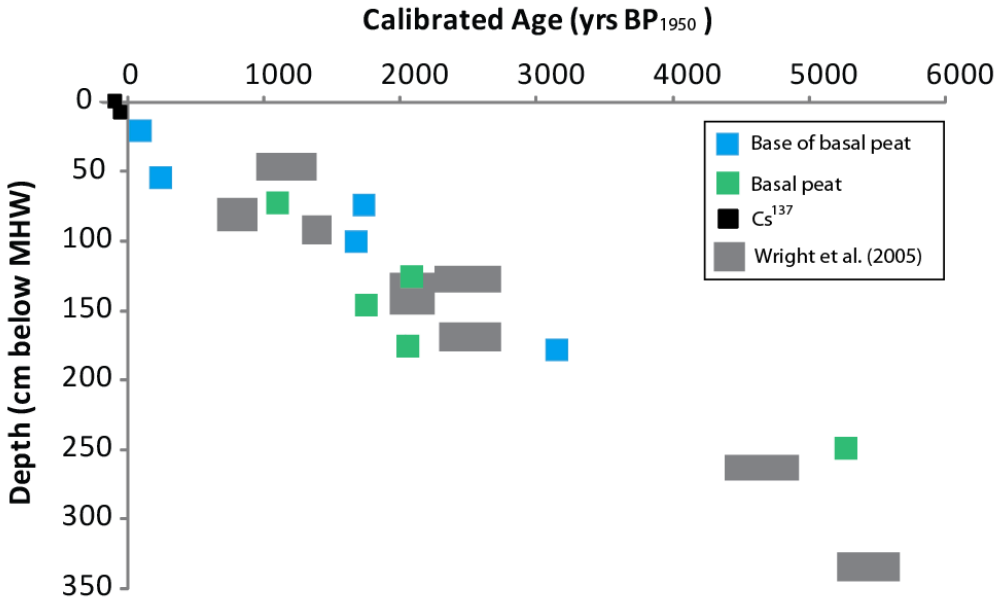

Figure 16. A sea level curve for the Eglin region based on our peat samples and other data as cited.

Modern transects spanning from the upland to the intertidal zone are used to determine the distribution of modern foraminifera relative to the duration and frequency of tidal inundation (elevation). The modern dataset is used to quantitatively estimate former elevations of fossil foraminiferal assemblages found in the long peat core and basal peats sections to reconstruct past relative sea level. Foraminiferal assemblages and radiocarbon dated in situ plant macrofossils within the salt marsh peats identify the timing and magnitude of changes in the rates of relative sea level over the past 5000 years. Geochemical data (Carbon and Nitrogen) corroborate the paleo-environment over the same time span of the relative sea-level record.

The results indicate an average rate of SLR of approximately 0.6 mm/year over the last five millennia (Fig. 16), consistent with other reconstructions from the region based on radiocarbon dated salt marsh samples (e.g., Donnelly and Giosan, 2008, Milliken et al., 2008). While the scatter in the data may in part represent small scale (decimeter scale) oscillations in sea level over the last several thousand years superimposed on this long term trend, the scatter could also indicate that uncertainties in age and vertical position of recovered samples is larger than we report here. For example, if the sample data is reworked material from an older stratigraphic interval. The new sea level data from Choctawhatchee Bay and other available data does rule out more complex sea level behavior over the last several millennia such as the proposed sea-level high stands inferred from the age and position of relict beach ridge plains (Blum et al., 2003;

Morton et al., 2000). Except during event scale (e.g., tropical cyclones) inundation, MSL has never been above modern levels over the past several thousand years (see discussion in Donnelly and Giosan, 2008).

5.2.3 Northern Gulf of Mexico Tropical Cyclone Activity Over the Past 4500 Years From Sediment Archives

The most striking feature of the seismic data collected in Choctawhatchee Bay is a significant erosional unconformity (a buried erosional surface) within the sediments (Figs. 17, 18). This erosional feature, located just north of the modern flood tidal delta associated with East Pass, has an area greater than 2km^2 and is cut into as much as 4 m of the underlying, primarily horizontally bedded, sediment. The deepest portion of the unconformity has subsequently been filled in with sediment. Radiocarbon dates on shell material collected in cores date the erosional event between 700 and 600 years ago.

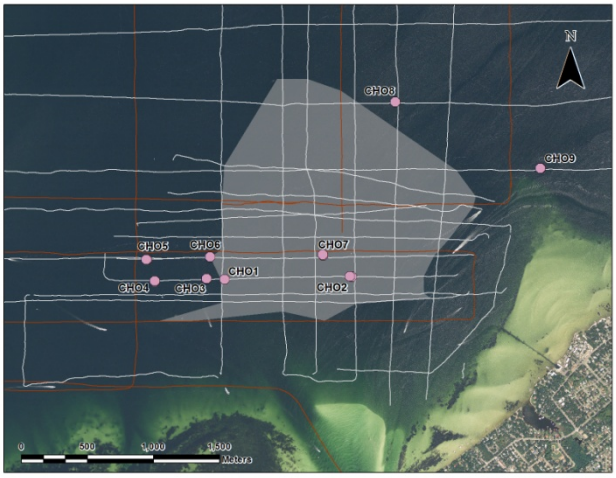

Figure 17. The location of chirp seismic profiles carried out in Choctawhatchee Bay just to the north of the east inlet. Also shown are the locations of sediment cores. The grey area is a packet of sediment overlying an unconformity within the bay and marks the region where material has been excavated during the formation of the unconformity surface. There is another packet of sediment to the west (the boundaries of which are not constrained) penetrated by core CH04.

Elemental analysis of cores from Choctawhatchee Bay via XRF scanning (Fig. 19) reveals that the bay was marine influenced (higher ratios of Calcium (Ca) and Strontium (Sr) relative to Titanium (Ti)) between 5800 and 3200 years ago, suggesting an effective connection to the ocean. Sediments from this interval also contain more coarse material (sand), suggesting higher energy waves and/or currents. Beginning about 3200 years ago, both sand content and Ca/Ti and Sr/Ti ratios fall, suggesting less marine-derived sediments and lower energy conditions within the bay. This change of state is likely related to the closing of the bay by barrier spit extension or inlet closure. Evidence of an east to west progradation of the barrier or inlet migration is evident in GPR profiles (Fig. 20). Beginning around 2500 years ago, the deposition of a series of sand layers in the sediments of Choctawhatchee Bay without any concomitant increase in Sr/Ti and Ca/Ti ratios

likely reflects increased overwashing of the barrier without the maintenance of a long-lived proximal inlet (an inlet may have existed to the west as is seen in GPR records (Fig. 21)). Increases in Ca, Sr, and sand in the sediments after ~1000 years ago indicate an increase in the flux of marine derived sediments. This increased flux of marine sediment to the bay and an opening (or at least significant widening) of the inlet around 1000 years ago followed a few centuries later by the large-scale erosional event around 700 years ago.

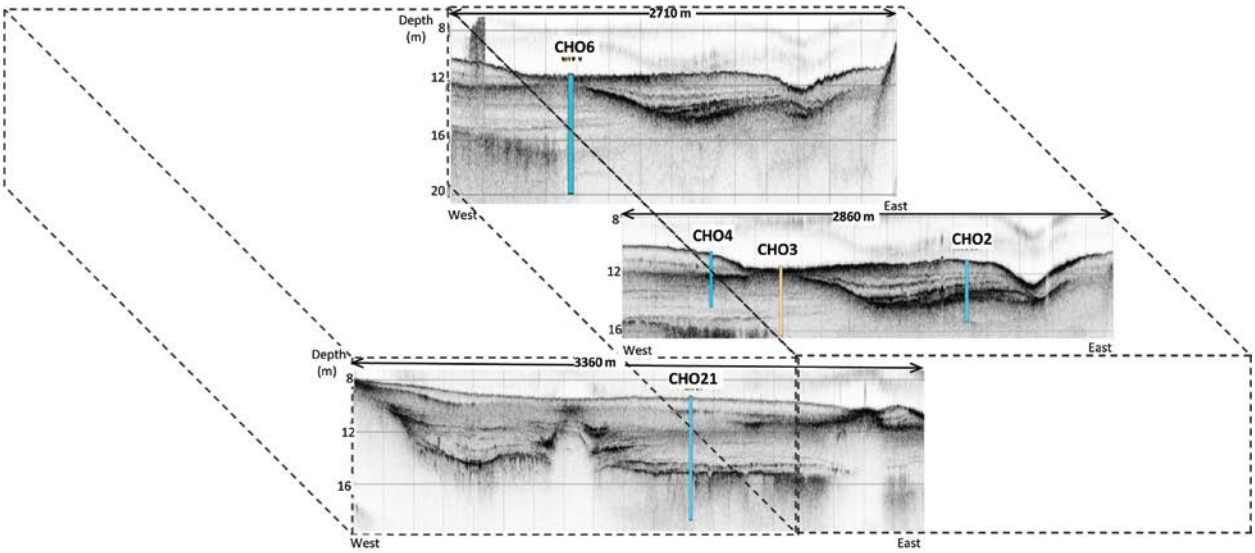

Figure 18. Seismic reflection profile from within Choctawhatchee Bay showing the unconformity with overlying sediment package outlined in Figure 17. The locations of cores are shown. Data from CH03 and CH04 are shown in Figure 19.

Sediment cores from Basin Bayou, on the northern shore of Choctawhatchee Bay were collected and used to further develop a storm history for the region (Rodysill et al., 2013). We collected three vibracores in July, 2012 that are aligned along the long axis of Basin Bayou, oriented roughly perpendicular to Choctawhatchee Bay. The cores were collected in a transect with increasing distance from Choctawhatchee Bay to test whether the coarse deposits we identify are spatially extensive and decrease in thickness and grain size with increasing distance from the bay, as would be expected of bay-source coarse deposits. Two high-energy deposits are present in the recent historical sediments of Basin Bayou, one of which dates to the early 20th century and the other to the late 19th century. The NOAA Best Track (Landsea et al., 2004) data set provides values of hurricane tracks all over the world between 1842 and the present. We used SLOSH hindcasts of the storms from this data base that impacted the region dating back to 1851 to assess which storms are likely responsible for the event beds. Category 3 hurricanes in 1917 and 1882 passing within 75 km west of the site resulted in the highest surge at basin Bayou and are likely responsible for the

deposits recovered. Many other weaker storms or hurricanes that made landfall further from Basin Bayou over the last 160 years resulted in minimal surge and are not recorded in the sediments at the site. Thus, the Basin Bayou record provides a reconstruction of only the more intense hurricanes making a direct landfall in Choctawhatchee Bay. The cores highlight periods of heightened intense storm frequency from 2800 to 2300, 2000 to 1900, 1700 to 1600, and 1300 to 600 years ago. Periods of relatively low storm frequency occurred from 2300 to 2000, 1600 to 1300, and 600 to 135 years ago.

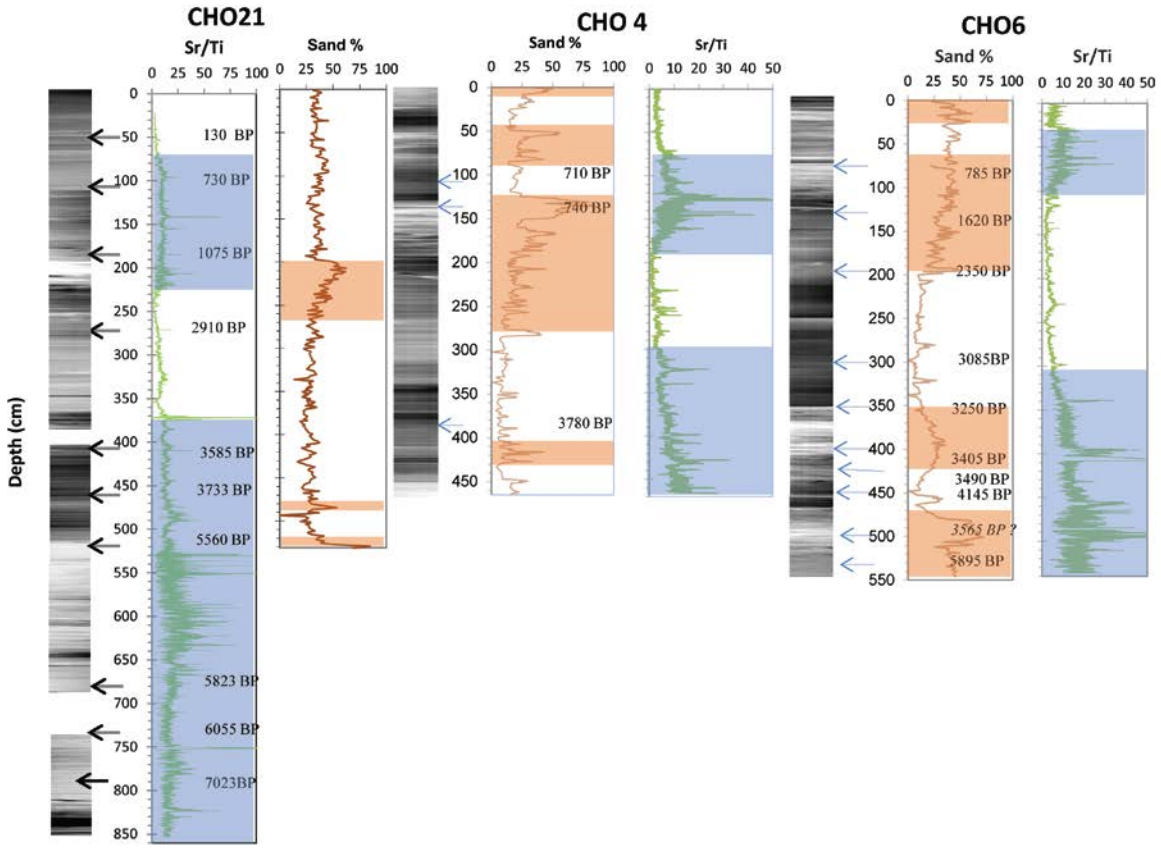

Figure 19. XRF and sedimentological analyses from three cores in Choctawhatchee Bay. Areas shaded in blue represent periods when there was a higher marine component to the sediment deposition within the bay. These data suggest changes in the opening in the barrier, presumably as a result of changes in storminess, with the most recent increase in exchange with the ocean occurring between ~700-1000 years ago, roughly contemporaneous with an observed spike in storm activity in the region. Core CH06 penetrates a bright reflector, or unconformity (dashed line), that was likely formed as a result of high energy erosive event(s) and transitions from marine to terrestrial input in this core represent older events. The sediment that overlies this unconformity shows a higher marine influence and CH04 penetrates a young packet of sediment with marine origin, including thick layers of high sand content likely representing storm deposits that date at around 200-300 years ago.

Our sediment records from the Eglin region provide a record that is remarkably similar to intense storm reconstructions from the northern gulf coast 200 km east of our study site (Lane et al., 2011; Brandon et al., 2013). The most active interval is between 2800 and 2200 years ago with frequency peaking at 5.5 landfalls per century about 2500 years ago. Activity falls off dramatically to less than 1 storm per century between 2100 and 1500 years ago. Intense hurricane activity increases after 1500 years ago and peaks at 3.5 storms per century about 1200 years ago and 4 storms per century about 800 years ago before dropping precipitously 600 years ago. The last 600 years have been among the most quiescent of the last 4500 years with less than 1 storm per century. Only four events are recorded in Basin Bayou in the last 600 years including the 1882 and 1917 events. The coherent pattern of event bed deposition between Basin Bayou (this study), Mullet Pond (Lane et al., 2011), and Spring Creek Pond (Brandon et al., 2013) suggests regionally synchronous levels of intense hurricane activity throughout the northeast Gulf of Mexico over the last several millennia. A similar pattern of variability in hurricane-induced event bed deposition over the last 1500 years is also evident in Belize (Gischler et al., 2008). These sites together suggest the occurrence of intense northern Gulf of Mexico storms during the last two millennia is related to the influence of the Loop Current and El Niño activity on creating a stronger ocean surface to lower stratosphere temperature gradient and providing a deeper layer of warm surface water that maintains storm strength (Lane and Donnelly, 2012; Brandon et al., 2013).

We further note that while there had previously been a discrepancy between our results and published work from Western Lake, 40 km west of EAFB (Liu and Fearn, 2000), a correction to the dates used in that study would likely bring it into line with our analysis. Recent work in the coastal lakes of the northeastern Gulf of Mexico suggest significant carbon reservoir corrections need to be applied to radiocarbon dates obtained on bulk organic carbon samples (e.g., Lambert et al., 2008). Our results do not entirely overlap with those reported in RC-1700 final report for Eastern and Western Lake (Donoghue et al., 2013) in terms of storms per century or in terms of timing of the most active periods, particularly for the last ~500 years, although they do see a peak in activity around 800 years ago. This likely reflects limitations in applying isotopic proxies of bulk lake organic matter in Eastern and Western Lakes as a proxy of hurricane inundation (i.e. other mechanisms are responsible for modest shifts in isotopic composition), the low resolution of the archive (sedimentation rates are more than two times higher in Basin Bayou), or both.

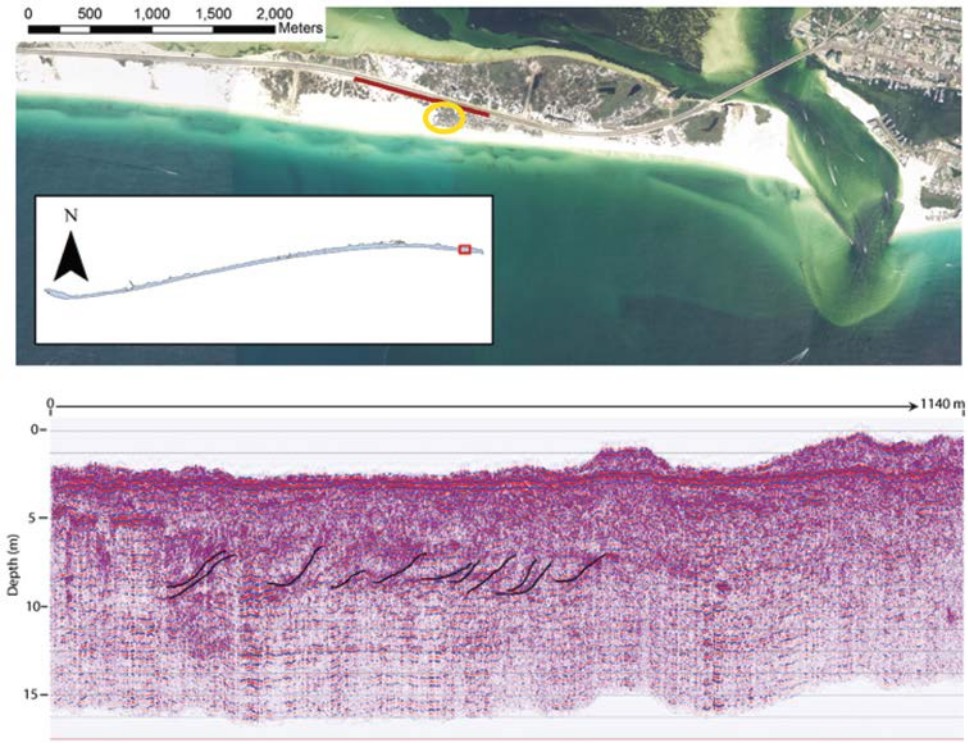

Figure 20. (lower) Ground penetrating radar data from the section of barrier close to East Pass inlet showing a sequence of westward dipping reflectors indicating deposition during westward barrier growth or inlet migration. The red line in the top panel shows the region of radar coverage. The yellow ellipse shows the location where 3 samples were taken for OSL dating. OSL dates of sediments from the dunes are younger than 200 years, supporting the idea that this section of barrier is dynamic and quickly evolving.

The opening of East Pass about 1000 years ago and the erosional event 700 years ago occurred at a time of relatively high intense hurricane activity (Fig. 19). Given that the water depth in this portion of the bay was quite deep 700 years ago (~12 m, accounting for <1m meter of SLR in the last 700 years), a significant flow would be required to excavate the sediments that were eroded from the bay bottom. A possible mechanism for this erosive event is the outflow of a very large storm-surge event (or events) through an inlet close to the current East Pass location. The beginning of the interval of frequent overwash in the Choctawhatchee Bay cores coincides with the very active intense hurricane interval, but persists through the relatively inactive interval between 2100 and 1500 years ago. Thus, the barrier fronting the bay likely had low elevation, at least during the lull in intense storms, in order to have been overwashed so frequently. The decrease in marine influence that begins around 3200 years ago occurred when intense hurricane activity was at intermediate levels (generally between 2 and 3.5 storms per century). The rate of SLR slows at about this time from about 1mm/yr to 0.6mm/yr (Fig. 15) and may point toward a link between the decreasing rate of SLR and barrier formation.

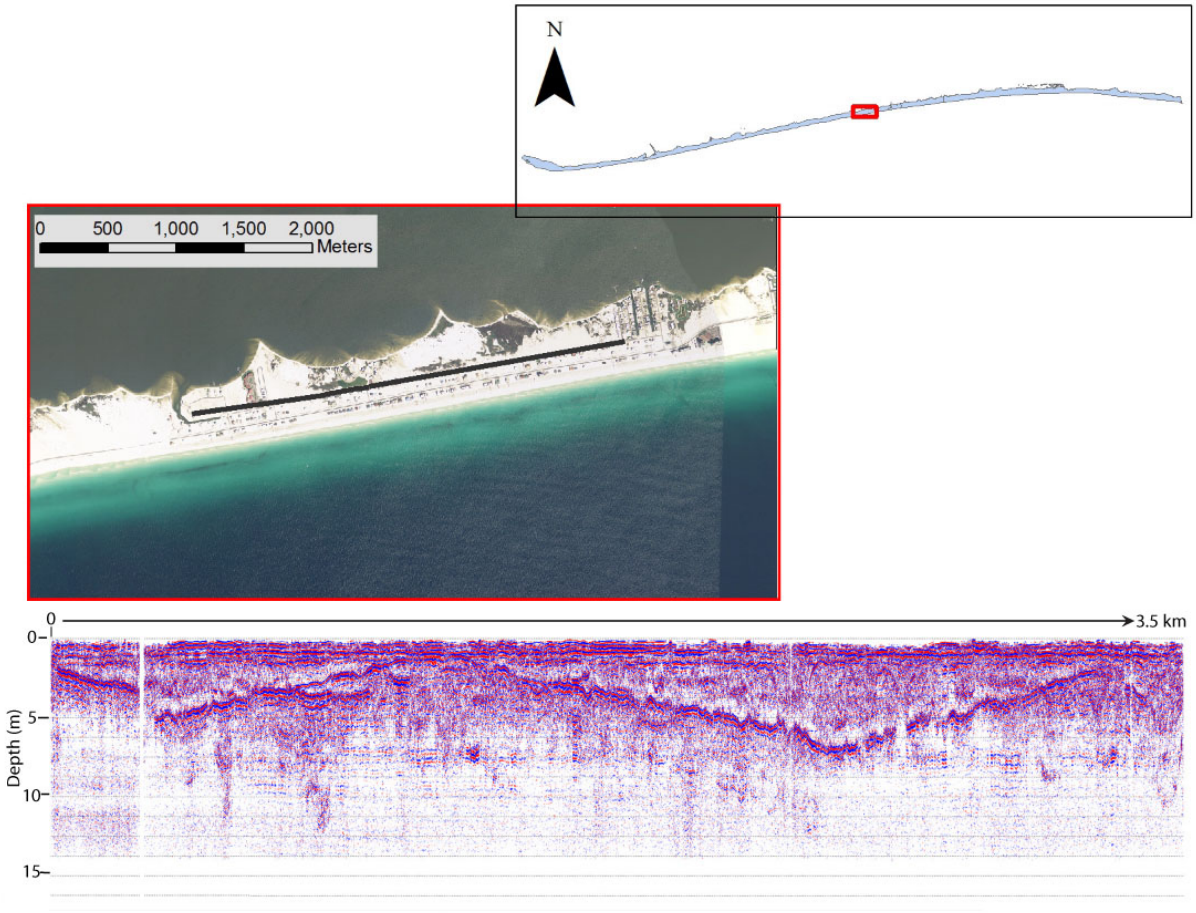

Figure 21. A ground penetrating radar profile from Santa Rosa Island showing the presence of a large paleo-inlet.

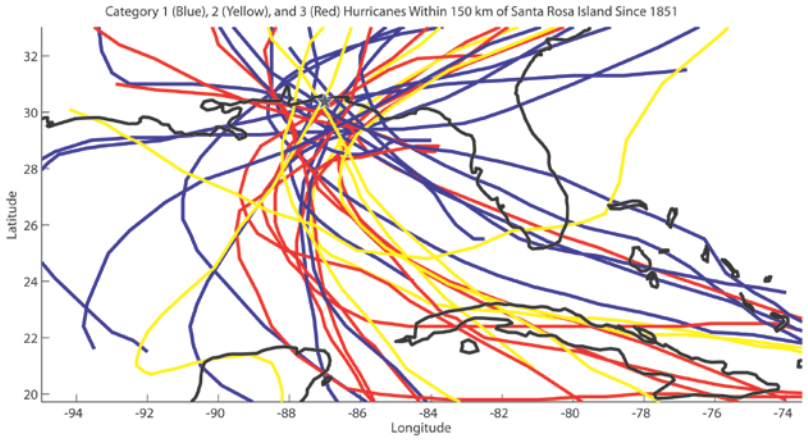

Figure 22. Historic storms that have impacted the Eglin area as found in the NOAA Best Track data base.

5.2.4 Recent Storm History

In 1917, a Category 3 hurricane made landfall directly over Choctawhatchee Bay, and in 1926 a Category 3 hurricane came onshore 155km west of the bay. The SLOSH model simulated a surge of 1.1 m for the directly landfalling 1917 storm and 0.9 m for the 1926 storm. These surge heights are very similar and it is possible that wind-driven waves could overtop the barrier during the 1926 storm despite the fact that the still water surge height was below the elevation of the barrier. The single bed seen in cores from Basin Bayou may therefore represent both of these events, or it may only represent the closer land-falling hurricane in 1917. The hurricane in 1917 was more proximal to our coring site in Basin Bayou, which more likely caused greater local wind velocities that produce larger wave heights than the more distal 1926 storm, causing sand deposition in Basin Bayou in 1917. We therefore attribute the two sand layers in the historical portion of our core record to the direct land-falling Category 3 hurricanes in 1882 and 1917.

Eight other Category 3 hurricanes have passed within 185 km of Choctawhatchee Bay documented in the Best Track dataset that do not correspond to sand beds seen in cores (Knapp et al., 2010). These storms occurred in 1877, 1894, 1916, 1975 (Eloise), 1985 (Elena), 1995 (Opal), 2004 (Ivan), and 2005 (Dennis). The three closest are Eloise (1975), Opal (1995), and Dennis (2005), which produced simulated surge heights in SLOSH of 0.8m, 0.9m, and 0.7m, respectively. Each of these surge heights are below the modern barrier elevation

5.2.5 Field Estimates of Overwash Flux.

Critical to understanding the future behavior of any barrier is an estimate of the flux of sediment transported across the barrier either by winds or water during storm events.

We have carried out coring and radar analyses of a sequence of overwash fans within the military portion of Santa Rosa Island. These fans were deposited in part during Ivan, with additional volume added by Dennis. The volume of the fan shown in Figure 23 is roughly 1.5 x10^4 m^3. There are 6 identifiable areas of similar size in a roughly 1.5km stretch of barrier. This constitutes about 7-10% of the volume of the barrier above sea level being moved landward. Events with a storm surge of more than 1.5m (above MSL) occur, based on our climatology/surge modeling, about 4 times per century, although two storms with this surge occurred in the last decade alone. The flux of sediment estimated from these events is less than 5 m^3/m/yr.

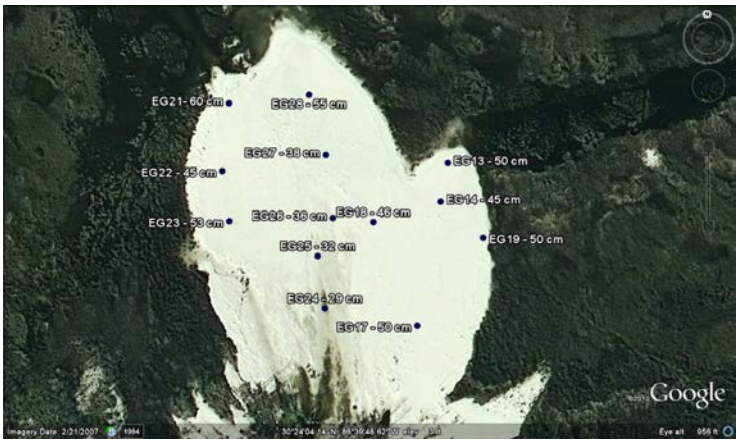

Figure 23. Thicknesses of sediment deposited in an overwash fan on Santa Rosa Island. The fan was emplaced by both hurricanes Ivan and Dennis.

LIDAR data collected over Santa Rosa Island have been used to quantify changes in the barrier morphology due to storm events. Dramatic changes are seen in the elevation and the shoreline position of the eastern portion of Santa Rosa Island in the last decade (Figs. 24, 25, 26). Beach profiles show loss of material close to the beach and shoreline that is accreted landward, between the new beach and the dune line. Additionally, some material is transported further back behind the dune field. Low-lying areas of barrier near the beach generally show only a net loss of material. The vertical growth of the middle portions of the barrier along this portion of the barrier island contrasts with observations from portions of the island further west where backshore accretion is limited (particularly in regions with greater overwash penetration) (Houser, 2008; 2009).

As a result of Hurricane Ivan, the shoreline retreated in places by as much as 10m (Figs. 24, 25). The beach itself has been raised by around 1m. Hurricane Ivan was a category 3 storm with an observed storm surge from local tide gauges of around 2m. This surge was insufficient to completely inundate the eastern portions of the barrier island.

In addition to sediment transport by storm surge and waves, significant sediment transport appears to be facilitated by winds. The sediment trap array data show some clear patterns, although they also point to the complexity of wind driven transport. The windrose for the region shows a prevailing wind from the south-southeast, with significant events also from the east (Fig. 1). At face value, this would suggest predominant transport towards the back-barrier, as well as alongshore to the west (i.e. in the same direction as the net alongshore drift). The bulk sediment trap data support this model. As expected, accumulation of sediment was typically greater in traps closest to the shoreline with many traps sited towards the back of the barrier and particularly those in the dune field having little to no accumulation. This suggests that Aeolian transport may not extend across the entire barrier, except for the low lying stretches of barrier, although the build-up of large dune fields places a significant volume of sediment on the barrier that is potentially moveable landward during large storm events.

Analysis of sediment trap data suggests that such transport contributes significantly more flux than that estimated from overwash flux. Although there is significant variability between traps, and not all flux is landward directed, the best estimate of across shore flux is ~30 m^3/m/yr and a similar flux is found for the alongshore westward barrier transport.

Radar data and OSL dating along the portion of the barrier fronting Choctawhatchee Bay show evidence for a rapidly evolving, dynamic barrier system (Fig. 20). Sequences of reflectors show progradation of the barrier to the west, consistent with the net direction of alongshore sediment transport. These reflectors may indicate barrier progradation or downdrift migration of a previous inlet. Sediments sample from dunes shoreward of this radar profile have OSL dates younger than 200 years, also suggesting a dynamic and changing environment.

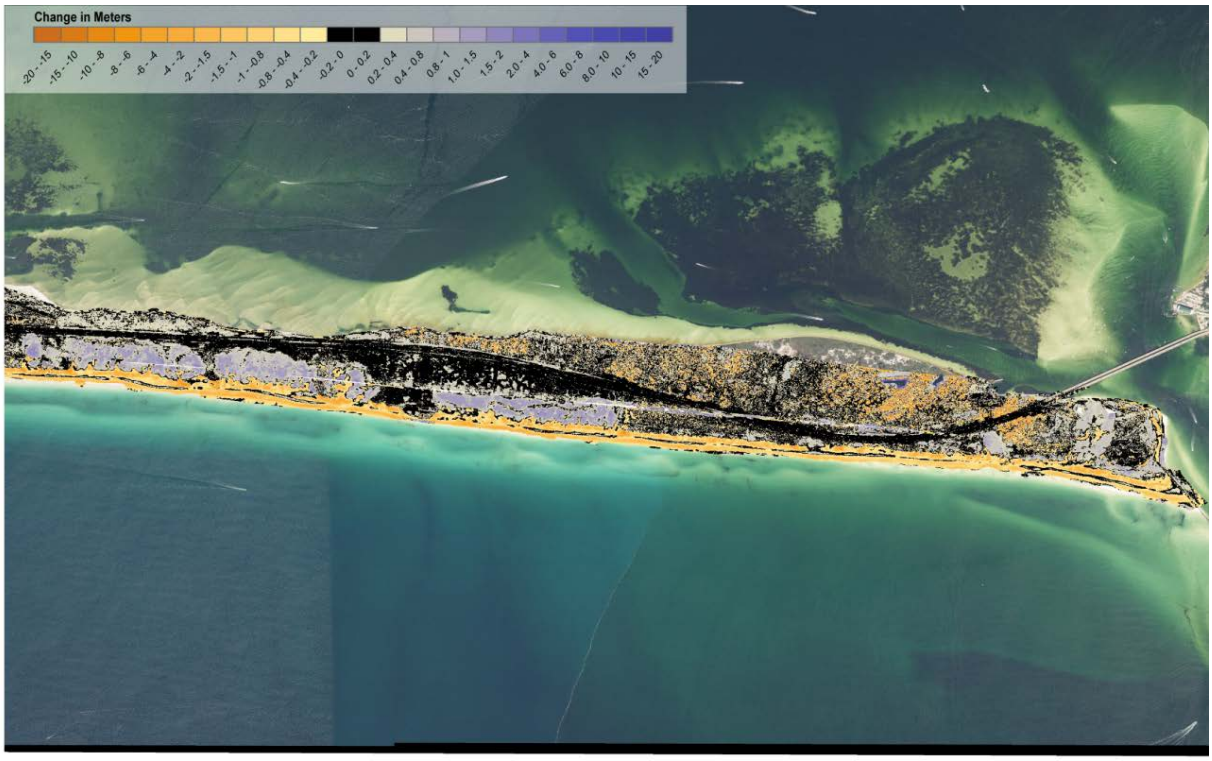

Figure 24. Changes in elevation following Hurricane Ivan on the eastern portion of Santa Rosa Island, immediately fronting EAFB. There is a loss of material on the beachface accompanied by backshore accretion. There are also areas of material loss on the bayside of the barrier.

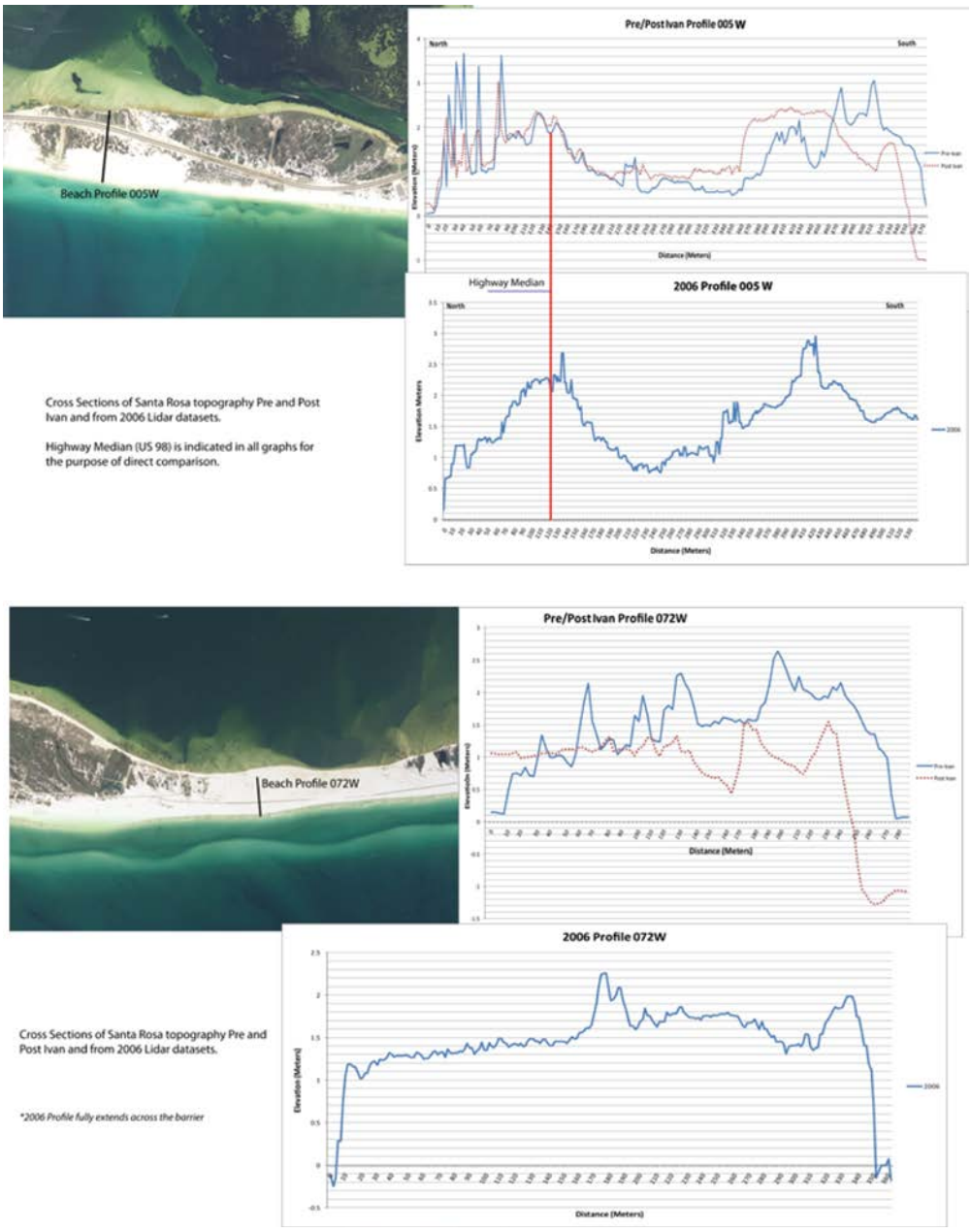

Figure 25. Example beach profiles on Santa Rosa Island taken before and immediately after Hurricane Ivan. (a) Shows a fairly common response in which there is a net loss of material at the beachface that is accreted onto the backshore. The barrier is essentially narrowed as a result of the transport. (b) In contrast shows a profile through a low-lying section that was likely inundated during the storm resulting in a net loss of elevation.

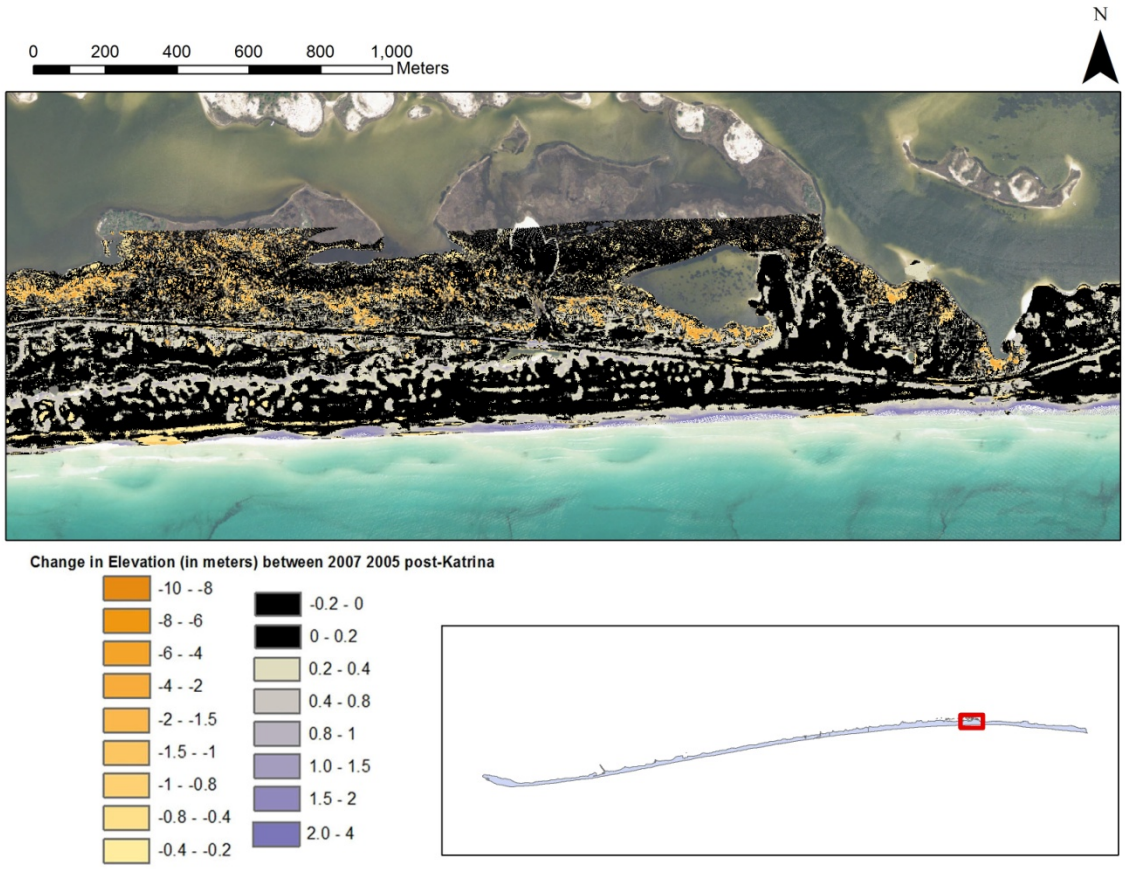

Figure 26. A differential LIDAR map of the section of Santa Rosa Island where we studied the overwash fan shown in Figure 23. Two LIDAR surveys from 2005 and 2007 were differenced, covering a period of post-storm recovery. There are areas of significant sediment gain, notably on the beach face, and smaller areas of sediment loss, mostly behind the dunes. There is some apparent accretion to the dunes, although the signals are small and are close to the noise levels of the data, particularly within vegetated zones. There were no major storms during this period and so differences are presumably the result of offshore gains (likely from post-storm recovery of the shoreface) at the beachface and aeolian transport elsewhere. The net gain of sediment on this stretch of beach is ~10-20 m^3/m/yr, slightly greater than the net flux estimated from the volume of the overwash fans.

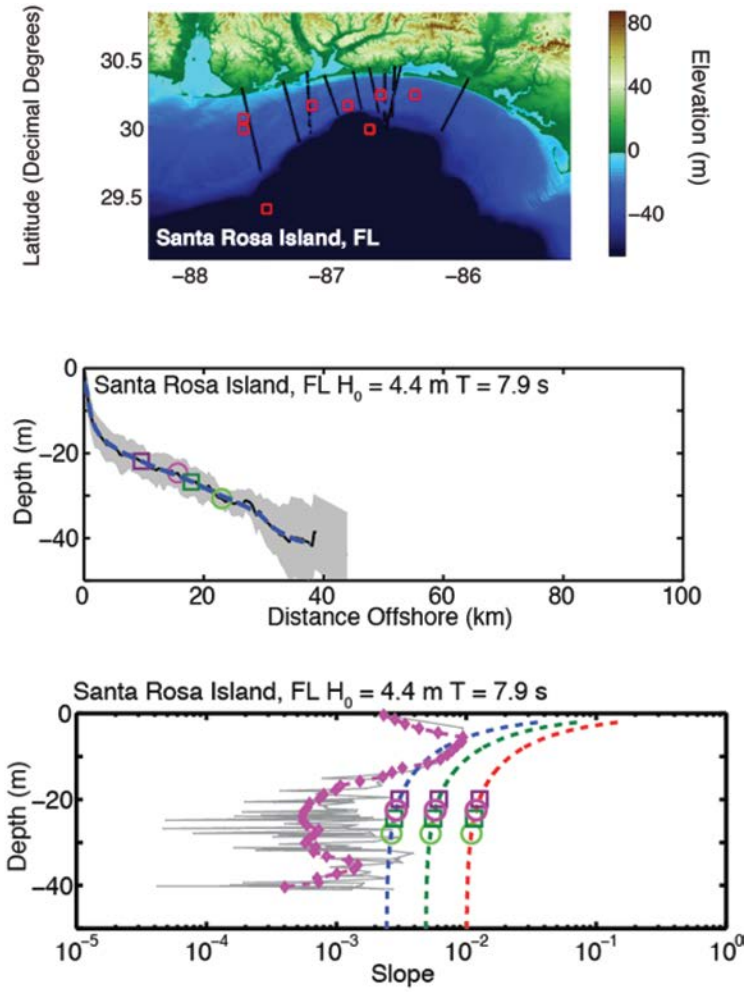

Figure 27. Santa Rosa Island shoreface characteristics. (Top) Profiles and WIS virtual buoy data used. (Middle) Averaged shoreface profiles with computed morphodynamic depths of closure. (Bottom) Measured and computed dynamic equilibrium shoreface slopes versus depth.

5.2.6 Shore Face and Wave Climate Characteristics

Wave data from ~20 years of Wave Information Study (WIS) buoys (Fig. 27) were used to calculate the morphodynamically representative wave height and wave period for waves impinging on Santa Rosa Island. We calculate a weighted histogram of the significant wave height to the fifth power for each buoy. The cross-shore sediment flux, q_s, is proportional to local wave height to the fifth power ($q_s \propto H^5$) as described above (Fig. 28). Comparison of computed equilibrium and measured profile slopes shows reasonable similarity in the top 15-20m of the profile (Fig. 27). Beyond this point, the observed profile is low-sloped, perhaps indicating that the slope is controlled by the underlying geological framework.

Weighting of wave events based upon their contribution to sediment transport emphasizes the effect of infrequent high-energy events on shoreface dynamics. For Santa Rosa Island, this results in an effective cross-shore effective wave height (H_x = 4.7m, weighted by sediment transport potential) more than twice as large as the average wave incidence height (which is less than 2m) (Fig. 28, upper right). Even with this weighting of large, infrequent wave events, the probability density function (PDF) of effective wave events shows a relatively smooth, single mode distribution. Although hurricanes contribute to the infrequent events affecting this site, their influence does not result in a separate population of effective events (as can be seen, for example, at Onslow Bay, which we discuss below).

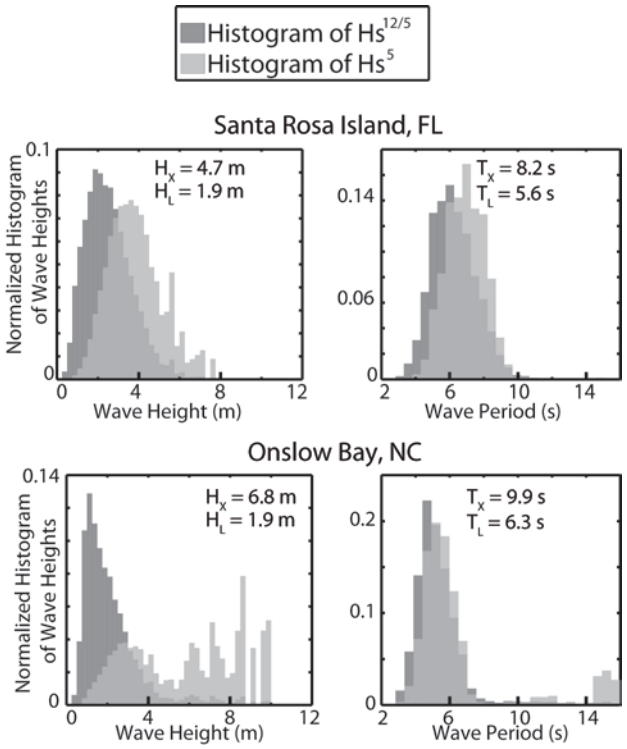

Figure 28. Wave climate data for Santa Rosa Island (top) and Onslow Bay, NC (lower). Data are based on 20 years of WIS buoy observations. Locations of the buoys are shown in Figures 27 and 42

5.2.7 Likelihood Estimates of Storm Surge at Eglin

The suite of 10,000 synthetic storms (Fig. 29) generated for the Eglin region have been used to estimate return intervals for storm events and, by running each storm event through SLOSH, to calculate surge statistics as a function of storm category (Figs. 30-32).

Under modern climate conditions, the 1/100 year event at EAFB corresponds to a ~3m surge event. The 1/50 year event is a 2m surge. Thus, Hurricane Ivan in 2004, which resulted in approximately 2m of surge was likely a good example of a 1/50 year event along this coast. Based on this analysis

Hurricane Opal was roughly a 1/44 year event and Hurricane Dennis was a 1/30 year event, with 1.85m and 1.5m of surge recorded at the Pensacola tide gauge, respectively.

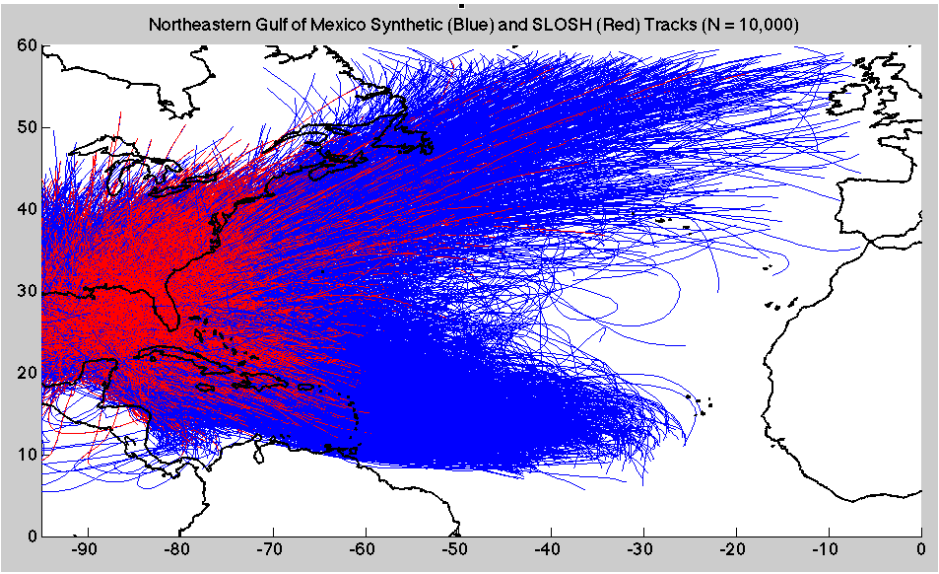

Figure 29. The population of 10,000 synthetic storms with at least 40 knot maximum sustained winds while within the northeast Gulf of Mexico.

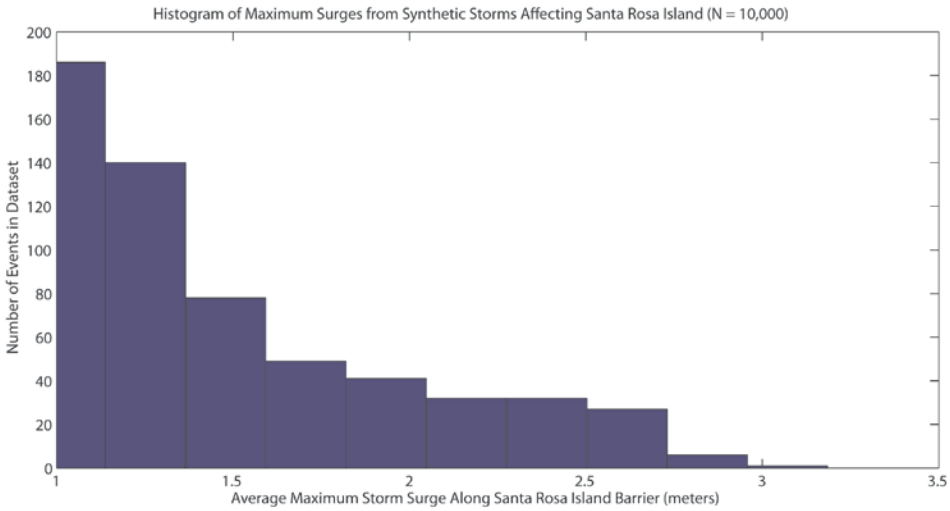

Figure 30. A histogram of storm events in the synthetic dataset as a function of storm surge along the Santa Rosa Barrier.

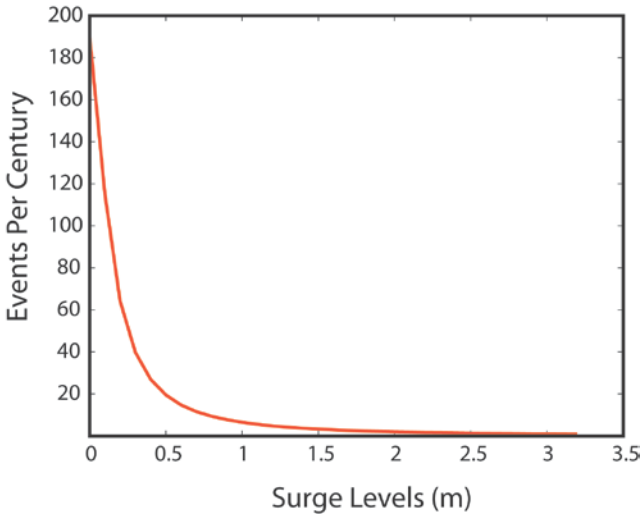

Figure 31. The frequency of storm surge levels expected to hit the Eglin area under modern climate conditions based on analysis of the suite of 10,000 synthetic storms.

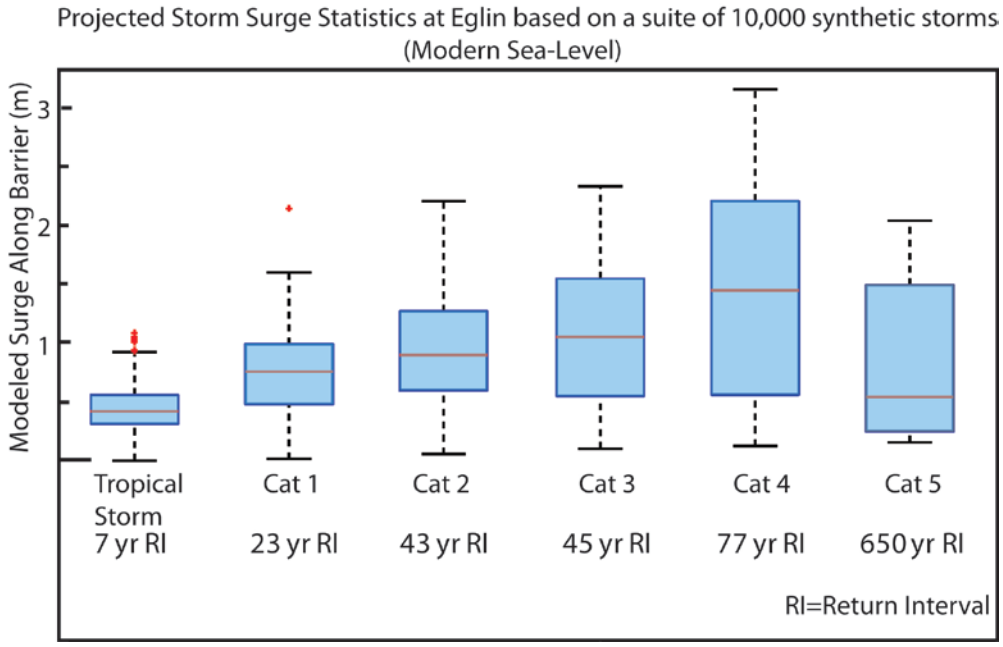

Figure 32. Storm surge levels as a function of storm size for the Eglin region along with estimate return intervals for each category of storm. On each blue box, the central red line denotes the median, the edges of the box are the 25th and 75th percentiles, the black bars extend to the most extreme data points not considered outliers, with outliers plotted individually as red crosses.

Significant surges around EAFB, the 100-year event for example, are more likely to result from storms of moderate intensity (category 2 and 3 storms) than from extremely intense storms. This is partly due to the overall higher frequency of category 2 and 3 storms when compared to higher category storms. The inverse relationship between a storm's intensity and the size of its wind field also plays a role. As a storm intensifies to category 5, its wind field contracts and the fetch and time over which the wind stress acts also decrease, resulting in smaller surge. The surges generated by smaller storms also impact shorter stretches of coastline. Another factor to consider is that category 5 storms are rare. Even though our analysis considers a multi-millennial hurricane climatology, any one location that we query with a radius filter might only pick up a handful of category 5 events of which few may be direct strikes. As a result the statistics produced can be driven by a handful of near miss storms.

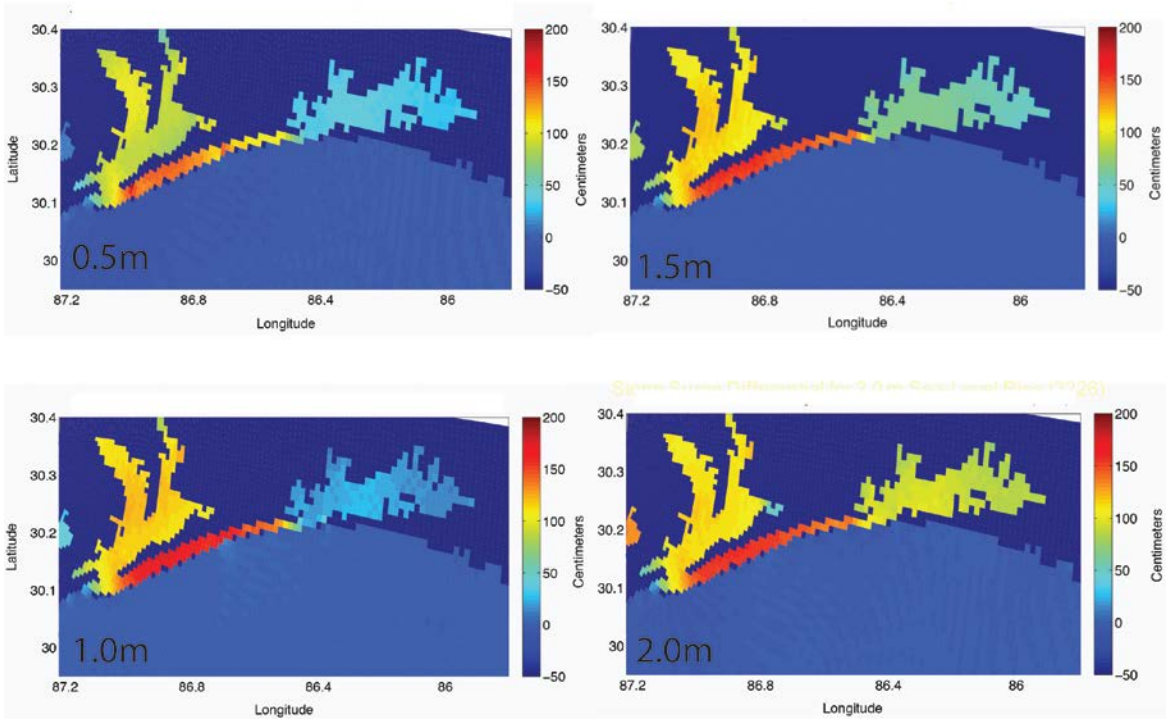

Figure 33. Storm surge differential (difference between surge calculated under current and projected sea-levels) at the end of the century for the 4 sea-level scenarios for a category 2 storm passing to the west of Santa Rosa Island. The low elevation at the western end of the barrier leads to a threshold behavior with significantly more surge in the backbarrier even at fairly small levels of SLR. Higher surge levels, for this westerly storm track, only occur in Choctawhatchee Bay for the 2m SLR scenario.

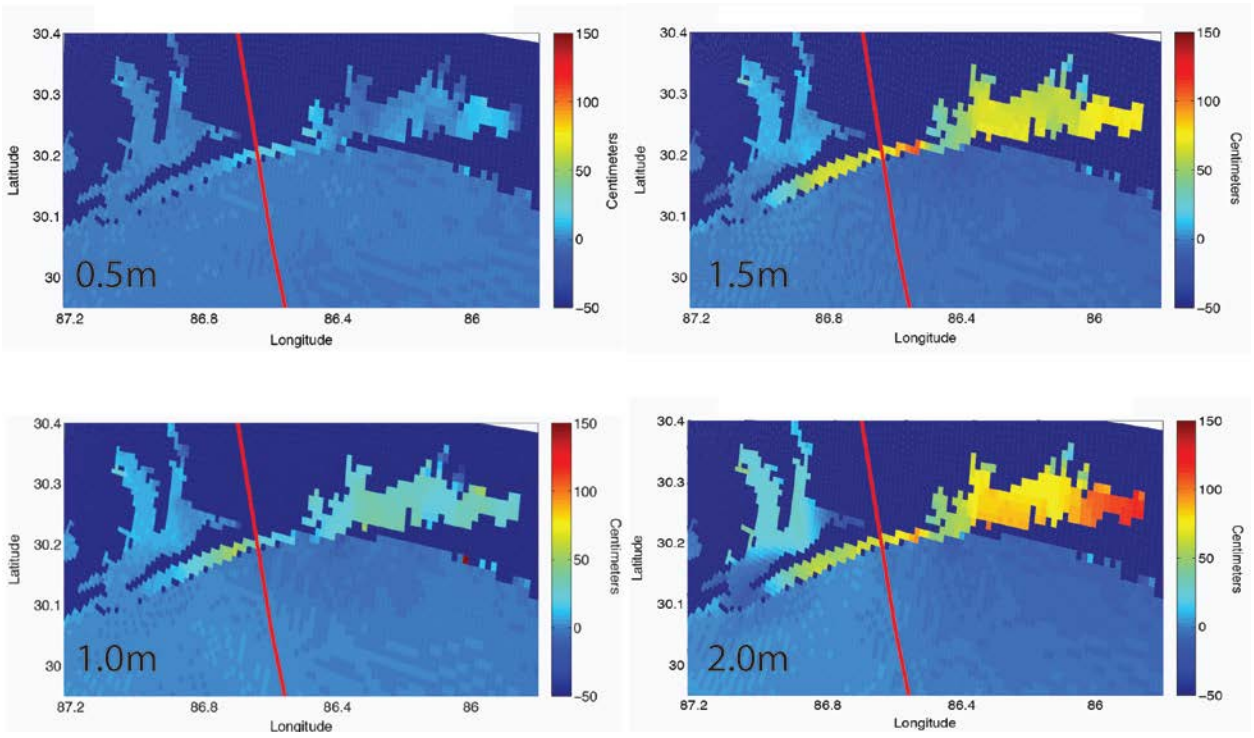

Figure 34. Storm surge differential (difference between surge calculated under current and projected sea-levels) at the end of the century for the 4 sea-level scenarios for a category 3 storm crossing Santa Rosa Island (red track). Higher surge levels, for this westerly storm track, occur in Choctawhatchee Bay for the 1.5m and 2m SLR scenarios.

In order to assess potential changes in hurricane surge propagation related to increased sea level, we modeled the surge using SLOSH for a series of synthetic storms for each of the AD 2100 sea level scenarios. Differencing the surge obtained in these scenarios with simulations of these events with current sea level yields spatial plots of the impacts of SLR on surge patterns. This approach does not consider changes in barrier geometry related to sea-level change and storm impacts. Nevertheless, the results highlight some important feedbacks between barrier drowning and back-barrier surge characteristics. Barrier drowning has a profound impact on back-barrier surge levels, even for relatively modest increases in sea level. For example, a SLOSH simulation of a category 2 hurricane making landfall to the west of Pensacola yields very little surge in Pensacola Bay under modern sea level as the Santa Rosa barrier effectively shields the bay (Fig. 33). However, given the height of the barrier fronting Pensacola Bay is relatively low-lying, with only 0.5m of sea-level rise the barrier is submerged during this event and surge is allowed to propagate into Pensacola Bay resulting in an additional 1 to 2 meters of surge there. Only modest additional surge is simulated in the bay for more extreme sea level scenarios. Thus dramatic changes in the vulnerability to hurricane surges can be expected in back-barrier bays fronted by low-lying barriers with modest

increases in sea level. With a much higher barrier fronting it, Choctawhatchee Bay only sees an appreciable increase in surge under the 2m SLR scenario for this storm.

In a second synthetic example, a category 3 storm making landfall near Navarre Beach, the greatest impact on surge in Choctawhatchee Bay, occurs under the 1.5m SLR scenario with surge increasing in the bay by roughly 0.75m (Fig. 34). The 2m SLR scenario increases surge at the head of Choctawhatchee Bay by about 1.5m. These results point to significant threshold behavior with respect to surge propagation to back-barrier locations that is controlled by barrier elevation relative to sea level. If barriers are unable to build to maintain elevation relative to future sea level, significant changes to back barrier surge vulnerability should be expected, even under modest SLR in areas with low lying barriers.

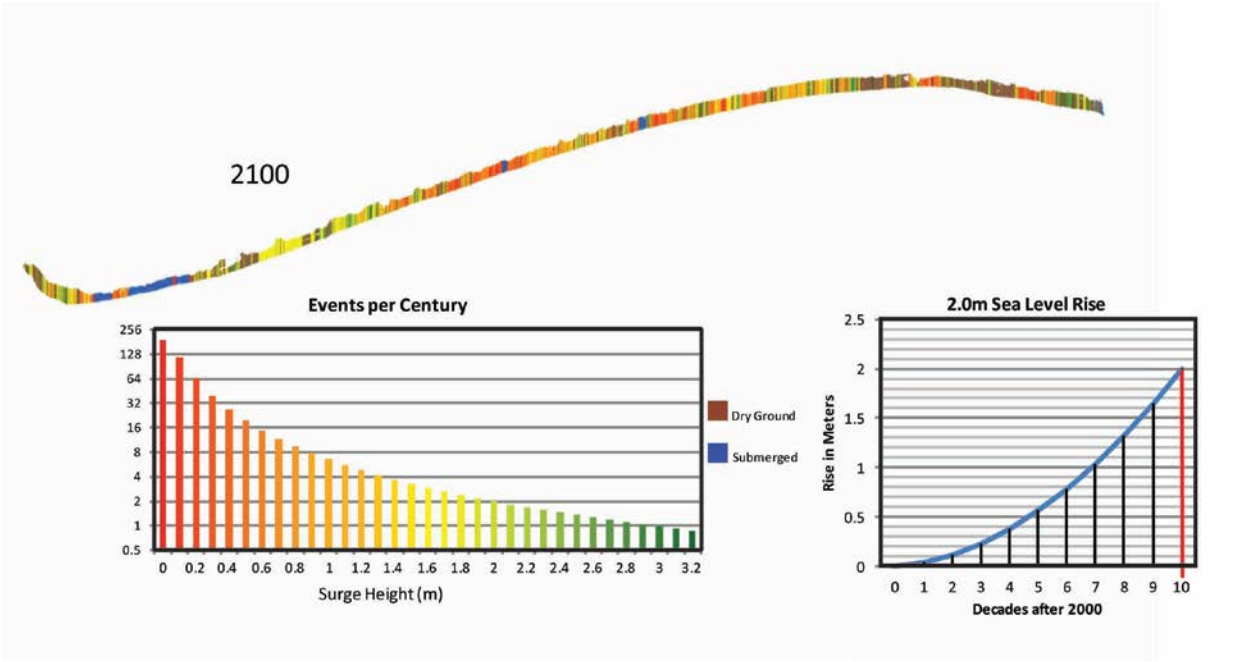

Figure 35. An example of a storm surge probability map for Santa Rosa Island. The example shown is for 2 m of SLR and for year 2100. Areas in blue are essentially permanently inundated. This approach does not account for changes in barrier morphology due to the rising sea-level (i.e., the barrier maintains the current day geometry).

The combination of storm surge return intervals and topography on the barrier allow us to calculate inundation probabilities for Santa Rosa Island (Fig. 35). Although this modeling does incorporate the 4 SLR scenarios in the calculation of surge, as for the surge modeling in Figures 33 and 34, it does not account for changes in barrier morphology resulting from the change in sea level. The

inundation probability shown in Figure 35 does not include wave run-up, but this has been calculated separately using the high resolution modeling using the UH-ORE model package described in the next section.

5.2.8 High Resolution Inundation Modeling at Eglin

Hurricane Ivan (2004) was used as a test case for high-resolution model validation including wave run-up. This hurricane event generated a significant storm surge combined with large storm waves that overtopped Santa Rosa Island and led to significant geomorphologic changes.

The maximum flow depth during the overtopping is rather small (~1.0m). However, the waves run up to an elevation of around 5m, which infers that the flow regime was very energetic during the event. The maximum flow speed recorded during the model run of the event is more than 2m/s along most parts of the shoreface and even over the barrier island itself. The individual storm waves show a much higher flow speed than the storm surge itself, which moves rather slowly. It can be assumed that the storm waves are responsible for pick up and erosion of sediment whereas the storm surge has the potential to redistribute this sediment through suspended load transport. The direction of the maximum flow speed was primarily in a landward direction and into the tidal inlet, where a lot of sedimentation was recorded. Some locations show an offshore-directed flow, indicating very strong recirculation currents induced by the storm waves thought to be responsible for substantial erosion at the shoreline and deposition of substrate around the area of wave breaking. Erosion and accretion plots made from pre- and post-storm LIDAR data confirm that large amounts of material were deposited on the barrier, around the area of wave breaking, during the event.

Four hypothetical hurricane tracks were modeled to show the range of likely impacts on the region for the 4 different sea-level scenarios (Fig. 36). Tracks 1, 3, and 4 pass close to the site and therefore produce high surge levels. Track 2 has only very limited inundation effects from a small amount of storm surge and produces relatively small storm waves due to its southwestern path. The inundation and overtopping scenarios are generally similar to what was observed during hurricane Ivan. Independent of the direction of wave approach, overtopping occurs predominantly in the lower parts of the barrier with fast flow speeds. The maximum flow speed is more than 2m/s in most parts of the inundation area and generally reaches supercritical flow stage, whereas the maximum flow speed of the pure storm surge is much smaller and mostly subcritical. Results for the track 3 storm are shown in Figure 37 for modern conditions and for the 0.5m and 1.0m sea-level scenarios.

For the increased sea-level scenarios, the surge levels are obviously increased for a given storm event. The numerical computations show an almost linear increase of the storm surge level with

SLR scenarios, however, the maximum flow depth as well as flow speed from the combined surge and storm waves behave in a slightly nonlinear manner. We observed a 10-20% higher flow depth and speed under 0.5 and 1.0m SLR situations. This effect is linked to the shoreward translation wave breaking at higher water levels that causes an elevated energy regime closer to shore, over parts of the barrier that were previously dry. Less dissipation offshore also produces faster flows at the shoreface with the potential for significant sediment transport and hence erosion.

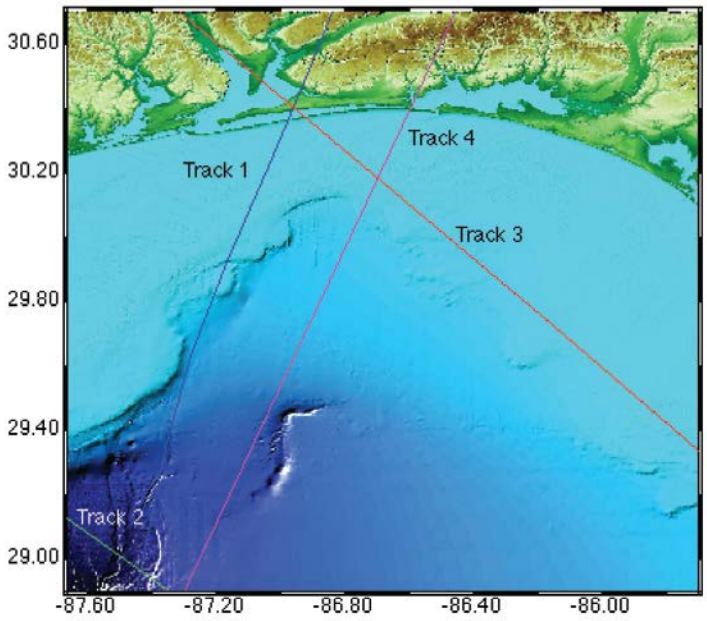

Figure 36. Tracks of the 4 storms used for high resolution synthetic modeling with the UH-ORE package.

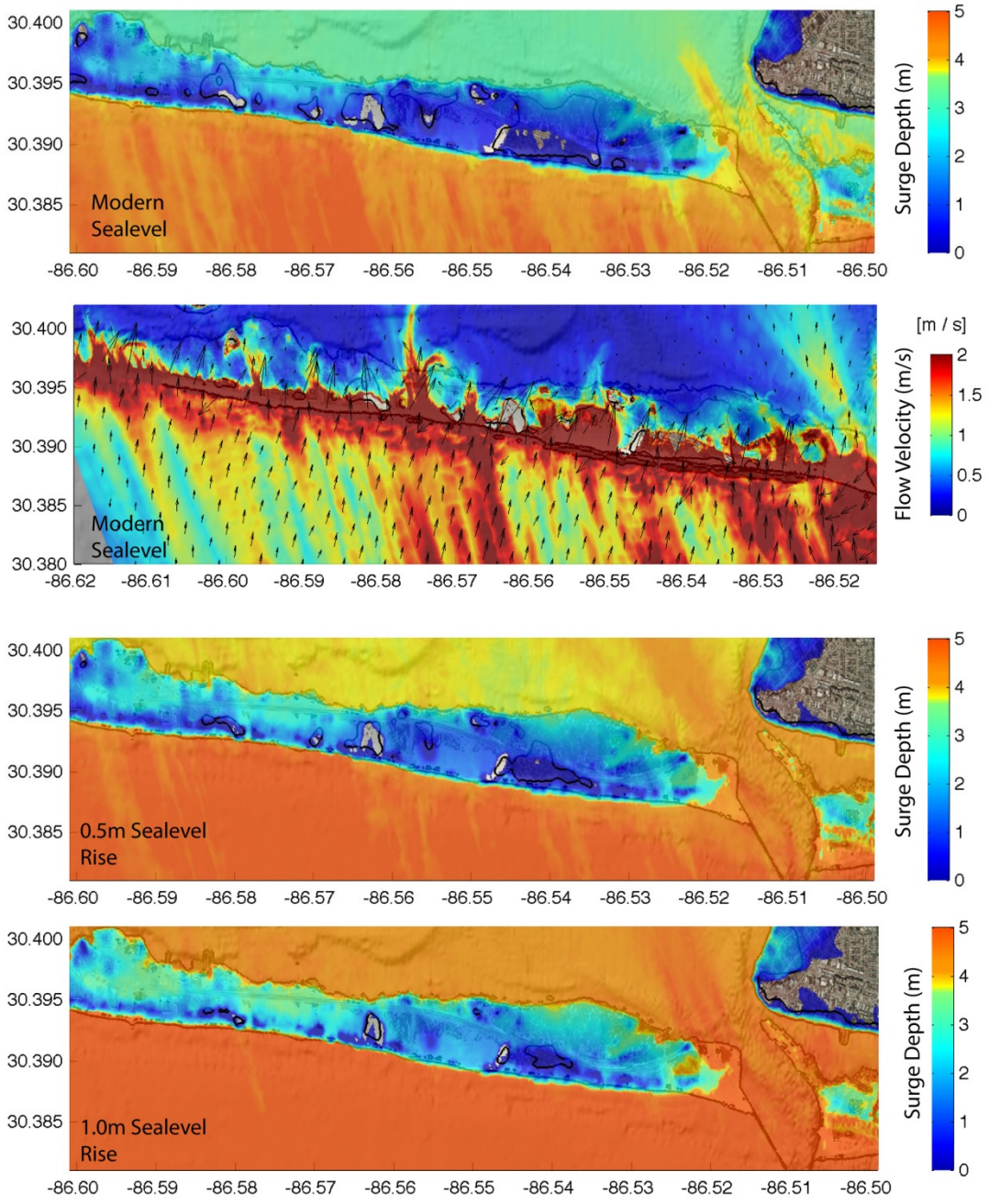

Figure 37. High resolution inundation modeling results for the storm track 3 shown in Fig. 36. The top two panels show results for modern sea level for surge level and flow velocity (including wave effects). Surge levels for 0.5m and 1.0m of SLR are shown as labeled in the lower panels.

5.2.9 Model Results for Eglin Using Field Observations of Overwash Flux

Simulations applied to Santa Rosa Island investigate how barriers with geometries matching that of Santa Rosa Island may respond over the next 100 years. These simulations differ from the behavioral models described in section 4.1 as they specifically treat the project-defined SLR scenarios, including sea-level acceleration over the coming century. A prototype barrier geometry is developed using bathymetric and topographic profiles along the island (Fig. 1). For Santa Rosa Island, the visually apparent break in shoreface slope (17m) appears to be slightly shallower than the computed morphodynamic depth of closure (24m). With limited knowledge of the shelf environment, we use the shallower of the two for the model implementation. A suite of simulations was performed to understand the potential long-term evolution of single barrier profiles for different sea-level scenarios and for different values of the maximum overwash rate.

As the potential rate of landward barrier overwash flux varies, so does the response of the modeled barrier (Fig. 38). With no overwash, the barrier height remains unchanged and the shoreline recedes as the shoreface oversteepens and sediment is transported offshore—in a manner predicted by Bruun rule with rates dependent upon the shoreface slope and SLR. The shoreline recession rates even in the absence of overwash, on the order of 25m for 0.5m SLR and 90m for a 2m SLR, are not insignificant, and in this case are determined by the shoreface geometry. However, at face value, this situation of low shoreline change and limited overwash would probably be considered more ideal for management of the island, as infrastructure would not be exposed at the shoreline and the transportation corridors would not be overwashed. However, over the long term, the non-overwashing barrier is essentially drowning in place, particularly for the higher SLR scenarios as general elevations of Santa Rosa Island are on the order of 2m. The short-term benefit of the lower shoreline recession results in relative drowning of the barrier, a threat to its long-term preservation for significant rates of SLR. Shoreline recession is only one part of the SLR response.

As overwash rates increase, shoreline recession rates also increase to around several hundred meters by the end of the century, such that the barrier would roll over its entire terrestrial footprint (Fig. 39). Although such rapid overwash and shoreline recession rates would negatively impact operations on the barrier, the barrier itself would be better able to protect inland sites and maintain itself as a landform as sea-level rises. Note, however, that the geometric constraints of the barrier are such that rates of overwash must be high for the barrier to maintain its elevation, on the order of 40–80 m^3/m/yr or higher. These rates are significantly greater than the volumetric overwash rates, which we estimate are on the order of 5-10 m^3/m/yr over the last decade (which included several large storms), but if we include our estimate of ~30 m^3/m/yr aeolian transport, measured over a year without hurricane strikes, then the total flux is close to the lower end of this limit. Note also that the increase of shoreline retreat with increasing potential overwash rates diminishes for

high overwash fluxes (Fig. 38). In this case, there is sufficient overwash to establish the barrier at the same relative elevations and width after sea level has risen.

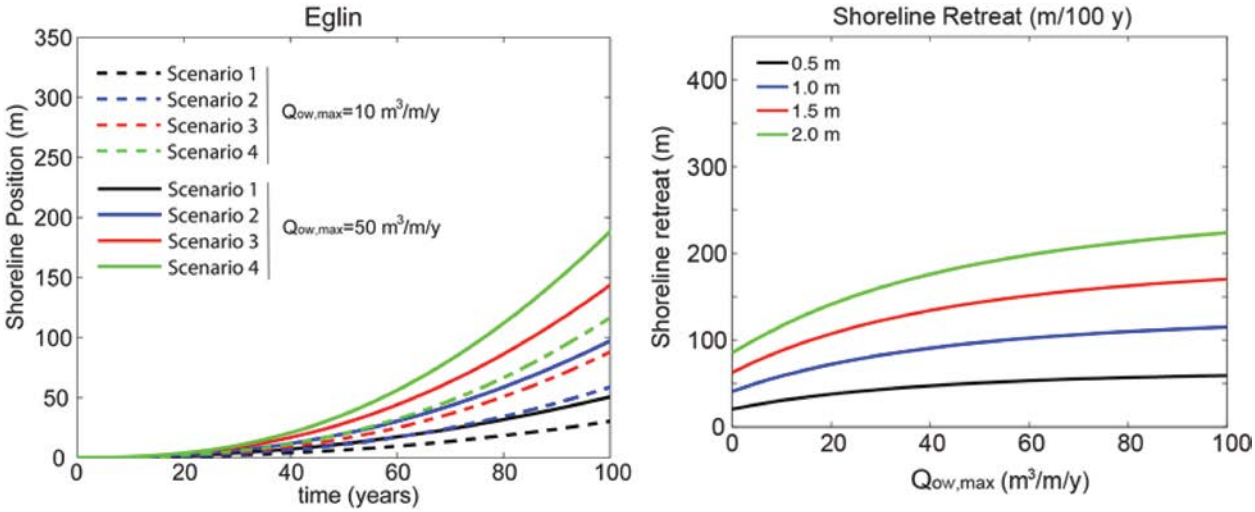

Figure 38. Santa Rosa Island geomorphic modeling results. (Left) Representative shoreline evolution for the project scenarios for selected values of $Q_{OW,max}$ and K = 10,000 m^3/m/y. (Right) Shoreline recession versus $Q_{OW,max}$ for the four prescribed SLR scenarios and a relatively rapid shoreface response (K = 7,500 m^3/m/y).

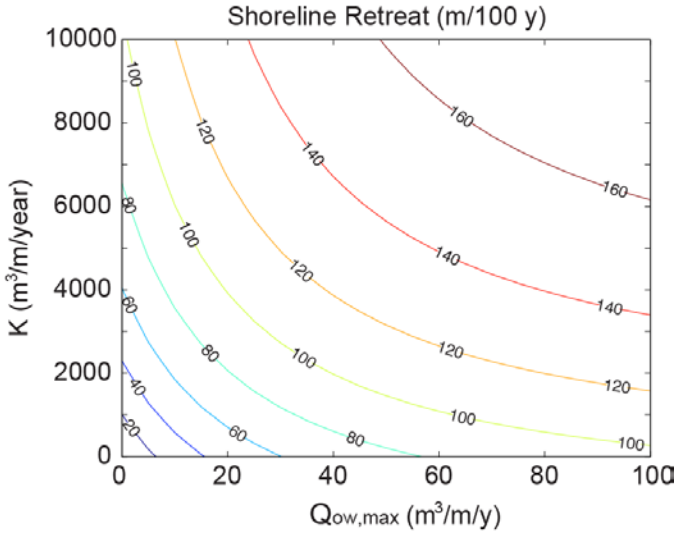

Figure 39. Compilation of model results after 100 years for differing values of the maximum overwash flux and shoreface response rate for the 2m SLR scenario.

Symbol	Meaning	Typical value range
D_T	Shoreface toe or closure depth	17 m
$\dot{z}$	SLR rate (Holocene and future predictions)	Scenario 4 (2m/100y)
D_B	Back-barrier slope	2 m
W_e	Critical barrier width	400 m
H_e	Critical barrier height	2 m
α_e	Shoreface slope at static equilibrium	0.012
K	Shoreface response rate	7,500 m^3/m/y
$Q_{OW,\max}$	Maximum overwash sediment flux	0-100 m^3/m/y
$V_{d,\max}$	Maximum deficit volume	$V_{d,\max} = H_e W_e$

Table 3. Santa Rosa Island geomorphic model input parameter values.

5.3 Camp Lejeune

5.3.1 Storm History Over the Last 8000 years at Camp Lejeune

New River, North Carolina was targeted for coring in an attempt to reconstruct a sedimentary record of geomorphological changes and historical events in the area. Three sites in New River were cored based on CHIRP sub-bottom stratigraphy surveys (Fig. 40). Seismic profiling identified a bright seismic horizon within the estuary. This surface is channel-like in geometry and its location links in with present day bathymetry, but if it was created by fluvial processes, it is not clear how it links to the past drainage of the region. Another possibility is that the channel is the result of scouring processes associated with past inundation events. Cores were collected using push-core and vibra-core methods. A total of 7 cores were collected.

Grain size analysis of one of the cores collected (NR3) contains sequences of coarse sediment, indicative of storm impacts. Relatively few recent event beds are evident, but a coarse grained event bed dating to the late 1950s or early 1960s was likely deposited by Hurricane Donna (1960), which suggests that historically the region was not impacted by many storms intense enough to produce event beds at the site. In contrast, numerous event beds occur between 1400 and 1650 CE. The period of greatest storm activity seen in the record was between 1,000 and 4,000 years ago.

The record also preserved the paleo-transition between a fluvial and estuarine environment around 7,000 years ago. This is indicated by the change in Ti:Sr ratio and the change from a basal sand layer to fine organic sediments, normally present in estuaries.

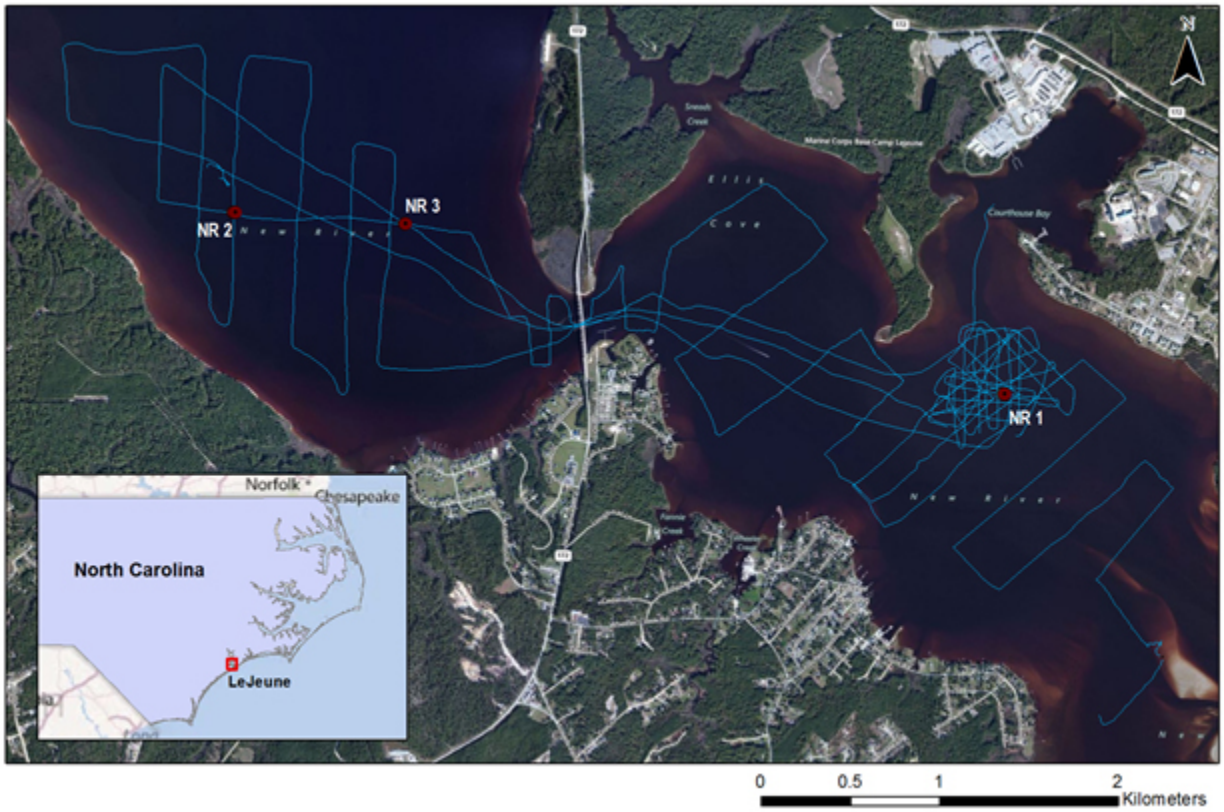

Figure 40. The location of seismic coverage and coring within New River inlet.

The results from New River, NC match well with other records of hurricane activity from the western North Atlantic. In combination, these archives point toward regionally synchronous intervals of intense hurricane activity over the last 1300 years or more (Fig. 41). For example, two intervals of historically unprecedented intense hurricane activity are evident in the Salt Pond reconstruction from Woods Hole, MA over the last 1300 years at 1400-1675 and 750-1100 CE (Donnelly et al. submitted). The most recent active interval at Salt Pond from 1400 to 1675 CE contains at least 9 significant events in 275 years (Fig. 41). Similarly, the Thatchpoint reconstruction (van Hengstum et al., 2013) also reveals a dramatic increase in the frequency of coarse event beds during this interval. Mallinson et al. (2011) document that the Outer Banks of North Carolina had a significant number of inlets cut through the barrier islands during this interval, which was likely a consequence of the increased intense hurricane activity at this time

(Fig. 41). The age of overwash deposits preserved at Onslow Beach fronting CL (Foxgrover, 2009; Yu, 2012) are consistent with these active intervals suggesting these intervals of more frequent intense hurricane activity resulted in overwash (Fig. 41). Radiocarbon dates from backbarrier marsh sediments recovered from the ocean side of the Onslow Beach barrier suggest that the barrier was seaward of its current position prior to 500 years ago. Thus overwash during the interval of increased intense hurricane activity between ~1450 and 1650 CE may have contributed to significant landward translation of the Onslow barrier.

5.3.2 Recent Storm History

According to the NOAA Best Track data set (Landsea et al., 2004), between 1861 and 1999, 13 storms have passed within a 30 nautical mile radius of Jacksonville, NC (Table 3.) This radius encompasses all of New River estuary, the New River Inlet, including the coring sites. The most recent storms that hit are Hurricane Floyd (Cat 2, 1999), Hurricane Bonnie (Cat 2, 1998), and Hurricane Bertha (Cat 2, 1996). One of the most destructive hurricanes to hit this area was Hurricane Donna (Cat 2, 1960.)

5.3.3 Shore Face and Wave Climate Characteristics

Wave data from ~20 years of WIS buoys were used to calculate the morphodynamically representative wave height and wave period for waves impinging on Onslow Bay, NC. Again, we calculate a weighted histogram of the significant wave height to the fifth power for each buoy. ($q_s \propto H^5$). Results are shown in Figures 28 and 42.

Again, this weighting by sediment transport potential results in effective morphodynamic shoreface wave heights that are much larger than the average wave conditions. For Onslow Bay, this results in an estimated effective wave height of 6.8 m, conditions that are rarely exceeded (Fig. 28). In contrast with the Santa Rosa Island case, the weighted distribution for Onslow Bay shows a marked bimodal distribution, with a distinct population of infrequent, high-wave events compared to background conditions. There are two consequences. First, this demonstrates (a perhaps surprising) larger importance of storms in shoreface evolution for Onslow Bay versus Santa Rosa Island, at least over the 20-year wave record we have analyzed. Second, the distribution of the influence of high-energy events is not smooth, suggesting that the 20-year record is insufficient to characterize shoreface dynamics at this site. We note that given the non-stationarity of hurricane strikes we discuss elsewhere, longer records of wave conditions may be averaging over different storm regimes.

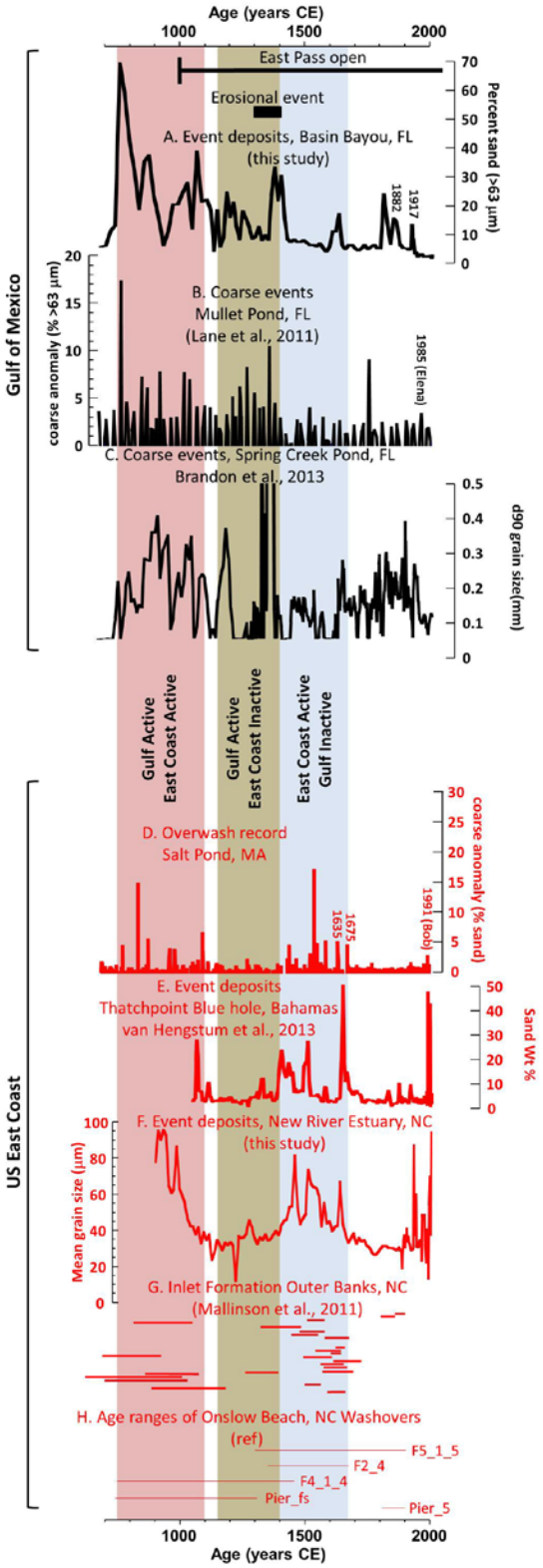

Figure 41 – Hurricane landfall reconstructions and select coastal storm evidence for the last two millennia (black are from the northern Gulf of Mexico; red are records from the East Coast and Bahamas). (A) Overwash event deposits from Basin Bayou, Choctawhatchee Bay, FL. The interval where East Pass is open based on geochemical archive from bay sediments (see Fig. 19). Also noted is age of the large erosional event recorded in bay sediments. (B) Coarse grained anomaly record from Mullet Pond, FL (Lane et al., 2011). The most recent event identified in the archive, Hurricane Elena (1985), is noted. (C) Coarse event beds recorded Spring Creek Pond, FL (Brandon et al., 2013). (D) Overwash record from Salt Pond, MA. Deposits associated with historic hurricanes in 1991, 1675 and 1635 AD are noted. (E) Coarse grained event deposits from Thatchpoint Blue Hole, Bahamas (van Hengstum et al., 2013). (F) Event deposits recovered from New River Estuary, NC. (G) Timing of inlet formation on the Outer Banks of North Carolina (from Mallinson et al., 2001). Length of bar indicates the age uncertainty of inlet activity. (H) Age of washover events from Onslow Beach fronting the New River Estuary (Foxgrover, 2009; Yu, 2012). Shaded light blue interval is when the East Coast of North America experienced heightened intense hurricane activity and the Gulf of Mexico was relatively quiescent. In contrast, the tan shaded interval is when the Gulf of Mexico experienced heightened intense hurricane activity and the East Coast of North America was quiescent. The pink shaded interval is when both the East and Gulf Coasts experienced heightened intense hurricane activity.

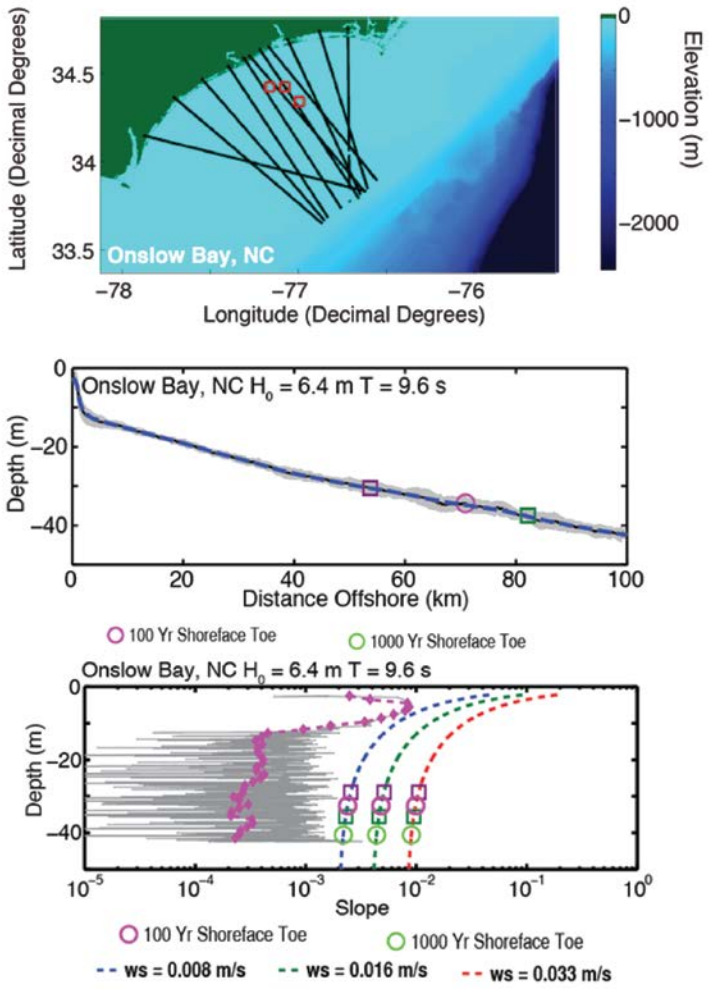

Figure 42. Onslow Bay shoreface characteristics. (Top) Profiles and WIS virtual buoy data used. (Middle) Averaged shoreface profiles with computed morphodynamic depths of closure. (Bottom) Measured and computed dynamic equilibrium shoreface slopes versus depth.

5.3.4 Likelihood Estimates of Storm Surge at Camp Lejeune

The suite of 10,000 synthetic storms generated for the CL region have been used to estimate return intervals for both storm events and, by running each storm event through SLOSH, to calculate surge statistics as a function of storm category (Figs. 43 and 44).

Results shown for CL are filtered for events coming within 125 km of a point along the coast between Wilmington and CL. The diameter of this circle is roughly the same as a coastal segment from Myrtle Beach to Cape Lookout. About 15% of the 10,000 east coast storms pass through this

region and virtually all of the storms generating at least 0.5m surge at CL pass within it. We have chosen to use the radius method to include storms that may parallel the coast either to the east or west that could still generate surge but which would not intersect a coastal segment.

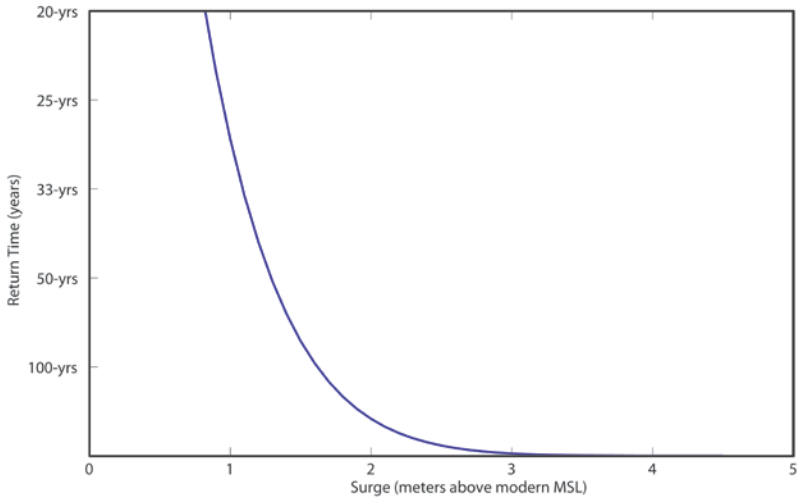

Figure 43. Return times for surge levels at CL under modern climate and sea-level conditions. Return intervals are: 1m surge -28 years; 2m -240 years; 3m -3750 yrs.

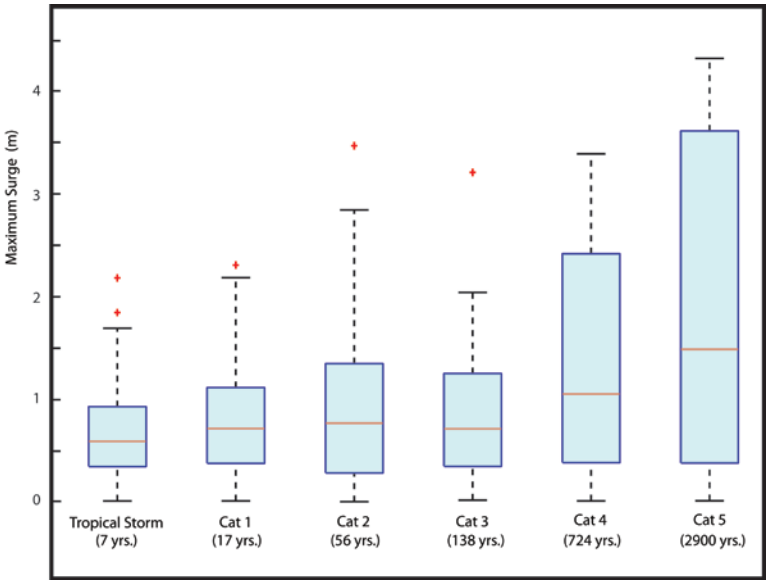

Figure 44. Inundation statistics for the CL region estimated using a suite of 10,000 synthetic storms and the NOAA SLOSH model to calculate storm surge levels. Return intervals for storms of each category are in the parentheses.

5.3.5 Impacts of Nor'Easter Storm Events

The high-resolution modeling package was refined to estimate the impacts of a Nor'Easter event on the barrier fronting CL. As for EAFB, the model was run for a real event for which some level of data are available to act as a groundtruth. The event run was the extra-tropical storm that developed from Hurricane Ida (Nor'Ida), which was a slow moving system lasting several days. The barometric pressure dropped only slightly below 1000hPa near CL on 13-Nov-2009 and hence the barometric pressure setup was only on the order of 0.15 m. The wind direction changed significantly over the course of the storm but reached a maximum around midnight on 12-Nov-2009. The maximum setup from the tides, however, occurred at 17-Nov-2009 around 11 AM when the wind speed had already significantly decayed. The combination of high tide, wind, and barometric setup was calculated to be 0.85 m, not including the wave setup. This value is about 0.3 m lower than the recorded storm surge levels near Wilmington and Beaufort about 70 miles to the southwest and northeast respectively (Fig. 45).

The storm surge at present sea-level and topography does not show significant overtopping of the barrier island near CL. At some locations, the storm waves cause minor overtopping. The very gentle bathymetry leads to wave breaking far offshore, which dissipates substantial energy. However, the maximum flow speed nearshore exceeds the critical flow stage and might have the potential for strong erosion and redistribution of the sediment. Near the New River Inlet waves were able to propagate into the lagoon system and fast moving flow was calculated far behind the barrier, consistent with our suggested model of sediment mobilization from past events in the estuary.

Overtopping becomes much more severe at 0.5 m SLR. Assuming a constant bathymetry and topography (i.e. the present day barrier location and morphology), the storm waves are able to overtop the barrier over wide sections in front of CL (Fig. 46). Compared to the Santa Rosa Island, CL faces more severe problems from storm surge and waves at an elevated sea level of only 0.5 m. Similar to the Gulf site, the wave energy envelope is able to propagate closer to shore at elevated sea levels. Due to the very gentle slope, this shoreward migration of energy results in significantly larger wave heights nearshore than under present sea level conditions. A SLR scenario of 1m causes even more extensive overtopping across virtually the entire dune system. Higher SLR calculations of 1.5 and 2.0 m drown the barrier and open the path for the storm waves to enter the lagoon system (Fig. 47). At this stage, large parts of CL would be inundated and exposed to erosive waves during storm events.

It should be noted that these scenarios were computed with the same bathymetry and topography as the modern sea-level scenarios and only the water level was raised. This provides good insight into the hydrodynamic conditions for such constellations of sea floor and water level, however, it is

highly unlikely that the barrier island systems maintain their current shape and composition over the course of the next century.

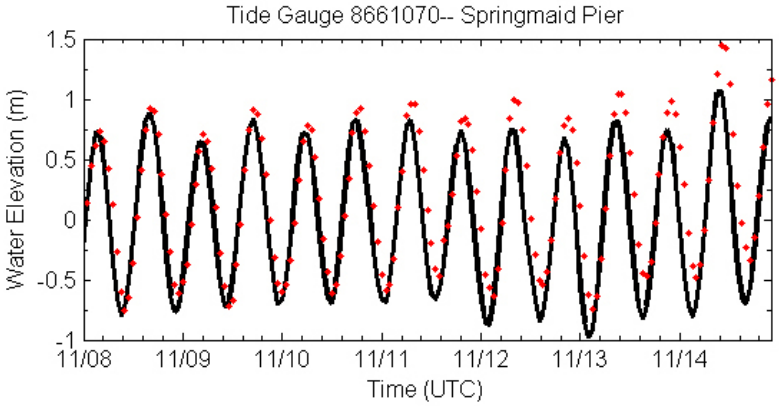

Figure 45. Modeled and observed tide levels for the duration of the Nor'Ida event.

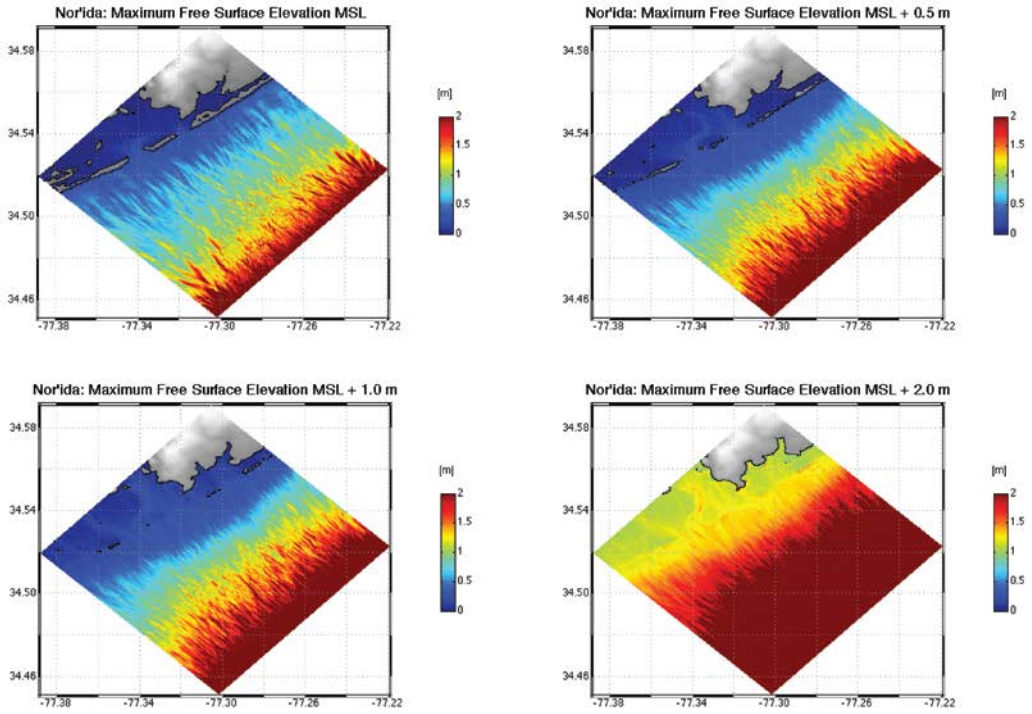

Figure 46. The projected impacts of Nor'easter storm Nor'Ida for the 4 sea-level scenarios. The barrier is fixed at its present day morphology for each run.

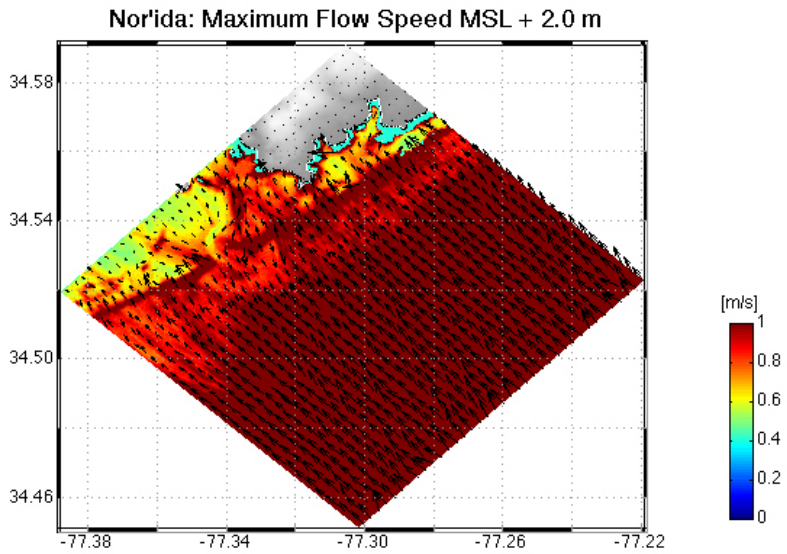

Figure 47. Maximum flow speed during an event with the same characteristics as the Nor'Ida storm but at 2m higher sea-level. In this situation, the present day barrier would be completely overtopped with storm waves impacting the mainland coast.

Extratropical storms are only rarely expected to result in complete barrier inundation, and then only at barriers with exceptionally low elevations, although some events can result inoverwash of sediment. The anaylsis of the Nor-Ida event at CL, does not show overtopping under modern conditions. As such, sediment is likely removed from the beachface into the offshore region, but under conditions of reasonable K parameter (wave action) most, if not all of this sediment will be replaced onto the barrier over the months following the storm.

5.3.6 Model Results for Camp Lejeune Using Field-Based Observations of Overwash Flux.

Similar to the model application to Santa Rosa Island, we perform exploratory model experiments for Onslow Beach in CL. The prototype barrier geometry (Figs. 48, 49) shows a rather shallow break in the submarine slope at ~11m. Previous studies (e.g., Riggs et al., 1996) demonstrate that the lower portions of this shoreface are dominated by outcropping hard lithology. Consequently, the lack of offshore mobile bed sediment causes the relevant shoreface depth for this coast to be significantly more shallow than the morphodynamic closure depth we compute (~30m). A suite of simulations was performed to understand the potential long-term evolution of single barrier profiles for different sea-level scenarios and for different values of the maximum overwash rate (Fig. 49).

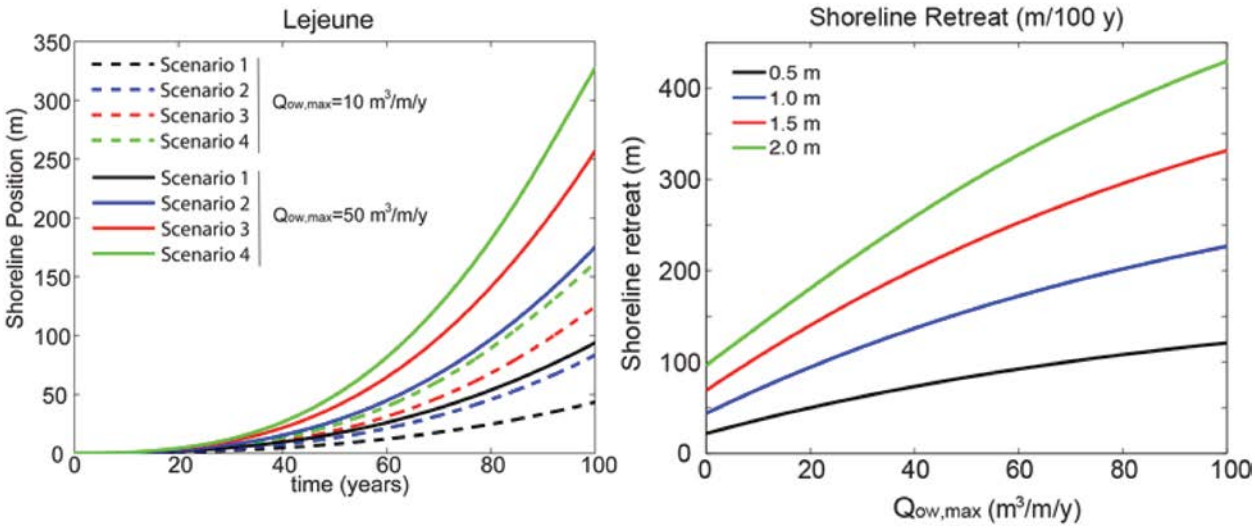

Figure 48. Onslow Beach geomorphic modeling results. (Left) Representative shoreline evolution for the project scenarios for selected values of $Q_{OW,max}$ and K = 10,000 m^3/m/y. (Right) Shoreline recession versus $Q_{OW,max}$ for the four prescribed SLR scenarios and a relatively rapid shoreface response (K = 10,000 m^3/m/y).

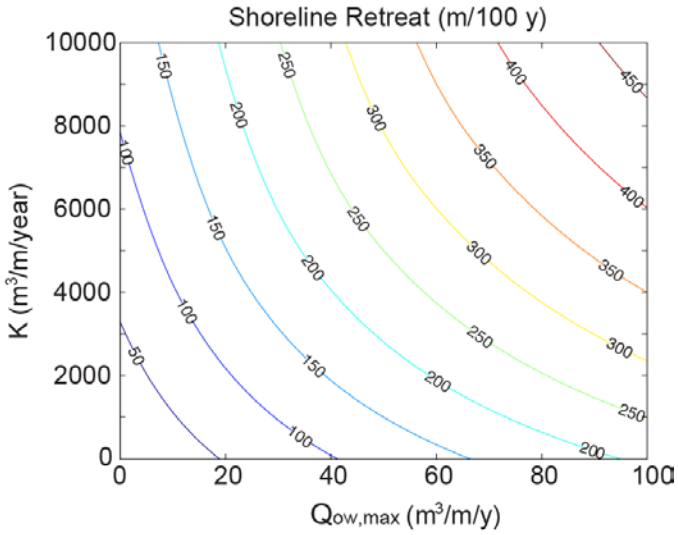

Figure 49. Compilation of model results after 100 years for differing values of the maximum overwash flux and shoreface response rate for the 2m SLR scenario.

Symbol	Meaning	Typical value range
D_T	Shoreface toe or closure depth	11 m
$\dot{z}$	SLR rate (Holocene and future predictions)	Scenario 4 (2m/100y)
D_B	Back-barrier depth	5 m
W_e	Critical barrier width	200 m
H_e	Critical barrier height	3 m
α_e	Shoreface slope at static equilibrium	0.005
K	Shoreface response rate	10,000 m^3/m/y
$Q_{OW,\max}$	Maximum overwash sediment flux	0-100 m^3/m/y
$V_{d,\max}$	Maximum deficit volume	$V_{d,\max} = H_e W_e$

Table 4. CL input parameter values.

Estimates of modern rates of barrier overwash flux for the CL site are not as clear as those for the Eglin site. In results for the DCERP project, Foxgrover (2009) demonstrates that overwash deposits along Onslow Beach have average depths of ~1 m and are within the general range of 0.5-2 m. For an estimated barrier width of 250 m, this suggests a width-averaged volume of ~250 m^3/m. The timing of this emplacement, however, is undetermined, and may represent decadal, centennial, or longer deposition. Assuming the deposit occurred in a single event, and using the return times of ~30yr for a 1m surge and ~240yr for a 2m surge event suggests that the overwash flux in the southern portions of the barrier, where elevation is between 1-2m, is in the range of 1-10m^3/m/yr. This estimate does not include aeolian transport. Given the uncertainty, we emphasize two scenarios with a high-estimate flux (50 m^3/m/y) and a more modest rate (which may still be higher than current rates, 10 m^3/m/y). We note that the lower lying southern reach of the island is experiencing shoreline erosion of up to 3m/yr, perhaps suggesting that higher rates are applicable (Foxgrover, 2009).

Even in the absence of overwash, model results suggest higher rates of shoreline recession at CL. With no overwash, the model reproduces Bruun-type shoreline change, driven by the shoreface slope. The lower slope of the Onslow Beach shoreface suggests higher shoreline recession for a given SLR. Note also that the increase in shoreline change for increasing overwash does not show the same limiting behavior as overwash fluxes approach 100m^3/m/y for CL as for EAFB. This suggests that the local geometry of the Onslow Beach barrier requires a greater quantity of

overwash to translate the existing barrier geometry intact as sea-level rises. This increased potential for shoreline recession is beyond that suggested by the shoreface slope, and is driven by the subaerial barrier geometry. There therefore exists a much greater potential for SLR-driven shoreline recession at this site. In the absence of sufficient overwash flux, this makes the loss of barrier more likely.

6. Conclusions and Implications for Future Research/Implementation

6.1 Barrier Morphology Under Conditions of Accelerated Sea-Level Rise

The barriers at EAFB and CL have developed and built themselves through wave-driven coastal processes, including barrier overwash which has helped develop barriers above sea level as they have slowly risen over the previous millennia. Continued existence of these barriers for higher sea levels over the coming century requires continued and possibly increased rates of overwash. The geomorphic model simulations presented here demonstrate the importance of overwash in maintaining intact barriers as sea level rises. Given the uncertainty in quantifying future overwash rates, the model is able to provide envelopes of shoreline change for different potential overwash fluxes. We have attempted to estimate current overwash fluxes at both sites as a guide for potential future barrier configurations. Both sites are currently experiencing low overwash rates that would be insufficient for barriers of the same width and height to maintain themselves for all four given SLR scenarios. Note, however, that the field/model inter-comparisons are limited as we are comparing modern measured overwash fluxes, which may be less than the maximum potential rate. Overwash fluxes may increase as sea level rises and inundation events become more frequent. As such, the model results presented here allow an estimation of how increases in overwash may affect shoreline change. Also, climate-change-induced variations in wave climate and storm frequency may change the potential rates of inundation and overwash.

The modeling does not account for the potential of human activities to alter the beach. Such activities include “beach nourishment” (placement of sandy fill on the upper shoreface), inlet alteration/dredging, and emplacement of engineering structures. Other human-induced changes to the barrier will also affect the future trajectory of these barriers. While the hydrodynamic simulations demonstrate the susceptibility of these barriers to damaging storms, the geomorphic modeling also demonstrates the interconnection between shoreline change and SLR. Sea-level rise will drive shoreline retreat along all sandy coasts, and management of base infrastructure at the shoreline should be performed to accommodate these changes. Hard armoring practices may prevent or delay buildings from loss, but such engineering activities will not prevent or reverse shoreline erosion. Consequently, beaches will be lost in front of and adjoining any hard armoring.

Given the increase in shoreline recession caused by overwash, shoreline change could be reduced by other activities such as dune and berm construction which could reduce overwash frequency. However, SLR will continue to drive coastal profiles landwards. In this case, reduction of overwash will increase the potential for in-place drowning of barriers.

6.2 Climatic Forcing of Regional Hurricane Patterns: Tying into the Basin-Wide Picture

Climate controls the characteristics of hurricane populations by providing the range of environmental conditions that influence the formation and life histories of tropical cyclones (e.g., Gray, 1968; Emanuel, 1987; Emanuel, 1988; Emanuel et al., 2004; Kossin et al., 2010). Tropical cyclones are also important, active components of Earth's climate system as they facilitate significant heat transport within and between the atmosphere and ocean (Emanuel, 2001; Emanuel, 2002; Scott and Marotzke, 2002; Sriver and Huber, 2007; Hart et al., 2007; Korty et al., 2008; Sriver et al. 2008; Hart, 2010; Woodruff et al., 2011). The manner in which climate and hurricane activity co-evolve has critical implications for society and is not well understood. Fluctuating components of the climate system like the El Niño Southern Oscillation (ENSO) (Gray, 1984), Madden-Julian Oscillation (MJO) (Klotzbach, 2010), Quasi-Biennial Oscillation (QBO), Atlantic Multidecadal Oscillation (AMO), and the Atlantic Meridional Mode (AMM) (Vimont and Kossin, 2007) influence Atlantic hurricane activity on timescales ranging from the intraseasonal to the multidecadal. Unfortunately, the short observational record is neither sufficient for identifying the components of climate that are influencing storm activity on centennial and longer timescales, nor capable of resolving hurricane-climate interactions during climatic regimes not analogous to the instrumental period (e.g., global warming or cooling, significant shifts in ocean-atmospheric circulation).

Kossin and Vimont (2007) argue that AMM dynamics provide an overarching framework for understanding hurricane activity in the modern climate, particularly for storms forming in the main development region (MDR) (Fig. 50). We suggest that examining the role of AMM-like dynamics on centennial timescales is essential for examining tropical cyclone dynamics on geological timescales as well. Kossin and Vimont (2007) convincingly argue that the AMM plays a significant role in driving interannual hurricane variability. The AMM is a dynamical mode of coupled ocean and atmosphere variability in the Atlantic, which manifests as a cross equatorial gradient in sea surface temperature (SST) and a shift in the Intertropical Convergence Zone (ITCZ) toward the warmer hemisphere, in other words: a positive (negative) AMM shifts the ITCZ northwards (southwards).

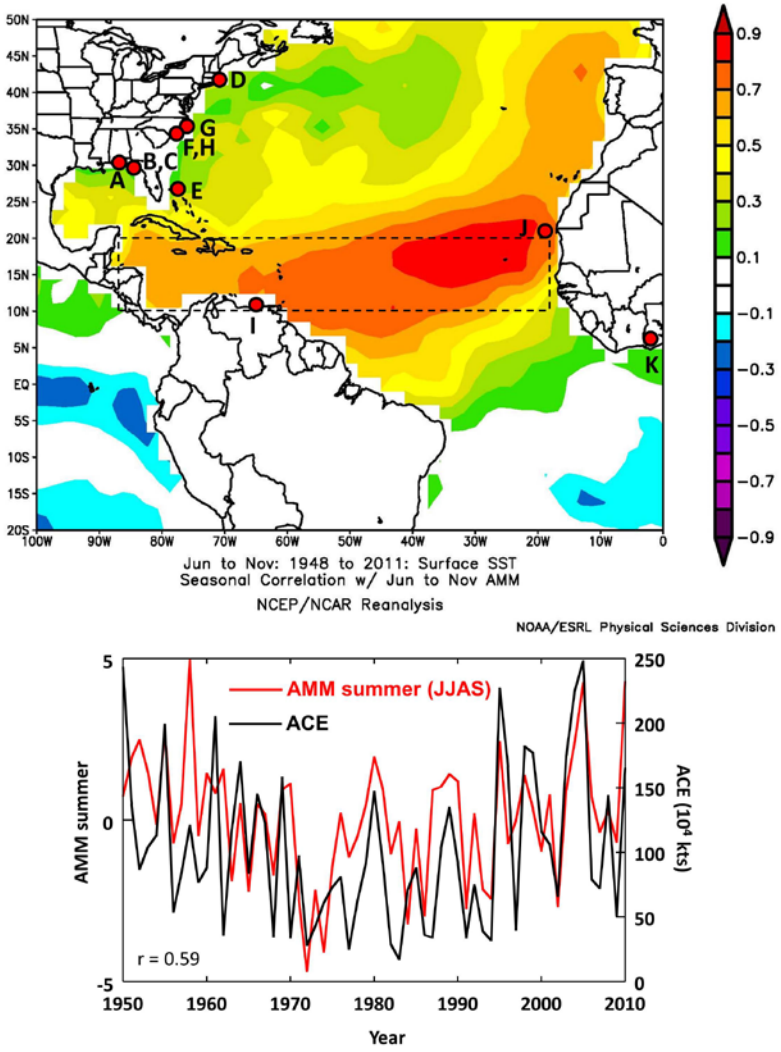

Figure 50 – (top) Correlation map of boreal summer SST and Atlantic Meridional Mode (AMM). SSTs are warmer during positive AMM. The main development region for North Atlantic tropical cyclones is noted in the dashed box. Locations of paleo-proxy records (A-K) shown in Figure 41 and 52 are as labelled. (bottom) 1950 to 2010 time series of Atlantic accumulated cyclone energy (ACE) and summer AMM.

Furthermore, the AMM influences several other factors that are critical tropical cyclone modulators across the MDR, including vertical wind shear, low-level vorticity, static stability, and sea level pressure (Kossin and Vimont, 2007). In addition to warmer SST in the MDR of the tropical North Atlantic (Fig. 50), a positive AMM phase is also characterized by increased low-level vorticity, decreased vertical wind shear and sea level pressure, which collectively increase cyclogenesis and potential intensity. The relationship of AMM to tropical cyclone activity in the North Atlantic is easily seen when comparing the AMM Index with accumulated cyclone energy (ACE) index (Fig. 50) and manifests itself on multi decadal timescales with the relationship between AMO and Atlantic hurricane activity (e.g., Goldenberg et al., 2001; Zhang and Delworth, 2006; Klotzbach, 2011). Tropical Atlantic precipitation is also impacted by AMM/AMO. Some

modeling studies suggest a shift toward more positive AMM-like conditions over the next century in response to greenhouse gas forcing (e.g., Doi et al., 2013). AMM/AMO-like variability occurs through much of the Holocene at multidecadal (e.g., Knudsen et al., 2011; Wei and Lohmann, 2012) as well as centennial to millennial timescales (e.g., Haug et al, 2001; Shanahan et al., 2009; etc.), with changing SSTs and the position of the ITCZ resulting in significant variability in precipitation across the tropics. These AMM-like shifts in ITCZ position and MDR SST have been linked to variability in Atlantic Meridional Overturning Circulation (e.g., Knudsen et al., 2011; Wei and Lohmann, 2012; Mulitza et al., 2008). AMM-like variability significantly impacts modern hurricane activity and likely played an important role in driving hurricane activity on longer timescales, yet has been relatively neglected in paleo-hurricane analysis over the late Holocene.

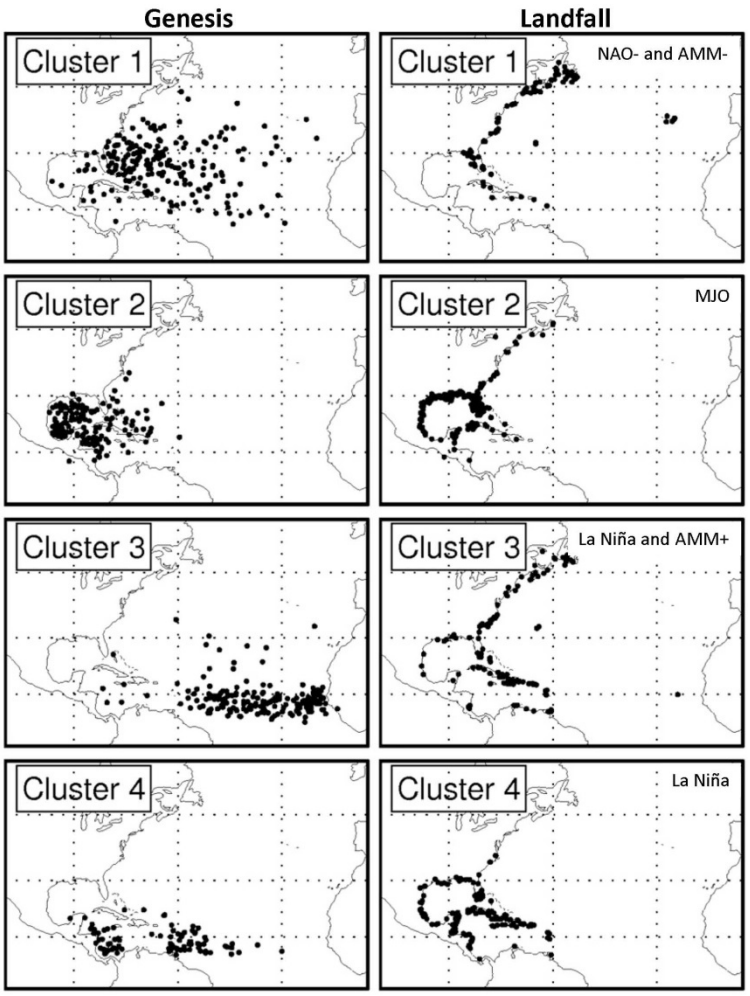

Figure 51. Different hurricane populations based on their location of genesis and track, as revealed by Cluster Analysis (Kossin et al., 2010). These populations accord well with known hurricane climate forcings: Cluster 1-Negative North Atlantic Oscillation (NAO) and negative AMM and southward ITCZ, Cluster 2-MJO, Cluster 3-La Niña and Positive AMM and northward ITCZ, Cluster 4-La Niña.

Obviously, total Atlantic hurricane activity is a function of when and where cyclogenesis occurs, track, and intensity (Elsner, 2003; Kossin and Camargo, 2009; Kossin et al., 2010; Colbert and Soden, 2012). The location of cyclogenesis also significantly impacts ultimate storm intensity, as longer lived storms tend to become more intense. Cluster analysis of Atlantic tropical cyclones from 1950 to 2007 further reveals the relationships between four different hurricane populations and various modes of climate variability, including AMM (Fig. 51; Kossin et al., 2010). Cluster 1 comprises tropical cyclones forming north of the MDR and off the southeastern coast of the US. These storms make up a substantial portion of the hurricane landfalls along the eastern seaboard of the North America. For example, 53% of the landfalling hurricanes in New England since 1851 CE (10 of 19) were Cluster 1 storms. Kossin et al. (2010) found that the rate of Cluster 1-type hurricanes increase during a more negative NAO. In addition, increased cyclogenesis off the southeastern U.S. is more frequent when AMM is negative (Kossin and Vimont, 2007). In contrast, Cluster 2 storms that form in the extreme western Caribbean and Gulf of Mexico are most strongly influenced by the Madden-Julian Oscillation (MJO) (Kossin et al., 2010). Cluster 3 storms, which generally form in the MDR, are enhanced by La Niña and positive AMM, and in the case of Cape Verde type storms, are sensitive to the strength and position of the African Easterly Jet. The majority of landfalling Cluster 3 storms impact the Caribbean and eastern seaboard of North America (e.g., 35% of the New England hurricane landfalls have been Cluster 3 storms). Finally, Cluster 4 hurricanes form in the western MDR and southern Caribbean and they tend to track westward and make landfall in the Caribbean and Gulf of Mexico. These Cluster 4 storms are most strongly modulated by ENSO, with La Niña conditions favoring their development. Thus, this Kossin et al. (2010) cluster analysis provides a useful framework for understanding the past geographic patterns of hurricane activity occurring at longer timescales, as observed through sedimentary reconstructions.

Mann et al. (2009) produced a statistical model to estimate basin-wide hurricane activity over the last 1500 years primarily based on reconstructions of Niño3 SST and MDR SST. The model predicts increased basin-wide activity between 900 and 1100 CE, when La Niña like conditions existed in the eastern tropical Pacific and MDR SSTs were relatively warm. This interval overlaps with the interval in which both the Gulf and East Coasts are very active between 750 and 1100 CE, but the model does not predict the increased activity between 750 and 900 CE. Nor does the model predict other intervals of increased intense hurricane activity reconstructed in our new high-resolution records (Fig. 41). For example, in addition to the 750-1100 CE interval, both the Gulf sites (Basin Bayou, Mullet Pond and Spring Creek Pond) and East Coast (Salt Pond) experienced elevated levels of intense hurricane landfalls between 400 and 625 CE. In contrast, they were anti-phased from 1150 to 1400 CE when the Gulf was active and East coast (i.e., Salt Pond) was quiescent, and they were also anti-phased from 1500 to 1675 CE when Salt Pond and Thatchpoint

record the highest frequency of major events of the last two millennia, but the Gulf Coast was quiescent (Fig. 41). Neither the active interval in the Gulf between 1150 and 1400 CE, nor the active interval in along the East Coast between 1500 and 1675 CE are predicted by the Mann et al. (2009) model. The anti-phasing of intense hurricane activity between the East and Gulf coasts may point to basin-wide changes in hurricane tracks (as suggested by Elsner et al., 2000; Liu and Fearn, 2000). However, given the variability is in the most intense storms, regional controls on the frequency of intense hurricanes (e.g., loop current penetration in the Gulf of Mexico; Lane, 2011; Lane and Donnelly, 2012) and/or changes in the location of cyclogenesis that favor more intense hurricanes striking the Gulf or East Coast likely also have driven spatial variability in Atlantic paleohurricane records. Therefore, factors other than ENSO and MDR SSTs (at least as reconstructed by Mann et al., 2009) are at times likely driving active hurricane intervals in the Gulf of Mexico versus the East Coasts.

A large number of tropical paleoclimatic proxy records point to significant and spatially coherent centennial-scale changes in SST and the position of the ITCZ over the last several millennia (e.g., Haug et al., 2001; Hodell et al., 2005; Moy et al., 2002; Poore et al., 2004; Conroy et al., 2008; Shanahan et al., 2009), similar to those of the AMM and AMO discussed above. For example, we show the Ti based runoff record from the Cariaco Basin off Venezuela (Haug et al., 2001; I on Figs. 50 and 52), the summer SST reconstruction off West Africa (deMenocal et al., 2000; J on Figs. 50 and 52), and the Si based lake-level record from Lake Bosumtwi (Shanahan et al., 2009; K on Figs. 50 and 52). These records display a pattern of variability that indicates centennial scale AMM-like variability with warm summer SST phases off West Africa accompanying increases in runoff in Venezuela (Ti increases; Fig 52F) and higher lake levels in tropical West Africa (Si increases; Fig. 52G) indicating a more northern position of the ITCZ. Conversely, when summer SSTs are cooler off West Africa, Venezuelan runoff is reduced (Ti decreases) and lake levels decline in tropical West Africa (Si decreases), which indicates that the ITCZ occupied a more southerly position.

Intervals when both the Gulf and East Coasts experienced elevated levels of intense hurricane strikes (400-625 CE and 750-1100 CE) occurred when the ITCZ was in a northerly position and SSTs in the MDR were warmer. When the East Coast experienced heightened intense hurricane activity (e.g., 1400-1675 CE), but the Gulf is quiescent, the ITCZ was transitioning south or was at a more southerly position. The interval between 1150 and 1400 CE, when the Gulf experienced heightened intense hurricane landfalls, but the East Coast is inactive, is one in which the ITCZ is transitioning north or was at a more northerly position.

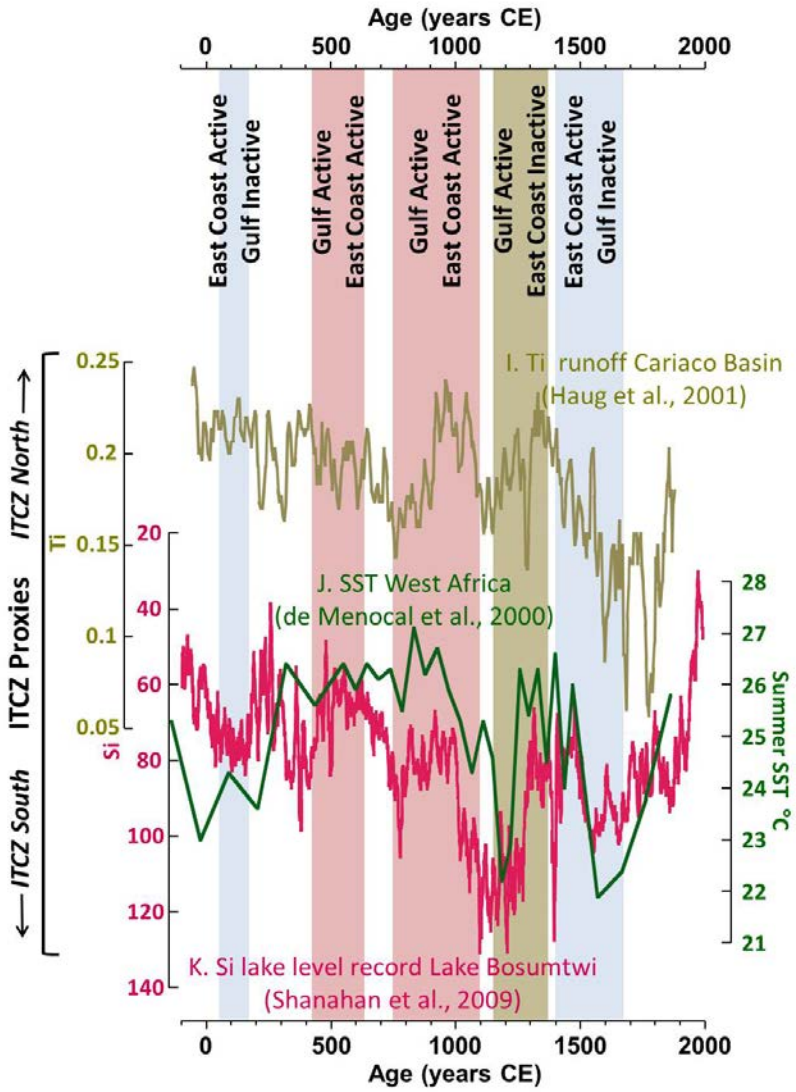

Figure 52 – (I) Ti based runoff record from the Cariaco Basin, Venezuela (Haug et al., 2001). (J) Summer SST reconstruction from off West Africa (deMenocal et al., 2000). (K) Si based lake level proxy from Lake Bosumtwi, Ghana (Shanahan et al., 2009). Shaded light blue intervals when the East Coast of North America experienced heightened intense hurricane activity and the Gulf of Mexico was quiescent. In contrast, tan shaded intervals are when the Gulf of Mexico experienced heightened intense hurricane activity and the East Coast of North America was quiescent. The pink shaded intervals are when both the East and Gulf Coasts experienced heightened intense hurricane activity.

These correlations between regional intense hurricane landfalls and tropical proxy records of MDR SST and ITCZ position, combined with the modern climatological connections between AMM/AMO variability and modern hurricane activity suggest that both basin-wide and regional controls on hurricane activity have been at play over the last few millennia. Intervals when the ITCZ is in a more northerly position and both the Gulf and East Coasts are active suggest more cyclogenesis in the deep tropics is responsible for the elevated levels of activity. At other times when only one of the regions experiences elevated intense hurricane activity regional climatic controls are likely at play.

The point we are making here is that the storminess encountered in a given region is subject to interplay between many complex climate variables. We see in the sedimentary records at both EAFB and CL evidence for major variations in storminess well before the impacts of human induced climate change that are corroborated at other locations across their respective ocean basins. Even as a result of natural climate variability storms can turn on and off in a given location, although there are basin wide trends to the activity levels. With future climate changes this behavior seems likely only to become more complex, and so understanding the base drivers for storms is an important starting point. It is also worth pointing out that areas that currently don't experience hurricane impacts (southern California) for instance, could do so in the future with appropriate changes in driving conditions.

6.3 Generalized Approaches for Assessment of Barrier System Vulnerability

The results of our program highlight several critical issues that should be specifically evaluated or taken into consideration as part of any vulnerability assessment for installations fronted by or which rely on barrier beach systems.

The geometry of the barrier system, including the back-barrier lagoonal system and offshore bathymetry, provide the framework within which the barrier evolves. Detailed data of barrier topography and offshore bathymetry is needed for accurate inundation modeling, and geometric as well as geologic data are required to understand potential geomorphic changes, including the effect of geologic controls. Such characterization should include best modern practices, including, but not limited to: LIDAR surveys of the subaerial barrier, bathymetric mapping of the shoreface, and geologic characterization of the barrier, backbarrier, and shoreface environment. *We recommend that the geometry and geology of the entire system should be determined with a reasonably high level of precision and detail.*

Sea-level rise rate is obviously a critical parameter in determining the stability and viability of a barrier system, but it is not the only parameter. For a given barrier and shelf geometry, the two critical environmental parameters that act as predictors of barrier behavior are the flux of sediment transported across the barrier towards the back-barrier region and the offshore wave climate. In our analysis, we have assumed that wave climate remains consistent through the coming century. The flux of sediments is largely controlled by the frequency of major storms hitting a given area: in a somewhat counter-intuitive manner, storm impacts can actually be beneficial to the long-term health of a barrier by facilitating landward migration of the barrier. However, as we have seen from sediment cores, the natural variability in storm activity in a given region can give rise to periods of heightened storm impacts, with short return intervals of major storms shaping the barrier morphology by cutting inlets which do not have time to heal before the next storm hits. Under such conditions, the shoreline morphology is likely one of shortened and segmented stretches of barrier

with increased exchange between the ocean and backbarrier and potentially greater exposure of the mainland to storm impacts. Although the probabilities of both extra-tropical and tropical storm inundation events, where they both occur, should be considered, we note that our modeling of the Nor-Ida event at CL does not show evidence of overtopping under modern conditions. As such, sediment is likely removed from the beachface into the offshore region where it is available to be returned to the beach during calmer conditions. *We recommend an analysis of storm recurrence intervals for a given region using statistical approaches to determine likely intervals between inundation events.*

In the light of the importance of overwash flux, estimates of the landward transport of sediment, either through storm-driven overwash or through aeolian transport, is a critical parameter in assessing the long-term health of the barrier. We have demonstrated several ways of estimating this flux for modern conditions, which may shed light on future potential overwash flux rates. In many communities, armoring does not permit overwash to occur with potentially serious implications for the decadal barrier evolution. *We recommend that field studies be carried out to gain an understanding of across-barrier sediment transport.*

Understanding net rates (and for deeper depths, in some cases the direction) of sediment transport across the wave-dominated shoreface remains a cornerstone challenge of coastal sediment transport. In particular, measuring and estimating lower shoreface transport processes across long time-scale remains a challenge, particularly as bed changes should asymptote to rates of relative SLR, on the order of a few mm/y. The effects of outcropping or slightly buried lithology presents an additional control on shoreface sediment transport and dynamics. *In addition to continued emphasis on shoreface sediment transport processes, we recommend field studies to characterize the shoreface and underlying geology. Given significant gaps in knowledge, modeling or other predictive exercises should explore a broad range of parameter space when assessing estimates of long-term shoreface sediment transport. Most importantly, we emphasize that wave conditions should be weighted by their influence on morphologic processes.*

Understanding inundation risk arising from large storms can be accomplished through use of one of a suite of available tools. We stress the importance of benchmarking the chosen model suite against one or more known events. We also stress the importance of sampling the suite of likely events that might threaten a given location: a small change in storm track can result in very different storm surge. In many cases, the NOAA Best Track database of historical storms does not adequately represent the range of storms possible for a given location. *We recommend running a detailed suite of inundation models with a large ensemble of storm events that are plausible for a specific location or installation.*

Finally, we note that storminess is highly non-stationary: regions experience great variability in storminess and regions that are not perceived to be at risk at present could experience events in the future, especially under conditions of climate change. *We recommend evaluating the sedimentary record in a given area to understand the long term risk of storm impacts.*

6.4 Gaps in Ability/Knowledge

In our analysis, we have assumed that wave climate remains consistent through the coming century. Clearly, the potential exists for changes in wave climate related to broader climate change. Assessment of such changes relies on future scenario climate models.

Significant disagreement exists between model projections for how Atlantic hurricane activity will respond to future anthropogenic forcing (Knutson and Tuleya, 2004; Vecchi and Knutson, 2008; Knutson et al., 2008; 2010; Vecchi and Soden, 2007). Global-scale numerical climate models (GCMs) have had difficulty simulating intense tropical cyclones in both present and projected climate conditions (Gualdi et al., 2008; Knutson et al., 2008; Zhao et al., 2009). Some studies over the last decade have proposed a linked human-induced climate change, which is thought to have increased sea surface temperatures (Levitus et al., 2000; Levitus et al., 2001), and the frequency and intensity of tropical cyclones (Webster et al., 2005; Emanuel, 2013; Emanuel et al., 2008). However, detection of historic trends in tropical cyclone activity and thus any attribution to human-induced warming is hampered by the shortness and observational biases of the instrumental record (e.g., Holland and Webster, 2007; Kossin et al., 2007; Landsea, 2007; Mann et al., 2007; Elsner et al., 2008; Chen et al., 2009). However, recent advances have been made toward more realistic hurricane intensity distributions in storm climate modeling (Emanuel et al. 2008, Bender et al. 2010). One such technique is the statistical-deterministic downscaling method of tropical cyclone climate developed by Emanuel et al. (2006). In this method, a large number of synthetic but climatologically-plausible tropical cyclone events are generated.

While many modeling studies have pointed toward an overall global decrease in tropical cyclone frequency with a shift to more intense storms (see Knutson et al., 2010 for review), significant regional variations in the response of tropical cyclone activity to future warming are possible. For example, recent downscaling of several Coupled Model Intercomparison Project (CMIP)5 models indicate that climate warming may cause more frequent and intense hurricanes along the eastern seaboard of the U.S. over the coming decades (Emanuel, 2013).

Coupling event (e.g. storm) driven sediment transport to the longer term barrier evolution requires a coupling between two distinct modeling approaches, presumably through a statistical approach, that has not yet been solved. A significant challenge for modeling long-term coastal behavior is

that we have to integrate changes that typically occur during short temporal scales (storms). In our current version of the model we approach this issue by assuming the existance of a single characteristic event, which is responsible for controling the long-term evolution of the barrier, but in reality temporal changes in the frequency and intensity of storms can vary significantly (e.g., Donnelly and Woodruff, 2007; Lane et al., 2011). Moreover, our current model uses a simplified relationship for storm overwash, which relies upon the critical width concept (Leatherman, 1983). This formulation is obviously a simplification as barrier overwash depends not only on the barrier geometry but also on the hydraulic forcing caused by storms. Thus, a major future modeling effort would be required to (1) extend the barrier evolution model to incorporate changes in the storm frequency and intensity, and (2) develop wave and flow-driven sediment transport parameterizations that will permit the barrier evolution model to capture changes in hydraulic forcing. Such parameterizations will need to be sufficiently complex to allow the range of driving processes to interact in a physically realistic manner, yet simple enough that the contributions from each component can be analyzed and understood. Estimating overwash flux from deposits has been done for the Eglin region but this does not capture sediment transported into the backbarrier lagoon. Aeolian flux can be simply added to the shoreward flux of sediment if a good estimate of the transport is obtained from field measurements. Tying estimates of overwash flux to predictions from hydrodynamic models, coupled with pre- and post-storm LIDAR data for a range of events is one way we can envision to improve our understanding of the volumes of sediment moved during storms. Ultimately the model will allow us to directly address the question of whether barriers can adequately survive a given frequency and intensity of storms (developed from our previous analyses of storm return intervals and the volumes of sediment transported during specific events) and at a given SLR rate. The geometries simulated using the model for barrier evolution will be input into the hydrodynamic model to determine the impacts of predicted landscape changes.

Communities frequently respond to coastal changes by stabilizing the shoreline via beach nourishment (i.e., periodic placement of sand at the eroding shoreline) and/or the construction of hard structures (e.g., sea walls and jetties). The effects of shoreline stabilization decisions will dynamically feedback into coastal evolution, but very few models explore these dynamics (Smith et al., 2008). We have extended the morphodynamic model for barrier evolution presented above to account for shoreline protection activities. This component of the model was not needed for either the Eglin or Lejeune systems, as neither are actively engaged in beach nourishment, but in many cases could be an important component of any projection modeling.

7.0 References

Amante, C. and B.W. Eakins, 2009. ETOPO1 1 Arc-Minute Global Relief Model: Procedures, Data Sources and Analysis. NOAA Technical Memorandum NESDIS NGDC-24, 19 pp, March 2009.

Ashton, A.D., A.C. Ortiz, 2011. Overwash controls coastal barrier response to sea-level rise. Coastal Sediments '11, Miami FL, ASCE.

Bagnold, R.A., 1963. Mechanics of marine sedimentation, The Sea: Ideas and Observations. Interscience, New York.

Bailard, J.A., 1981. An energetics total load sediment transport model for a plane sloping beach. J. Geophys. Res. 86, 10,938-910,954.

Bender, M.A., T.R. Knutson, R.E. Tuleya, J.J. Sirutis, G.A. Vecchi,S.T. Gerner, I.M. Held, 2010. Modeled impact of anthropogenic warming on the frequency of intense Atlantic hurricanes. Science. 327(5964), 454-458.

Bloom, A.L., 1964. Peat accumulation and compaction in a Connecticut coastal marsh. J. Sed. Petrol., 34, 599-603.

Blum, M.D., A.E. Sivers, T. Zayac and R.J. Goble, 2003. Middle Holocene sea-level and evolution of the Gulf of Mexico coast: Transactions - Gulf Coast Association of Geological Societies, v. 53, p. 64– 77.

Booij, N. C., R. C. Ris, and L. H. Holthuijsen, 1999. A third-generation wave model for coastal regions: 1. Model description and validation, J. Geophys. Res., 104(C4), 7649– 7666.

Bowen, A.J., 1980. Simple models of nearshore sedimentation. Beach profiles and longshore bars, in: McCann, S.B. (Ed.), The Coastline of Canada. Geological Survey of Canada.

Brandon, C.M., J.D. Woodruff, D.P. Lane, J.P. Donnelly, 2013. Tropical cyclone wind speed constraints from resultant storm surge deposition: A 2500 year reconstruction of hurricane activity from St. Marks, FL. Geochem., Geophys., Geosys. 14, doi:10.1002/ggge.20217.

Bruun, P., 1962. Sea-level rise as a cause of shore erosion. Proceedings of the ASCE, J. Waterways and Harbors Division, 88, 117-130.

Chen, K., J. McAneney, K. Cheung, 2009. Quantifying changes of wind speed distributions in the historical record of Atlantic tropical cyclones. Natural Hazards and Earth System Sciences. 9, 1749-1757.

Cheung, K.F., A.C. Phadke, Y. Wei, R. Rojas, Y. J.-M. Douyere, C.D. Martino, S.H. Houston, P.L.-F. Liu, P.J. Lynett, N. Dodd, S. Liao, E. Nakazaki, 2003. Modeling of storm-induced coastal flooding for emergency management, Ocean Eng., 30(11), 1353– 1386.

Cheung, K.F., L. Tang, J.P. Donnelly, E. Scileppi, K.-B. Liu, X.-Z. Mao, S.H. Houston, R.J. Murnane, 2008. Numerical modeling and field evidence of coastal overwash in southern New England from Hurricane Bob and implications for paleotempestology, J. Geophys. Res., 112.

Cleary, W.J. and P.E. Hosier, 1987. Onslow Beach, North Carolina: morphology and stratigraphy. Proc. Coastal Sediments '87. Am. Sot. Civ. Eng., New Orleans, p. 1745-1759.

Colbert, A.J., B.J. Soden, 2012. Climatological Variations in North Atlantic Tropical Cyclone Tracks. J. Climate 25, 657-673.

Cowell, P.J., P.S. Roy, R.A. Jones, 1995. Simulation of large-scale coastal change using a morphological behavior model. Marine Geology 126, 45-61.

Cowell, P., Hanslow, D., Meleo, J., 1999. The shoreface. Handbook of beach and shoreface

morphodynamics. Chichester: Wiley 37, 71.
Davis, W.R., 1954. Hurricanes of 1954: Monthly Weather Review: v. 82, p. 370-373.
Dean, W.E., 1974. Determination of carbonate and organic matter in calcareous sediments and sedimentary rocks by loss on ignition: comparison with other methods. J. Sed. Petrol. 44, 242-248.
Dean, L., K. A. Emanuel, and D. R. Chavas. 2009. On the size distribution of Atlantic tropical cyclones, Geophys. Res. Lett., 36, L14803, doi: 10.1029/2009GL039051.
Dean, R.G., 1991. Equilibrium Beach Profiles: Characteristics and Applications. J. Coastal Res. 7, 53-84.
deMenocal, P., Ortiz, J., Guilderson, T., Sarnthein, M., 2000. Coherent high- and low-latitude climate variability during the Holocene Warm Period. Science 288, 2198-2202.
Demuth, J.L., M. DeMaria and J.A. Knaff. 2006. Improvement of advanced microwave sounding unit tropical cyclone intensity and size estimation algorithms. J. App. Meteorology and Climatology. 45, 1573 – 1581.
Doi, T., G.A. Vecchi, A.J. Rosati, T.L. Delworth, 2013. Response of CO2 Doubling of the Atlantic Hurricane Main Development Region in a High-Resolution Climate Model. J. Climate 26, 4322-4334.
Donnelly, C., N. Kraus, and M. Larson, 2006. State of Knowledge on Measurement and Modeling of Coastal Overwash, J. Coastal Res., 22(4), 965-991.
Donnelly, J.P., and J.D. Woodruff, 2007. Intense hurricane activity over the past 5,000 years controlled by El Niño and the West African monsoon. Nature, 447**,** 465-468.
Donnelly, J.P., and L. Giosan, 2008. Tempestuous highs and lows in the Gulf of Mexico. Geology 36, 751-752.
Donnelly et al. in prep, Regional Oceanographic Forcing of Unprecedented Intense Hurricane Activity at the Transition between the Medieval Climate Anomaly and Little Ice Age.
Donoghue, J.F., J.B. Elsner, B.X. Hu, S.A. Kish, A.W. Niederoda, Y. Wang, M. Ye, 2013. Effects of near-term sea-level rise on coastal infrastructure, SERDP project RC-1700 Final Report.
Elsner, J.B. and A.B. Kara, 1999. Hurricanes of the North Atlantic: Climate and Society. Oxford University Press, New York. 488 pp.
Elsner, J.B., 2003. Tracking Hurricanes. Bull. Amer. Meteor. Soc., 84, 353–356.
Elsner, J.B., K.-B. Liu, and B. Kocher, 2000. Spatial variations in major US hurricane activity: Statistics and a physical mechanism. J. of Climate, 13**,** 2293-2305.
Elsner, J.B., J.P. Kossin, T.H. Jagger, 2008. The increasing intensity of the strongest tropical cyclones. Nature. 455, 92-95.
Emanuel, K.A., 1987. The dependence of hurricane intensity on climate. Nature, 326**,** 483-485.
Emanuel, K.A., 1988. The maximum intensity of hurricanes. J. Atmospheric Sciences, 45**,** 1143-1155.
Emanuel, K.A., 2001. The contribution of tropical cyclones to the oceans' meridional heat transport. J. Geophysic. Res., 106**,** 14771-14782.
Emanuel, K.A., 2002. A simple model of multiple climate regimes. J. Geophys. Res. 107(D9). 4077. doi: 10.1029/2001JD001002.
Emanuel, K.A., C. DesAutels, C. Holloway, and R. Korty, 2004. Environmental control of tropical cyclone intensity: J. Atmos. Sci., 61, 843–858.

Emanuel, K., S. Ravela, E. Vivant and C. Risi. 2006. A Statistical Deterministic Approach to Hurricane Risk Assessment. Bull. Am. Meteorological Soc., 87(3). 299 – 314.

Emanuel, K.A., R. Sundararajan, J. William, 2008. Hurricanes and global warming: results from downscaling IPCC AR4 simulations. Bulletin of the American Meteorological Society. 89, 347-367.

Emanuel, K. 2013. Downscaling CMIP5 climate models shows increased tropical cyclone activity over the 21st century. Proc. Nat Acad. Sci. 110, 12219-12224.

Foxgrover, A.C., 2009. Quantifying the overwash component of barrier island morphodynamics: Onslow Beach, NC., MSc. Thesis, College of William and Mary.

Frank, W.M. 1977. Structure and energetics of the tropical cyclone, part 1, Storm structure. Monthly Weather Review. 105. pp. 1119 – 1135.

Gehrels, W.R., 1999. Middle and late Holocene sea-level changes in eastern Maine reconstructed from foraminiferal saltmarsh stratigraphy and AMS 14C dates on basal peat. Quaternary Res., 52, 350–359.

Gehrels, W.R., Hayward, B.W., Newnham, R.M., Southall, K.E., 2008. A 20th century acceleration of sea-level rise in New Zealand. Geophys. Res. Letts., 35, L02717. doi:10.1029/2007GL032632.

Gischler, E., E. Shinn, W. Oschmann, J. Fiebig and N. Buster, 2008. A 1500-Year Holocene Climate Archive from the Blue Hole, Lighthouse Reef, Belize. J. Coastal Research 24**,** 1495-1505.

Goldenberg, S. B., C.W. Landsea, A.M. Mestas-Nunez and W.M. Gray, 2001. The recent increase in Atlantic hurricane activity: Causes and implications. Science 293, 474-479.

Gray, W. M., 1968. Global view of the origin of tropical disturbances and storms. Monthly Weather Review 96, 669-700.

Gray, W. M., 1984. Atlantic Seasonal Hurricane Frequency. Part I: El Nino and 30 mb Quasi-Biennial Oscillation Influences. Monthly Weather Review 112, 1649-1668.

Gualdi, S., E. Scoccimarro, A. Navarra, 2008. Changes in tropical cyclone activity due to global warming: results from a high-resolution coupled general circulation model. J. Climate. 21, 5204-5228.

Hart, R.E., 2010. An inverse relationship between aggregate tropical cyclone activity and subsequent winter climate. Geophys. Res. Letters, doi:10.1029/2010GL045612.

Hart, R., R. Maue, M. Watson, 2007. Estimating the atmospheric and SST memory of tropical cyclones through MPI anomaly evolution. Monthly Weather Review 135, 3990-4005.

Haug, G.H., K.A. Hughen, D.M. Sigman, L.C. Peterson and U. Rohl, 2001. Southward Migration of the Intertropical Convergence Zone through the Holocene. Science 293, 1304-1308.

Hemming, J.M., J.M. Brown, M. Brim, R. Jarvis, 2005. Sediment quality survey of the Choctawhatchee Bay system in the Florida Panhandle: Marine Pollution Bulletin, 50, 903.

Hodell, D. A., M. Brenner, J.H. Curtis, R. Medina-González, E. Ildefonso-Chan Can, A. Albornaz-Pat and T.P. Guilderson, 2005. Climate change on the Yucatan Peninsula during the Little Ice Age. Quaternary Research 63, 109-121.

Holland, G.J., P.J. Webster, 2007. Heightened tropical cyclone activity in the North Atlantic: Natural variability or climate trend? Phil. Trans. Royal Soc. London. Ser. A. doi:10.1098/rsta.2007.2083.

Houser, C., C. Hapke, S. Hamilton, 2008. Controls on coastal dune morphology, shoreline erosion and barrier island response to extreme storms. Geomorphology 100, 223-240.

Houser, C., and S. Hamilton, 2009. Sensitivity of post-hurricane beach and dune recovery to event frequency. Earth Surface Processes and Landforms 34, 613-628.

Jelesnianski, C.P., J. Chen, J. and W.A. Shaffer, 1992. SLOSH: Sea, Lake and Overland Surges from Hurricanes, NOAA Technical Report NWS 48, NOAA, Washington, DC.

Jiménez, J., Sánchez-Arcilla, A., 2004. A long-term (decadal scale) evolution model for microtidal barrier systems. Coastal Engineering 51, 749-764.

Kalnay et al., 1996. The NCEP/NCAR 40-year reanalysis project, Bull. Amer. Meteor. Soc., 77, 437-470.

Kemp, A.C., B.P. Horton, R. Corbett, S.J. Culver, R.J. Edwards and O. van de Plassche, 2009. The relative utility of foraminifera and diatoms for reconstructing late Holocene sea-level change in North Carolina, USA. Quaternary Res., 71, 9-21.

Klotzbach, P.J., 2010. On the Madden-Julian-Atlantic hurricane relationship. J.Climate. 23, 282-293.

Klotzbach, P.J., 2011. The Influence of El Nino-Southern Oscillation and the Atlantic Multidecadal Oscillation on Caribbean Tropical Cyclone Activity. J. Climate. 24, 721-731.

Knapp, K.R., Kruk, M.C., Levinson, D.H., Diamond, H.J., Neumann, C.J., 2010. The International Best Track Archive for Climate Stewardship (IBTrACS): Unifying tropical cyclone best track data. Bull. Amer. Meteor. Soc. 91, 363-376.

Knudsen, M.F., M.S.,Seidenkrantz, B.H. Jacobsen, A. Kuijpers, 2011. Tracking the Atlantic Multidecadal Oscillation through the last 8,000 years. Nature Communications 2:178 doi:10.1038/ncomms1186

Knutson, T. R., and R.E. Tuleya, 2004. Impact of CO2-induced warming on simulated hurricane intensity and precipitation: Sensitivity to the choice of climate model and convective parameterization. J. of Climate 17, 3477-3495.

Knutson, T.R., J.J. Sirutis, S.T. Garner, G.A. Vecchi, I.M Held, 2008. Simulated reduction in Atlantic hurricane frequency under twenty-first-century warming conditions. Nature Geoscience. doi:10.1038/ngeo202.

Knutson, T.R., J.L. McBride, J. Chan, K. Emanuel, G. Holland, C. Landsea, I. Held, J. Kossin, A. Srivastava and N. Sugi, 2010. Tropical cyclones and climate change. Nature Geosciences 3, 157-163.

Korty, R.L., K.A. Emanuel, J.R. Scott, 2008. Tropical cyclone-induced upper-ocean mixing and climate: application to equable climates. J. of Climate 21 638-654.

Kossin, J.P., J.A. Knaff, H.I. Berger, D.C. Herndon, T.A. Cram, C.S. Velden, R.J. Murnane, and J.D. Hawkins, 2007. Estimating hurricane wind structure in the absence of aircraft reconnaissance. Weather and Forecasting, 22, 89-101.

Kossin, J., S.J. Camargo, 2009. Hurricane track variability and secular potential intensity trends. Climate Change 97, 329-337.

Kossin, J.P., S.J. Camargo, M. Sitkowski, 2010. Climate modulation of North Atlantic hurricane tracks. J. Clim. 23, 3057-3076.

Lambert, J.W., P. Aharon, A.B. Rodriguez, 2008. Catastrophic hurricane history revealed by organic geochemical proxies in a coastal lake sediments: a case study of Lake Shelby, Alabama (USA). J. Paleolimnol. 39, 117-131.

Landsea, C.W., C. Anderson, N. Charles, G. Clark, J. Partagas, P. Hungerford, C. Neumann and M. Zimmer, 2004. The Atlantic hurricane database re-analysis project: Documentation for the 1851-1885 addition to the HURDAT database. in R. Murnane and K. Liu eds. Hurricanes and Typhoons: Past, Present and Potential: New York, Columbia University Press.

Landsea, C.W., 2007. Counting Atlantic tropical cyclones back to 1900. Eos Transactions. 88(18), 197-202.

Lane, D.P., 2011. Late Holocene Hurricane Activity and Climate Variability in the Northeastern Gulf of Mexico. Ph.D. Thesis. MIT/WHOI Joint Program in Oceanography/Applied Ocean Science and Engineering. Massachusetts Institute of Technology. Boston, MA.

Lane, P., J.P. Donnelly, 2012. Extreme hurricane climates of millennia past: causes and implications. PAGES Special Issue: Paired Perspectives on Global Change. 20(1), p. 32.

Lane, P., J.P. Donnelly, J.D. Woodruff, A.D. Hawkes, 2011. A decadally-resolved paleohurricane record archived in the late Holocene sediments of a Florida sinkhole. Marine Geology. v. 287. p. 14-30.

Lawrence, M.B., L.A. Avila, J.L. Beven, J.L. Franklin, J.L. Guiney, R.J. and Pasch, 2001. Atlantic Hurricane Season of 1999: Monthly Weather Review, v. 129, p. 3057-3084.

Leatherman, S.P., 1979. Migration of Assateague Island, Maryland, by inlet and overwash processes, Geology(7), 104-107.

Leatherman, S.P., 1983. Barrier dynamics and landward migration with Holocene sea-level rise. Nature 301, 415-417.

Levitus, S., J.I. Antonov, T.P. Boyer, C. Stephens, 2000. Warming of the World Ocean. Science. 287**,** 2225-2229.

Levitus, S., J.I. Antonov, J. Wang, T.L. Delworth, K.W. Dixon and A.J. Broccoli, 2001. Anthropogenic Warming of Earth's Climate System, pp. 267-270.

Liu, K., M.L. Fearn, 2000. Reconstruction of prehistoric landfall frequencies of catastrophic hurricanes in northwestern Florida from lake sediment records. Quat. Res. 54, 238-245.

Lorenzo-Trueba, J., and V.R. Voller, 2010. Analytical and numerical solution of a generalized Stefan problem exhibiting two moving boundaries with application to ocean delta formation, J. Math. Anal. Appl., 366(2), 538-549.

Lorenzo-Trueba, J., V.R. Voller and C. Paola, 2013. A geometric model for the dynamics of a fluvially dominated deltaic system under base-level change, Comp. Geosci., 53(0), 39-47.

Lorenzo-Trueba, J., V.R. Voller, C. Paola, R. R. Twilley, and A. E. Bevington, 2012. Exploring the role of organic matter accumulation on delta evolution, J. Geophys. Res., 117(F3), F00A02.

Lorenzo-Trueba, J., V.R. Voller, T. Muto, W. Kim, C. Paola, and J.B. Swenson, 2009. A similarity solution for a dual moving boundary problem associated with a coastal-plain depositional system, J. Fluid Mech., 628, 427-443.

Lorenzo-Trueba, J., and A.D. Ashton, 2014. Rollover, Drowning, and Discontinuous Retreat: Distinct modes of barrier response to sea-level rise suggested by a simple model. J. Geophys. Res., DOI:10.1002/2013JF002941.

Love et al., 2009. Digital Elevation Models of the northern Gulf Coast: Procedures, Data Sources and Analysis, NOAA National Geophysical Data Center.

Madsen, A.T., A.S. Murray, 2009. Optically Stimulated Luminescence dating of young sediments: A review, Geomorphology, 109, 3-16.

Mallinson, D.J., C.W. Smith, S. Mahan, S.J. Culver, K. McDowell, 2011. Barrier island response to late Holocene climate events, North Carolina, USA, Quaternary Research 76, 46-57.

Mann, M.E., K.A. Emanuel, G.J. Holland, P.J. Webster, 2007. Atlantic tropical cyclones revisited. Eos Transactions. 88(36), 350-352.

Mann, M.E., J.D. Woodruff, J.P. Donnelly, Z. Zhang, 2009. Atlantic hurricanes and climate over the past 1,500 years. Nature. 460, 880-885.

Marks, D. G., 1992. The beta and advection model for hurricane track forecasting. NOAA Tech. Memo. NWS NMC 70, National Meteorological Center, Camp Springs, MD, 89 pp.

Masetti, R., S. Fagherazzi, A. Montanari, 2008. Application of a barrier island translation model to the millennial-scale evolution of Sand Key, Florida. Continental Shelf Res. 28, 1116-1126.

Masetti, R., S. Fagherazzi, and A. Montanari, 2008. Application of a barrier island translation model to the millennial-scale evolution of Sand Key, Florida, Cont. Shelf Res., 28(9), 1116-1126.

McCall, R.T., J.S.M. Van Thiel de Vries, N.G. Plant, A.R. Van Dongeren, J.A. Roelvink, D.M. Thompson and A.J.H.M. Reniers, 2010. Two-dimensional time dependent hurricane overwash and erosion modeling at Santa Rosa Island, Coast Eng., *57*(7), 668-683.

McNamara, D.E., and B.T. Werner, 2008. Coupled barrier island-resort model: 1. Emergent instabilities induced by strong human-landscape interactions, J. Geophys. Res., *113*(F01016,), doi:10.1029/2007JF000840.

Miller, J.K. and R.G. Dean, 2004. A simple new shoreline change model. Coastal Engineering, 51(7), 531-556.

Milliken, K.T., J.B. Anderson and A.B. Rodriguez, 2008. A new composite Holocene sea-level curve for the northern Gulf of Mexico, *in* Anderson J.B., and Rodriguez, A.B., eds., Response of upper Gulf Coast estuaries to Holocene climate change and sea level change: The Geol. Soc. America, Special Paper 443, 1-11.

Morang, A., 1992. Inlet Migration and Hydraulic Processes at East Pass, Florida: J. Coastal Res., 8, 457-481.

Morton, R.A., J.G. Paine and M.D. Blum, 2000. Responses of stable bay–margin and barrier–island systems to Holocene sea-level highstands, western Gulf of Mexico: J Sedimentary Res., v. 70, p. 478–490.

Moy, C.M., G.O. Seltzer, D.T. Rodbell and D.M. Anderson, 2002. Variability of El Nino/Southern Oscillation activity at millennial timescales during the Holocene epoch: Nature 420, 162-165.

Mulitza, S., M. Prange, J.B. Stuut, M. Zabel, T. Dobeneck, A.C. Itambi, J. Nizou, M. Schilz, G. Wefer, 2008. Sahel megadroughts triggered by glacial slowdowns of Atlantic meridional overturning. Paleoceanography 23, PA4206.

NOAA. 2007. Hurricane Research Division. HURDAT Re-analysis Project. <http://www.aoml.noaa.gov/hrd/hurdat/Data_Storm.html>

Ortiz, A.O. and A.D. Ashton, Exploring a Mechanistic Explanation for the Morphodynamic Depth of Closure. J. Geophys. Res., in prep.

Otvos, E., 1982. Santa Rosa island, Florida panhandle, origins of a composite barrier island. Southeastern Geol., 23 (1), 15– 23.

Pasch, R.J., and L.A. Avila, 1999. Atlantic Hurricane Season of 1996: Monthly Weather Review, v. 127, p. 581-610.

Pasch, R.J., L.A. Avila and J.L. Guiney, 2001. Atlantic Hurricane Season of 1998: Monthly Weather Review, v. 129, p. 3085-3123.

Pelletier, J. D., and T. Perron, 2012, Analytic solution for the morphology of a soil-mantled valley undergoing steady headward growth: Validation using case studies in southeastern Arizona. J. Geophys. Res., v. 117.

Perron, T., J.W. Kirchner and W.E. Dietrich, 2009, Formation of evenly spaced ridges and valleys: Nature, v. 460.

Phadke, A.C., C.D. Martino, K.F. Cheung and S.H. Houston, 2003. Modeling of tropical cyclone winds and waves for emergency management, Ocean Eng., 30(4), 553– 578.

Poore, R.Z., T.M. Quinn, S. Verardo, 2004. Century-scale movement of the Atlantic Intertropical Convergence Zone linked to solar variability. Geophys. Res. Letters 31, L12214, doi: 10.1029/2004GL019940.

Pritchard, D., Roberts, G. G., White, N. J., and Richardson, C. N., 2009, Uplift histories from river profiles: Geophysical Research Letters, v. 36.

Ridge, J.T., A.B. Rodriguez, S.R. Fegley, R. Browne, D. Hood, 2011. A new 'pressure sensitive' method of measuring Aeolian sediment transport using a Gauged Sediment Trap (GaST), Geomorphology, 134, 426-430.

Riggs, S.R., W.J. Cleary and S.W. Snyder,1995. Influence of inherited geologic framework on barrier shoreface morphology and dynamics. Marine Geology, 126, 213-234.

Riggs, S.R., W.G. Ambrose, J.W. Cook, S.W. Snyder, 1996. Sediment production on sediment-starved continental margins: the interrelationship between hardbottoms, sedimentological and benthic community processes and storm dynamics, J. Sediment. Res., 68, 155–168.

Ris, R. C., and H. Holthuijsen, 1999. A third-generation wave model for coastal regions: 2. Verification, J. Geophys. Res., 104(C4), 7667– 7681.

Roberts, M.L., K.F. von Reden, J.R. Burton, C.P. McIntyre, S.R. Beaupré, 2011. A gas-accepting ion source for Accelerator Mass Spectrometry: Progress and applications. Nuclear Instruments and Methods in Physics Research Section B: Beam Interactions with Materials and Atoms. 294, 296-299.

Rodriguez, A.B., J.B. Anderson, F.P. Siringan, and M. Taviani, 2004. Holocene evolution of the east Texas coast and inner continental shelf: Along-strike variability in coastal retreat rates, J. Sediment. Res., 74(3), 405-421.

Rodriguez, A.B., J.B. Anderson, and A.R. Simms, 2005. Terrace inundation as an autocyclic mechanism for parasequence formation: Galveston Estuary, Texas, USA, J. Sediment. Res., 75(4), 608-620.

Rodriguez, A. B., A.R. Simms, and J. B. Anderson, 2010. Bay-head deltas across the northern Gulf of Mexico back step in response to the 8.2 ka cooling event, Quaternary Sci. Rev., 29(27-28), 3983-3993.

Rodysill, J.R., J.P. Donnelly, D.P. Lane, R.L. Evans, A. Ashton, R. Sullivan, M. Toomey, D. MacDonald, 2013, Northern Gulf of Mexico tropical cyclone activity over the past 4500 years from sediment archives, PhD. Thesis, Chapter 5, Brown University.

Roeber, V., K.F. Cheung, M.H. Kobayashi, 2010. Shock-capturing Boussinesq-type model for nearshore wave processes, Coastal Eng., 57, 407-423.

Roeber, V., K.F. Cheung, 2012. Boussinesq-type model for energetic breaking waves in fringing reef environments. Coastal Engineering, 70(1), 1-20.

Roelvink, D., A. Reniers, A. van Dongeren, J. van Thiel de Vries, R. McCall, and J. Lescinski, 2009. Modelling storm impacts on beaches, dunes and barrier islands, Coastal Eng., *56*(11–12), 1133-1152.

Roelvink, J. A., 2006. Coastal morphodynamic evolution techniques, Coastal Eng., *53*(2–3), 277-287.

Schnurrenberger, D., J.M. Russell, K. Kelts, 2003. Classification of lacustrine sediments based on sedimentary components. J. Paleolimnol. 29, 141-154.

Scott, J.R., J. Marotzke, 2002. The location of diapycnal mixing and the meridional overturning circulation. J. Physical Oceanography 32, 3578-3595.

Shanahan, T.M. J.T. Overpeck, K.J. Anchukaitis, J.W. Beck, J.E. Cole, D.L. Dettman, J.A. Peck, C.A. Scholz, J.W. King, 2009. Atlantic Forcing of Persistent Drought in West Africa. Science 324, 377-380.

Sriver, R.L., M. Huber, 2007. Observational evidence for an ocean heat pump induced by tropical cyclones. Nature 447, 577-580.

Sriver, R.L., M. Huber, J. Nusbaumer, 2008. Investigating tropical cyclone-climate feedbacks using the TRMM microwave imager and the Quick Scatterometer. Geochemistry, Geophysics, and Geosystems. 9(9), Q09V11, doi:10/1029/2007.GC001842.

Stive, M.J.F., H.J. de Vriend, 1995. Modelling shoreface profile evolution. Marine Geology 126, 235-248.

Stolper, D., J.H. List, E.R. Thieler, 2005. Simulating the evolution of coastal morphology and stratigraphy with a new morphological-behaviour model (GEOMBEST). Marine Geology 218, 17-36.

Stone, G.W., 1991. Differential sediment supply and the cellular nature of longshore sediment transport along coastal northwest Florida and southeast Alabama since the Late Holocene.PhD Dissertation, University of Maryland, College Park, MD 376 pp.

Stone, G.W., F.W. Stapor, J.P. May, J.P. Morgan, 1992. Multiple sediment sources and a cellular, non-integrated, longshore drift system: northwest Florida and Southeast Alabama coast, USA: Marine Geology, 105, 141– 154.

Stone, G.W., F.W. Stapor, 1996. A nearshore sediment transport model for the Northeast Gulf of Mexico Coast. J. of Coastal Res., 12 (3), 786– 792.

Stone, G.W., P. Wang, D.A. Pepper, J.M. Grymes, H.H. Roberts, X. Zhang, S.A. Hsu, O.K. Huh, 1999. Studying the importance of hurricanes to the northern Gulf of Mexico, EOS Trans AGU, 80 (27), 301-305.

Stone, G.W., B. Liu, D.A. Pepper and P. Wang, 2004. The importance of extratropical and tropical cyclones on the short-term evolution of barrier islands along the northern Gulf of Mexico, USA: Mar. Geol., 210, 63–78.

Storms, J. E.A., and G. J. Hampson, 2005. Mechanisms for forming discontinuity surfaces within shoreface-shelf parasequences: Sea level, sediment supply, or wave regime? J. Sediment. Res., 75 (1), 67-81.

Swenson, J.B., C. Paola, L. Pratson, V.R. Voller, A.B. Murray, 2005. Fluvial and marine controls on combined subaerial and subaqueous delta progradation: Morphodynamic modeling of compound-clinoform development. J. Geophys. Res. -Earth Surface, 110, doi:10.1029/2004JF000265.

Tolman, H. L., B. Balasubramaniyan, L. D. Burroughs, D. V. Chalikov, Y. Y.Chao, H. S. Chen, and V. M. Gerald, 2002. Development and implementationof wind-generated ocean surface wave models and NCEP, Weather Forecasting, 17(2), 311 – 333.

van Hengstum, P.J., J.P. Donnelly, M.R. Toomey, N.A. Albury, P. Lane, and B. Kakuk, 2013. A heightened interval of hurricane activity from 1350 to 1550 AD on the Little Bahama Bank. Continental Shelf Res. (http://dx.doi.org/10.1016/j.csr.2013.04.032)

Vecchi, G., and B. Soden, 2007. Effect of remote sea surface temperature change on tropical cyclone potential intensity. Nature 450 1066-1070.

Vimont, D.J., J.P. Kossin, 2007. The Atlantic Meridional Mode and hurricane activity. Geophys. Res. Letters. 34, L07709, doi:10.1029/2007GL029683.

Webster, P.J., G.J. Holland, J.A. Curry, H.R. Chang, 2005. Changes in tropical cyclone number, duration, and intensity, in warming environment. Science, 309, 1844–1846.

Wei, W., G. Lohmann, 2012. Simulated Atlantic Multidecadal Oscillation during the Holocene. J. Climate 25, 6989-7001.

Wessel, P., and W. H. F. Smith, 1991. Free software helps map and display data, Eos Trans. AGU, 72(41), 441.

Woodruff, J.D., R.L. Sriver, D.C. Lund, 2011. Tropical cyclone activity and western North Atlantic stratification over the last millennium: a comparative review with viable connections. J. Quaternary Science, 27, 337-343.

Yamazaki et al., 2009. Depth-integrated, non-hydrostatic model for wave breaking and run-up, Int. J. Numerical Methods in Fluids, 61, 473-497.

Yu, W., 2012. Impacts of Storms and Sea-Level Rise on Coastal Evolution Between Two Capes: Onslow Bay, North Carolina MS thesis, University of North Carolina at Chapel Hill.

Zhang, R. and T.L. Delworth, 2006. Impact of Atlantic multidecadal oscillations on India/Sahel rainfall and Atlantic hurricanes. Geophys. Res. Letters, 33, L17712.

Zhao M., I.M. Held, S.J. Lin, G.A. Vecchi, 2009. Simulations of global hurricane climatology, interannual variability, and response to global warming using a 50km resolution GCM. J. of Climate. doi: 10.1175/2009JCLI3049.1

Appendices

A. List of Scientific/Technical Publications

Ashton, A.D., 2013. Beyond the Bathtub: Modeling the Morphologic Response of Coasts. Joint Penrose/Chapman Conference: Coastal Processes and Environments Under Sea-Level Rise and Changing Climate: Science to Inform Management, April 14-19, Galveston, USA

Ashton, A.D., Ortiz, A., Lane, P., Donnelly, J., 2011. Characteristic Timescales of Shoreface Response to Sea-Level Rise. Eos Trans. AGU Fall Meet. Suppl., Abstract OS43D-05. (Oral Presentation)

Ashton, A.D., Ortiz, A.C., 2011. Overwash controls coastal barrier response to sea-level rise. Coastal Sediments '11, Miami FL, ASCE.

Donnelly, J.P., P. Lane, M.R. Toomey, J. Rodysill, A. Hawkes, P. van Hengstum, P.N. Ranasinghe, D. Wallace, and D. MacDonald, 2013, North Atlantic Hurricane Activity over the Last Two Millennia: Patterns, Climatic Forcing, and Implications for the Future, Joint Penrose/Chapman Conference, Galveston, TX.

Donnelly, J.P., P. Lane, M.R. Toomey, J. Rodysill, A. Hawkes, P. van Hengstum, P.N. Ranasinghe, D. Wallace, and D. MacDonald, 2013, Late Holocene North Atlantic Hurricane Activity, Annual Meeting of the Geological Society of America, Charlotte, NC.

Donnelly, J.P., P. Lane, A. Hawkes, P. van Hengstum, P. N. Ranasinghe, M. Toomey, and D. MacDonald, 2012, Late Holocene Hurricane Activity: Patterns, Consequences and Potential Climatic Forcing, American Quaternary Association Biennial Meeting, Duluth, MN.

Lane, P., Donnelly, J.P., Woodruff, J.D., Hawkes, A.D., 2011. A decadally-resolved paleohurricane record archived in the late Holocene sediments of a Florida sinkhole. Marine Geology. v. 287. p. 14-30.

Lin, N., P. Lane, K. Emanuel, R. Sullivan, J.P. Donnelly, Climatological-hydrodynamic storm surge modeling for Apalachee Bay, Florida, in press, J. Geophys, Res (Atmospheres).

Lorenzo-Trueba, J., Ashton, A.D., 2012. Can human activities alter the drowning fate of barrier islands? Eos Trans. AGU Fall Meet. Suppl., Abstract EP33B-0855.

Lorenzo-Trueba, J., Ashton, A.D., 2013. A simple morphodynamic model of coastal barrier response to rising sea level. Joint Penrose/Chapman Conference: Coastal Processes and Environments Under Sea-Level Rise and Changing Climate: Science to Inform Management, April 14-19, Galveston, USA

Lorenzo-Trueba, J., and A.D. Ashton, 2014. Rollover, Drowning, and Discontinuous Retreat: Distinct modes of barrier response to sea-level rise suggested by a simple model. J. Geophys. Res. (Earth Surface), DOI:10.1002/2013JF002941

Ortiz, A., and A.D. Ashton, Exploring a morphodynamic explanation for the shoreface depth of closure, submitted to Journal of Geophysical Research.

Ranasinghe, P.N., J. Donnelly, R.L. Evans, A, Ashton, K. Condon, R. Sullivan, A. Beltzer, Changes in mid-late Holocene hurricane activity influence coastal dynamics in northeastern

Gulf of Mexico – A case study in the Choctawhatchee Bay, Destin FL., EOS Trans AGU, 2011.

Rodysill, J.R., J.P. Donnelly, D.P. Lane, R.L. Evans, A. Ashton, R. Sullivan, M. Toomey, D. MacDonald, 2013, Northern Gulf of Mexico tropical cyclone activity over the past 4500 years from sediment archives, PhD. Thesis, Chapter 5, Brown University.